Emergency Stability Control of Power Systems Using Wide Area Synchrophasor Measurements

By

Neethu Vettuthuruthel Raju

A Thesis submitted to the Faculty of Graduate Studies of
The University of Manitoba
For the partial fulfillment of the requirements of the Degree of
MASTER OF SCIENCE

Department of Electrical and Computer Engineering
University of Manitoba
Winnipeg, Manitoba

Copyright © 2018 by Neethu Vettuthuruthel Raju

Abstract

This thesis investigates novel ways of using wide area synchrophasor measurements for implementing response-based emergency control operations. Two synchrophasor measurement based Remedial Action Schemes (RASs), one to prevent cascaded tripping of transmission lines due to overloading when a major tie-line exporting power is tripped and the other to prevent uncontrolled islanding and blackouts due to transient instability, were developed.

The RAS proposed for overload prevention in Manitoba Hydro grid acts to quickly reduce the power delivered from HVdc converters during the tripping of tie-lines exporting power to USA. The proposed approach uses synchrophasors data to estimate the minimum required power reduction in the Bipoles based on the identified tripping event, in contrast to current RAS which reduces a fixed percentage of power flow in the tripped line.

The second RAS performs controlled islanding to prevent transient instability. It incorporates two previously proposed algorithms to detect impending instabilities and identify the critical coherent generator group using voltage magnitudes reported by phasor measurement units (PMUs). Then the loads are assigned to islands considering the phase angle differences and relative electrical distances between the loads and the generators in a coherent group. Finally, a frequency-based generator and load shedding scheme is applied to maintain the post-islanding generation-load balance. The effectiveness of the approach was demonstrated using the IEEE 39 Bus test system.

Acknowledgment

I would like to express my gratitude to Dr. Athula Rajapakse for his guidance and support throughout the years. It is a great privilege to work under his supervision.

I would also like to thank Dr. Ioni .T. Fernando and Mr. David Diakiw at Manitoba Hydro and Dr. Dinesh Rangana Gurusinghe at RTDS Technologies Inc. for their support with providing resources, technical guidance, and valuable feedback throughout the research.

I would like to thank the examining committee for spending their time in reviewing my thesis.

I must also thank the academic, technical and administrative staffs from the Department of Electrical and Computer Engineering especially to Mr. Erwin Driks, Ms. Traci Gledhill and Ms. Amy Dario. Special thanks to Amalnath Mani, Jordan Poitras, Nithin Thomas, and Amrutha Peedikayil for the comments made to improve my writing. Also, I would like to thank all my colleagues in the Department of Electrical and Computer Engineering for their support and best experiences at the University of Manitoba.

Last but not least, I would like to thank my family for their constant support at every step of my life.

Neethu Vettuthuruthel Raju

December 2018

Dedication

To my family and friends.

Contents

List of Tables

List of Figures

List of Symbols

$P_{t(i)}$	Power flow through the branch *i*
P_{th}	Threshold power setting
$S_{nR,i}$	Normal line rating of ith line
$S_{eR,i}$	Emergency rating of ith line
ΔP_{dc}	Amount of HVdc reduction
ΔS_i	Overloading of the *i*th line in MVA
$\Delta S_{\%,i}$	Percentage overloading of the *i*th line
S_i	MVA rating of the *i*th line
$S_{F,i}$	Sensitivity factor of the *i*th branch
m_i	Slope of the fitted curve
ΔP_{dc}^*	Amount of HVdc power reduction
ΔP_{dc1}^*	Amount of HVdc power reduction in MODE 1 operation
ΔP_{dc2}^*	Amount of HVdc power reduction in MODE 2 operation
$P_{BPrated,n}$	MVA rating of the Bipole *n*
$\Delta P_{BP,n}$	Total amount of power reduction in Bipole *n*
$ROCOV$	Rate of change of voltage magnitude at the generator terminal
ΔV	Voltage deviation at the generator terminal
V_{mag}	Terminal voltage measured at the generator end
$V_{mag,ref}$	Reference voltage magnitude

F_s	Reporting rates of PMUs in frames/sec
$V_{magG}^{(q)}(t)$	Voltage magnitude of the *qth* generator at time t
I_{pq}	characteristic impedance for the transmission line
Δt	length for the transmission line
n_g	fault distance from the sending of the transmission line
$\Delta\delta$	Phase angle difference between the generator and the load points
δ_{gen}	Phase angle value at the generator
δ_{load}	Phase angle value at the load point
$[Y]$	Normal admittance matrix of the system
f_{isl}	Average frequency of the selected island
$f_k(t)$	Frequency of the generator and load points in the island
$f_l(t)$	Total number of load points in the island
$f_g(t)$	Total number of generators in the island
$n^{'}$	Total number of generator and load points in the island
$V_{magG}^{(p)}(t)$	Voltage magnitude of the *pth* generator at time t

List of Abbreviations

HVac	**H**igh **V**oltage **ac**
GPS	**G**lobal **P**ositioning **S**ystem
WAMS	**W**ide **A**rea **M**onitoring **S**ystem
PMU	**P**hasor **M**easurement **U**nit
ROCOV	**R**ate **O**f **C**hange **O**f **V**oltage
RAS	**R**emedial **A**ction **S**cheme
SPS	**S**pecial **P**rotection **S**ystem
SCADA	**S**upervisory **C**ontrol and **D**ata **A**quisition
PDC	**P**hasor **D**ata **C**oncenrator
DG	**D**istributed **G**eneration
HVdc	**H**igh **V**oltage **dc**
UFLS	**U**nder **F**requency **L**oad **S**hedding
PSO	**P**article **S**wam **O**ptimisation
FACTS	**F**lexible **A**lternating **C**urrent **T**ransmission **S**ystem
SSR	**S**ub-**S**ynchronous **R**esonance
SVC	**S**tatic **V**oltage **C**ompensator
STATCOM	**S**tatic **S**ynchronous **S**eries **C**ompensator
TCSC	**T**hyristor **C**ontrolled **S**eries **C**ompensator
SSSC	**S**tatic **S**ynchronous **S**eries **C**ompensator
UPFC	**U**nified **P**ower **F**low **C**ontroller

OBDD	**O**rdered **B**inary **D**ecision **D**iagram
TEPCO	**T**okyo **E**lectric **P**ower **C**o
NCS	**N**orthern **C**ollector **S**ystem
MISO	**M**idwest **I**ndependent **S**ystem **O**perator
USA	**U**nited **S**tates of **A**merica
WACS	**W**ide **A**rea **C**ontrol **S**ystem
RED	**R**elative **E**lectrical **D**istance
ICI	**I**ntentional **C**ontrol **I**slanding

List of Appendix

Chapter 1

Introduction

This chapter presents the background, motivation behind the research and the goals of the research. A brief introduction to Wide Area Monitoring Systems (WAMS) that use synchrophasor technology, applications of synchrophasor measurements, particularly for emergency control, and Remedial Action Schemes (RAS) in practice is given. The importance of remedial action schemes or special protection schemes in power grid protection is discussed to highlight the relevance of research objectives to the power utility industry. The chapter concludes with the arrangement of the thesis.

1.1 Background

Utilities are compelled to operate closer to the maximum power transferability limits of their transmission assets due to increasing load demand, limited generation options, and environmental and economic constraints on the construction of new transmission lines. Generally, power systems are designed with sophisticated controls to operate within their voltage and frequency level under various disturbances including faults, sudden load variations, and generation loss. Nonetheless, when some unexpected event or simultaneous

multiple disturbances take place in a power system operating with limited stability margin, transmission lines and transformers in the system may become overloaded. Consequently, different generator groups in the system may lose their synchronism. If such conditions persist with sufficient time, ranging from several seconds to several minutes depending on the evolving phenomena, cascaded tripping of transmission equipment and lines can occur leading to collapse of the entire power system.

Rotor angle instability and voltage instability are two serious issues causing power system-wide impacts. Angular stability problems arise when one or several generators in a power system lose synchronism, i.e. some of them accelerate or decelerate with respect to the others resulting in out-of-step operation. This may result in wild fluctuations in the power flow, ultimately leading to uncontrolled system separation due to the operation of protection relays. The chances of voltage instability increase when the system becomes heavily loaded and reactive power resources reach closer to their limits. Overloading of transmission lines and equipment's usually occurs due to the power imbalance in the system following an outage. Tripping of equipment due to overloading, especially the transmission lines, can overload the remaining equipment resulting in cascaded tripping, which can potentially develop to a total system outage, if remedial action is not taken.

Among various methods in practice to regulate the effects of wide area power system disturbances discussed above, Remedial Action Schemes (RASs), also known as Special Protection Schemes (SPS), are in the top priority. Special protection schemes are commonly in use as they are highly cost-effective and simpler in design when compared to other available alternatives such as transmission line expansion or power plant construction. Traditional power system protection focused on individual equipment, such

as generators, transformers, and transmission lines. However, these methods cannot provide solutions for system-wide problems; in fact, they can aggravate wide area problems while trying to protect an individual equipment from abnormal operating conditions or overloading. To address the power system wide area network problems, proper information about the whole network, need to be collected and analyzed. This can be performed using modern technologies like synchrophasor measurement based wide area monitoring technology. Synchrophasor measurements provide time tagged measurements that are updated at a rate faster than traditional system control and data acquisition (SCADA) systems to a central station. This information can be used for analyzing the system condition and designing the emergency control methods. Even though wide area synchrophasor measurements are widely used for power system monitoring applications, the potential of advanced synchrophasor technology is not yet fully utilized for closed loop emergency control operations or wide-area protection. Some potential applications of wide area synchrophasor measurements for closed loop emergency control are investigated in this thesis.

1.1.1 Wide Area Measurement Technology

The increasing complexity and geographic extent of power networks make certain events and conditions to grow into system-wide phenomena that cannot be properly identified by local monitoring. System-wide coordinated responses based on wide area monitoring is becoming critical in managing these system-wide events. Proper monitoring facilities should be provided at appropriate points in the network. Measurements should then be sent to a central station through reliable and fast communication channels for the analysis of

data for identifying threatening events such as voltage, frequency and rotor angle instabilities. Receiving correctly time-aligned information from various locations in the power system has always been a challenge when considering the system protection measures. Time aligned measurements are important for conducting post-mortem analysis of major events, system model validation, wide area monitoring, control, and protection. Wide area monitoring based on synchrophasor measurements can be considered as an effective solution for possible applications mentioned above [1].

Synchrophasors provide measurements of voltage, current, phase angle, and frequency synchronized to a common time reference. Global positioning system (GPS) is typically used to provide the common time reference for synchronizing and time tagging the phasor measurements [2]. If sufficient monitoring points are available, the power system state can be continuously monitored on a near real-time basis through synchrophasor measurements collected using secure communication channels.

Wide area measurement system components are illustrated in Figure **1.1**. Phasor Measurement Units (PMU's) at different geographical locations gathers/collect the measurements. The measurements are time tagged and transmitted at one of the standard reporting rates through local area network to a local Phasor Data Concentrator (PDC) [2]. The PDC collects the measurements from the PMUs in the local substation, check the integrity of measurements, and record them in a sequential order according to the time tags. The local PDCs send the synchrophasor data to a higher level PDC located at a central control station through a wide area network. This central PDC provides time-aligned data for specific applications, long-term archives, and regional PDCs.

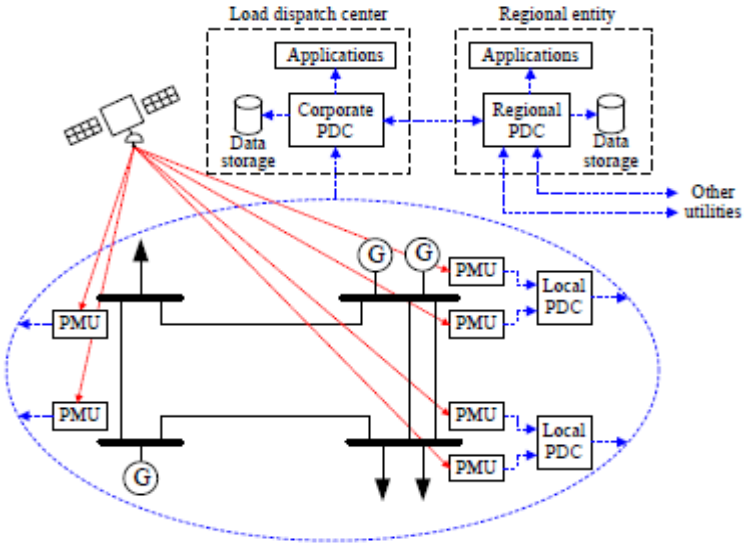

Figure 1.1 Components of a Wide Area Measurement system

1.1.2 Synchrophasor Applications

Various synchrophasor applications are found in the literature. The main synchrophasor application includes:

Monitoring applications: The measurements obtained from PMUs can be used to improve the situation awareness of the system operators so that they can identify the system abnormalities and take preventive actions to avoid undesirable system states. Various monitoring application includes voltage, frequency, and phase angle monitoring, small signal oscillations and damping monitoring, transmission line parameter monitoring, voltage stability monitoring, event detection, and fault location.

Power congestion management: These applications help to manage the economic load dispatch without violating the power transfer capacity with the help of real-time measurements.

Management of active distribution networks: As the popularity of distributed generation (DG) is increasing, PMUs are one of the best options to monitor and control the operation of distribution networks with DGs.

Offline Analysis: Synchrophasor technology can be used for offline power system studies. The measurements collected using the PMUs are processed even months after collecting the information for further analysis of the system characteristics. This enables the possibility of using the synchrophasor measurements for validating power system dynamic models. Post-event analysis can be conducted for determining the operating limits of the power system and for load characterization.

Power system protection and control applications: Synchrophasor measurements combined with secure communication channels enables the detection of abnormal operating conditions and predicting when there is a risk of the system becoming unstable due to phenomena such as voltage, frequency, oscillatory, or rotor angle instability. Synchrophasor measurement based wide are system protection schemes, based on such predictions, determine and activate suitable emergency control actions to avoid or reduce the potential instabilities. For example, the voltage, current and phase angle measurements obtained from the PMUs can be used as inputs for detecting the transient instability of a power system. Transient stability prediction assisted with the phasor measurements has proven to be faster when compared to other detection methods [3][4].

1.1.3 Special Protection Schemes/Remedial Action Schemes

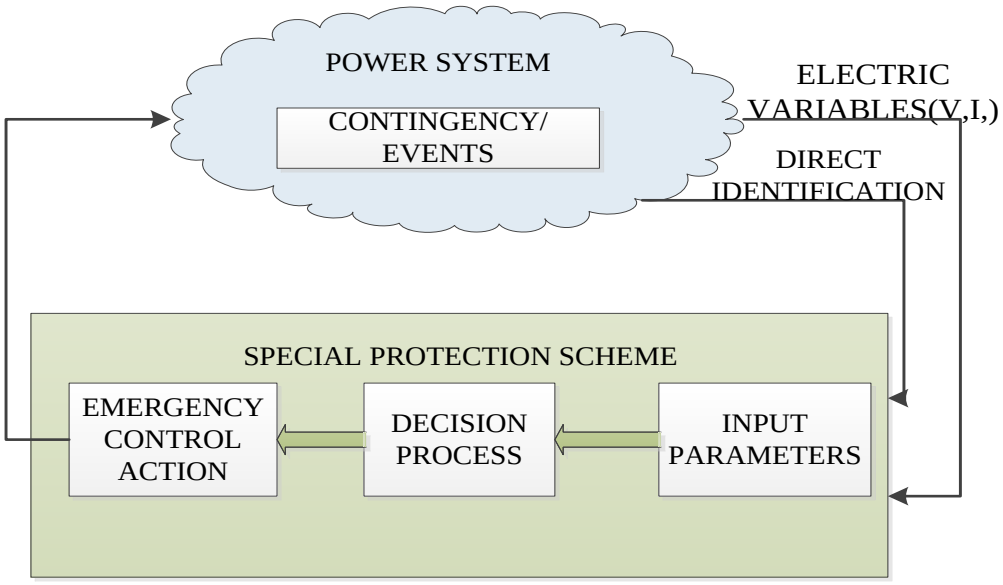

Figure 1.2 Structure of a Remedial Action Scheme (adapted from [5])

Special protection schemes (SPSs), which are also referred to as remedial action schemes (RASs), are designed to detect abnormal or predetermined system conditions and take corrective actions other than or in addition to the isolation of faulted components to maintain system reliability. Based on the method used for detecting abnormal or critical operating conditions, special protection schemes can be categorized as event-based special protection schemes and response based special protection schemes.

Event-based SPSs are designed to operate upon the recognition of a combination of events such as the loss of more than one line. An event-based SPS operates like an open loop control which directly detects the contingency and initiates sudden control action such as generator rejection, load shedding, system islanding, turbine fast valve control, etc. in response to the event.

Response-based SPSs act on the measured electrical variables such as voltages, currents, frequency, and phase angles. They initiate protective actions when a contingency causes the measured values to hit a trigger level or other defined condition. Response-based schemes monitor system response during disturbances and incorporate a closed-loop process to react to the evolving system conditions. The two most common response-based types of SPSs are under-frequency load shedding and under-voltage load shedding.

1.2 Motivation Behind Research

Although power systems are reliable, and multiple simultaneous faults and failures are rare, they are not completely impervious to major events that can lead to power blackouts. Blackouts leave people without power and are associated with large economic consequences. Many power systems demand special protection systems, which are designed to address wide area problems that cannot be completely identified and remedied by the conventional power system protection systems. These problems are often specific to the power system concerned, as well are the potential solutions. Special protection systems are usually designed during the planning stages and are generally not adaptive to new situations. Due to the increasing need for system expansion and the recurring contingencies that lead to unstable operating conditions, there is a need for adaptive emergency control and protection methods, which can be applied to prevent total blackout of the power grid.

Although there is potential for using synchrophasor measurement technology in designing response based special protection systems operating in a closed loop manner, there are only a few applications in practical use. According to a recent CIGRE report on PMU

applications [6], the majority of synchrophasor applications in practical use are monitoring applications. Therefore, there is a need for developing useful and practically applicable closed loop control and protection applications to utilize wide area synchrophasor measurements.

1.3 Objectives and Contributions

The main goal of this research is to explore the possibilities of using wide area synchrophasor measurements for designing response based remedial action schemes. The two applications investigated in this thesis are a measurement-based overload prevention scheme and an intelligent controlled islanding scheme for a power system subjected to severe rotor angle instability.

The objective of the first application is to prevent the transmission lines and transformers being overloaded after the tripping of a major transmission line used for power export. The power system example considered receives power through several HVdc links and therefore the emergency control action considered is a rapid reduction of power injected from the HVdc links. The contribution of the research is a method to determine the amount of HVdc power reduction in a way that minimizes the total power reduction while avoiding violation of emergency and continuous ratings of the affected transmission lines and transformers. The proposed method is designed and demonstrated with the help of PSS/E power system dynamic simulation software.

The objective of the second application is to perform controlled islanding in order to prevent total system collapse due to an impending out-of-step operation of generators consequent to a major fault event. The power system considered for this application is a

predominantly ac system, and controlled islanding is a last resort action usually taken when the system cannot be saved by any other means. The contributions of the research include an algorithm to determine the number of islands and the boundaries of the islands based on the phase angle differences measured using PMUs and the relative electrical distances (REDs) computed using the system parameters. The method also includes a frequency-based generator and load tripping scheme to ensure the post-islanding power balance in the individual islands. The proposed method is designed and demonstrated with the help of TSAT dynamic simulation software.

1.4 Thesis Organization

The rest of the thesis is structured as follows:

Chapter 2 includes a literature review, which discusses the power system stability, operating states and several special protection schemes in the literature that includes; frequency-based generator and load tripping, control of HVdc and FACTS devices, and Controlled islanding.

Chapter 3 presents the development of a measurement based remedial action scheme for overload protection in the Manitoba Hydro grid. The development of the methodology and its verification under different fault scenarios in the system are provided in this chapter.

Chapter 4 proposes an intelligent controlled islanding scheme for transient stability control. Different components in the scheme that include post contingency stability prediction, coherent generator groups recognition, assignment of loads to feasible islands, and post-islanding load and generator-tripping scheme are described. The chapter also presents application example and simulation results.

Chapter 5 summarizes the proposed emergency control schemes in this thesis and presents the research conclusions and the contributions. Some suggestions for future research is also provided in this chapter.

Chapter 2

Literature Survey

This chapter provides the essential background related to power system stability and the different operating states in the power system. A brief study on the Special Protection Schemes is conducted as a part of this review. Several special protection techniques in practice such as under-frequency load shedding, generator tripping, control islanding, power electronic devices etc. are explained in detail. Different control islanding methods in the literature are discussed as well in this section. Examples of some existing Special Protection Schemes are provided in the conclusion.

2.1 Power System Stability

Power System Stability is referred to the capability of a power system to return to a stable operating state following a contingency which can result in abnormal operation of the system. The three main subdivisions of power system stability are rotor angle stability, frequency stability and voltage stability[7].

Power systems being nonlinear in nature, the system stability is mainly affected by the extremity of the contingency along with the prevailing initial conditions of the network.

According to that, angular and voltage stability are divided as small and large-disturbance stability. The power system stability classifications are shown in Figure **2.1**.

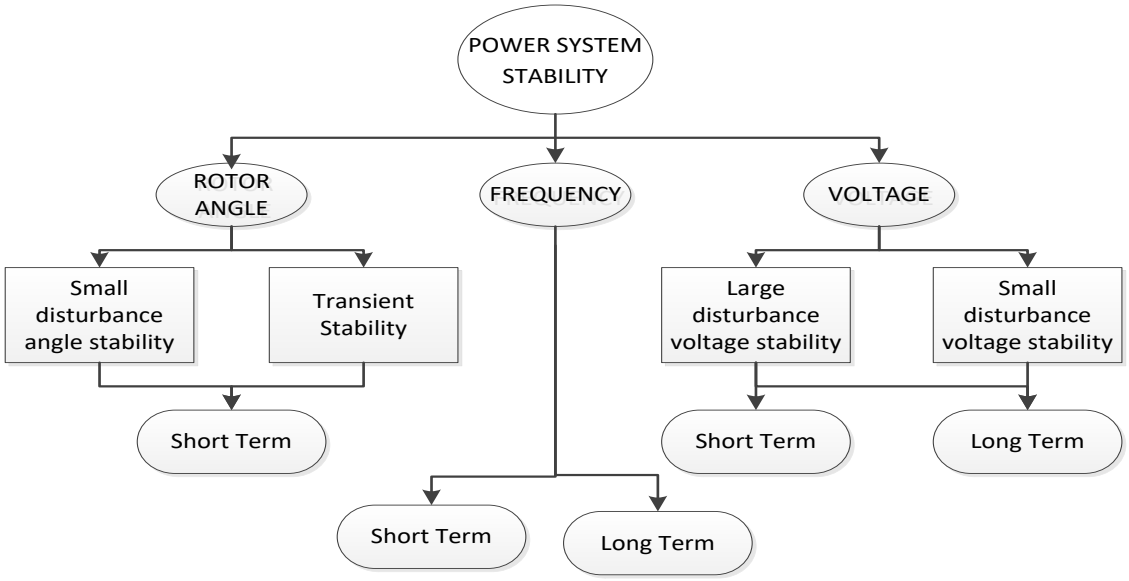

Figure 2.1 Power system stability classification

2.2 Different Operating States of the Power System

Proper knowledge about the power system state of operation is necessary for understanding the importance of emergency control schemes in system protection. The first categorization of the operating states of the power system was developed by DyLiacco in 1967. In DyLiacco's classification, the power system operating states are categorized as normal, emergency and restorative state. Fink and Carlsen introduced further extensions to the system stages as normal, alert, emergency, in extremis, and restorative in 1978. The power system can be generally described using differential equations with equality and inequality constraints. The equality constraints correspond to the generation and load balance whereas the inequality constraints identify the equipment capacity range, which includes the voltage and the power limits. Under the normal operating condition, the system will be in safe

operation range satisfying both equality and inequality constraints. Enough security margin for operation will be there under such conditions so that they will remain in the normal stage of operation following to a single contingency. The security margin can also be described as a range between the stable and unstable regions of operation. The system will move towards the alert state with the decrease in the stable operation margin while keeping the constraints under the safe level of operation. If the system is subjected to some abnormalities while in the alert state, it can cause the overloading of the power system network elements including the transmission lines, generators, and transformers leading the power system to step into the emergency state depending on the extremity of the contingency. The classification of the power system operating states is illustrated in Figure **2.2**.

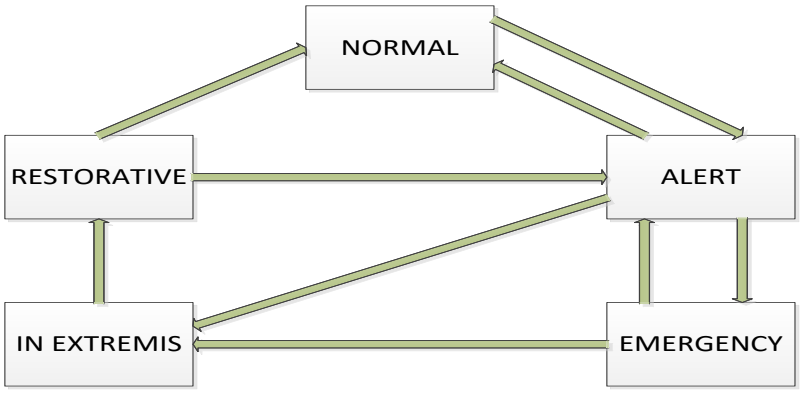

Figure 2.2 Classification of the power system states

Special protection schemes are initiated during the emergency state of operation. Emergency control actions are required to prevent the system from moving to the extremis state which can lead to a total power blackout. The network will transition to the restorative state right after the control action is implemented to recover the system from the abnormalities. Here in this thesis special protection schemes are proposed to implement in

the emergency state of operation to restore a power system subjected to overloading and transient instability.

2.3 Wide Area Measurement-Based Emergency Control

Power system emergency control operations can be continuous or discontinuous in nature as illustrated in Figure **2.3**. Issues related to angular stability can be eliminated using continuous control operations. For example, appropriate feedback controllers can be used for the continuous control of system variables like the excitation current of a generator, Flexible Alternating Current Transmission System(FACTS) device output etc. However, sudden system changes should be initiated for protecting the power network following transient instability, equipment overloading, and cascaded tripping. Such operations include the load shedding, reactive power source switching, generator tripping/rescheduling, HVdc control, system separation, etc., and are temporary in nature. These kinds of SPSs are termed as discontinuous controllers. Most of the designed SPSs operate for predefined set of events in the system and therefore, they are also termed as event-based emergency control schemes. On the other hand, emergency control using wide area measurement technology, detect abnormal system conditions by monitoring the changes in network variables and initiate control operations of discontinuous nature in response to observed changes. The emergency control scheme proposed in this thesis belongs to the above kind of control operations also termed as a response/measurement-based emergency control.

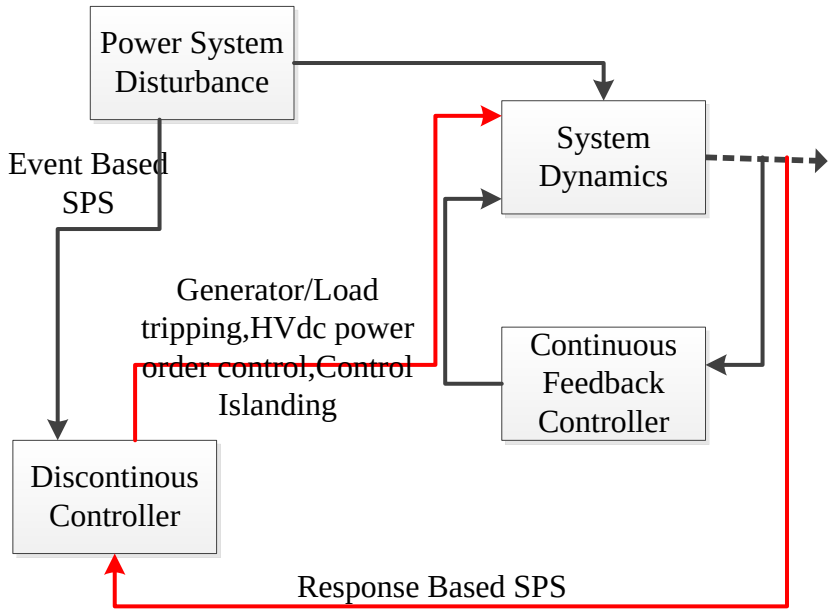

Figure 2.3 Power system stability controls (adapted from [8])

2.4 Special Protection Systems

Special protection systems, which are also termed as Remedial Action Schemes(RAS), are widely used in modern power transmission systems. RASs are emergency control schemes which are designed to protect the power system from a critical set of abnormalities by proper detection and fast initiation of control action thereby restoring the system stability. Generally, the emergency control actions that are initiated after the system steps into instability are tripping of transmission lines, generator rescheduling, HVdc power flow control, load tripping and intentional controlled islanding. The most common emergency control options in the literature are discussed in detail below.

2.4.1 Under Frequency Load Shedding

Under frequency load shedding (UFLS) is implemented when power system frequency declines due to lack of active-power generation. If emergency control actions are not initiated to remedy the situations of under-frequency, the frequency level will further deteriorate. If the under-frequency situation is prolonged for a considerable amount of time, it will damage the generating units. The generator protection devices will trip the affected generating units to protect them from damaging conditions, but it will result in a further increase in generation-load imbalance. In such situations, it is important to implement a scheduled load tripping pattern when the frequency goes below a certain threshold level. The primary frequency control will help in reducing the frequency imbalance to an extent through the governor control if the frequency deviation is of a small level. The emergency control schemes based on frequency variations helps in regulating the frequency variations to a certain extent providing sufficient time for the governor control to come into action [9].In literature, a number of strategies have been proposed for Under frequency load shedding. A conventional method like in [10] is the pioneer generation of UFLS schemes. The first step in this method is to identify the most critical event that will result in the generator tripping and calculate the maximum rate of frequency decline. Following that the amount of load shedding required to restore the frequency deviation and keep the system frequency within a permissible range of operation is determined. The total number of load shedding steps to be implemented and the amount of load to be curtailed under each step of operation is calculated through intense offline studies on the particular system. Identification of the critical contingency and designing a load shedding scheme is a tough task as it is system dependent. In the conventional method,

a certain amount of load is tripped in every step without considering the power imbalance. This increases the chance of over tripping the load without considering the frequency recovery following each stage of operation.

Adaptive UFLS methods proposed in [11][12][13] are designed to minimize the drawbacks of the conventional schemes. Forecasting the frequency deviation using heuristic optimization algorithms like Particle Swam Optimisation(PSO) is used in [11] to help determining the maximum frequency change in the system subjected to a fault and designing a load shedding scheme considering the predicted frequency deviation. In [14], a distributed under-frequency load shedding and load restoration scheme that exploits frequency and change in frequency rate measurements produced by PMUs as detectors of a large contingency is proposed. This method exploits the advantage of PMU's high reporting rates, remarkable measurement accuracy as well as time synchronization for the real-time implementation.

2.4.2 Over Frequency Generator Tripping

The load shedding procedure alone cannot guarantee the total system frequency recovery. When the load demand decreases, excess generation must be adjusted to restore the powe imbalance. Over-frequency generator tripping/rescheduling is an emergency control operation implemented to avoid frequency overshoots and assure its stability. The over frequency emergency control actions help in restoring the system frequency to an acceptable range by tripping the excess generation in several steps. This operation is repeated many times until the system generation balance out the total load demand.

Governor controls can also enable generation rescheduling to some extent, but its response is slow and limited.

An over-frequency generator tripping scheme is mainly designed based on the understanding of the system and through extensive validations using offline studies. These are considered to be system dependent and can vary with the power network expansion. A hybrid method is proposed in [15] which uses lookup tables developed offline for determining the generator tripping pattern. The information about the fault location, fault type, and the fault duration are collected online and provided as input to the lookup table for determining the generators to be shed. Look-up tables reduce the decision time of implementation.

Load shedding and generator tripping can also be performed by the respective actions of under and over-frequency relays by sequentially disconnecting discrete blocks of load or generation. Reference [16] introduces a generator tripping action regulated by the over-frequency relays. In the above method, the over-frequency relays are adjusted with a frequency deviation action level and time delay. After islanding, the system frequency violation is picked up by the relays and the generators are shedding according to the pre-set priority list. Proper relay coordination can help to avoid the excessive shedding of generators and thereby maintaining the island's frequency within an acceptable range.

Another method for over frequency generator tripping is described in [17]. It uses a trajectory sensitivity analysis method for identifying the critical generators to be tripped for the emergency at hand. The proposed method directly utilizes the state variable trajectories generated by time-domain simulation during stability assessment period for identifying the generators. Furthermore, a pattern search method is implemented among

the candidate generators to derive the optimal control strategy. The above method takes less computational time as both trajectory sensitivity analysis and pattern search are solved in parallel.

2.4.3 HVdc and FACT Devices

High voltage dc transmission (HVdc) and flexible ac transmission system (FACTS), technologies developed as a result of advancements in power electronics has enormous application in the power transmission and distribution industry. HVdc links can be used for interconnecting large power systems which cannot be linked through ac lines due to their different operational frequency. Back-to-back stations or long-distance transmissions carrying a large amount of power from the generating stations through overhead transmission lines or submarine cables are the examples. HVdc transmission links with increased power transfer capability are gaining more popularity because of their fast controllability of power compared to the ac lines. Moreover, the ability of HVdc links to transmit the power independent of the ac system conditions and requirement of no common frequency level makes HVdc an efficient option to rectify the problems such as power flow control and transmission line overloading [18].

Incorporating the FACTS technologies to the ac lines can help ac power flow control to exploit the transmission capacity to their maximum limit without sacrificing the system reliability. FACTS devices can be utilized to improve real power transfer capability in the lines, prevent sub-synchronous resonance (SSR) and damp oscillations. FACTS devices can be used as a part of a special protection system as they also provide fast controllability of real and/or reactive power.

FACTS devices are considered to be more economical and a fast solution to mitigate the overload and voltage violations in the system even though they may introduce smaller disturbance to the system. FACTS implementation can be divided into two stages: in the first stage, the operational needs of the FACTS control in the system is identified and the second stage deals with designing a control algorithm to satisfy the goals as described in [19]. The FACTS controllers/devices that have been developed for various applications include Static Var Compensator (SVC), Static Synchronous Compensator (STATCOM), Thyristor-Controlled Series Capacitor (TCSC), Static Synchronous Series Compensator (SSSC) and Unified Power Flow Controller (UPFC). FACT devices can be connected at decided locations in the power system in series, shunt or combination of both. While SVC and STATCOM are shunt connected, TCSC and SSSC are connected in series. UPFC are connected in both shunt and series configuration [20]. Among the FACTS devices, STATCOMs are connected to increase the power system transient stability limits. Along with the voltage stability increase, STATCOM can also provide power flow controllability in a network [21]. New research focussing on the application of STATCOM includes the transient stability and power oscillation damping performed on several IEEE test systems. TCSC provides fast control of line impedance if required to adjust the load flow, provide dynamic stability and for damping the power oscillations. SSSC emulates a variable inductor or capacitor in series with a transmission line and it imitates inductive or capacitive reactance to maintain effective line reactance [22].UPFC can provide power flow control through fast and efficient control of voltage, transmission line impedance, and phase angle as proposed in [21]. In general, we can conclude that FACTS and HVdc can

be used for power system stability control by effectively managing the network congestion and avoid complete blackouts.

2.4.4 Controlled Islanding

Large disturbances such as loss of major transmission line or major power plants have a high probability to propagate over the entire system causing out-of-step situations between different generator groups. Under such situations, it is essential to split the system into different islands to prevent an entire system failure. This operation can be performed in an intelligent manner considering the system conditions and by properly splitting of the system. Islands, formed by intentional controlled islanding of a power system are observed to be more stable and reliable than naturally isolated islands created due to the cascaded tripping of transmission lines following the occurrence of faults. Controlled islanding can be considered to be an effective method for system restoration as it aims in providing a balance between load and generation in the islands. Fast implementation of controlled islanding following a large disturbance can help in ensuring the post-disturbance stability of the power system.

Several works have been done in the area of islanding based on the system parameters, and network features. The controlled islanding techniques reported in the literature can be categorized under four major groups: slow coherency methods, graph theory-based methods, minimal cut set identification methods, and spectral partitioning/clustering.

System islanding based on generator coherency helps in arranging the coherent group of generators on the same island. Slow coherency-based controlled islanding procedure follows two main steps of operation. In the first step, generator clustering based on slow

coherency is conducted and in the second stage, the minimal cutset for separating the generator groups are identified using different search methods [23] [24]. Slow coherency-based methods are effective in maintaining the generator load balance and provide better transient performance after islanding. Slow coherency can be used to determine the weak links in the network and thereby help in identifying the lines to be tripped to prevent the propagation of the slow dynamics as in [25]. A coherent group identification technique based on hierarchical clustering algorithm is explained in [26]. The method helps to divide the power network into a minimum number of islands and provides power balance in separated islands for maintaining the system stability. Slow coherency based online approach for system separation is proposed in [27] where the leading and lagging group of generators for system splitting are identified based on the rotor angle variation of the generators.

Graphical representation of the power grid will reduce the difficulty in representing large power network. The power system is a complex network consisting of buses which are interconnected through transmission lines. They include generator and load buses of different power limits. Power flow through the transmission lines is directional in nature. In general, a power system network can be considered as a directional graph with certain values at the vertices. Several methods incorporating the features of graph theory and minimal cut-set representation are available in the literature for efficient islanding of a power system. The total generation and power flows through the transmission lines in the network can be obtained from power flow analysis. After islanding the system by tripping certain transmission lines, we can calculate the power generation-demand difference in the islands as the sum of the power flowing through the tripped lines (assuming the losses are

nil). In order to minimize the power imbalance due to islanding, the best option is to trip the lines carrying the minimum amount of power for the system splitting. Using this idea, the system separation problem can be converted as a minimal cut-set problem where the minimum cutset with minimum net-flow is identified for system islanding. A controlled islanding approach using minimal cutset with the minimum net flow is proposed in [23]. [8] proposes a two-phase method for the real-time system separation. The large power network is reduced to a small space with the help of ordered binary decision diagram (OBDD)-based algorithm at first and a splitting strategy based on power-flow measurement is implemented for the system separation. [28] shows the application of graph theory in partitioning of huge network and system splitting.

The latest research using graph theory techniques is based on spectral partitioning which is widely used in image processing, data mining, and machine learning tools. Spectral clustering techniques are more advanced than the traditional clustering algorithms in providing better solutions and it is similar to the minimal cutset problems. A spectral partitioning controlled islanding strategy is proposed in [29].It is based on the eigenvalue analysis performed on the dynamic graphs which gives an idea about the structure of the power system. Spectral clustering correlated with the graph theory will help in identifying the islanding boundaries in a network. This method is considered to be simpler and requires less computation time.

2.4.5 Examples of SPS in Literature

Some of the existing Special Protection Schemes implemented by different utilities around the world are discussed in this part of the review. A wide area protection scheme against

out-of-step operation was implemented by Tokyo Electric Power Co. (TEPCO). It used a prediction technique for determining the phase angle difference between groups of generators using the previous measurements. When the predicted phase angle difference is higher than a pre-set threshold value an emergency system separation is performed [30]. A control islanding scheme was proposed for the Manitoba Hydro system based on the normal form method [31]; for determining the coherent groups of generators after the system is subjected to some abnormalities. Islanding operation is conducted after identifying the boundaries separating the selected group of generators [31]. Post islanding stability of the system is attained by the rejection of loads and tripping the excess generation.

The Hydro-Quebec SPS described in [32] implements a generation rejection and load shedding scheme against cascaded line outages or bypassing of series compensated capacitor banks in key locations. As the power systems across the world become more heavily loaded, a number of countries are turning to SPS as a more economical way of increasing transmission capacity. An example from Chile is given in [33]. It has been designed to free congestion for cheaper power transmission.

A special protection scheme with two-stage operation is designed for the Taiwan Power Company [34]. The control scheme is designed to prevent system blackouts followed by transient instability. The entire SIPS installation comprises two stages. A generator tripping scheme for N-3 contingency is designed as a first stage operation. The second stage operation is based on generator tripping, load rejection, and bus-tie switching for preventing all extreme contingencies which can be considered as a modification to the first stage operation.

To conclude, many utilities have implemented special protection schemes which are complex in nature for real-time implementation. There is a potential for developing simpler and effective methods incorporating new technologies like phasor measurements. The main focus of this research is to present novel emergency control schemes based on wide area measurement technology for protection of power systems from instabilities and abnormal conditions.

2.5 Concluding Remarks

This chapter presented a brief review of emergency control schemes. Most emergency control actions are discontinuous in nature.Various emergency control actions commonly implemented in power systems were discussed in detail. These include load shedding, generator tripping and re-scheduling, HVdc power order control, FACT devices control, and system separation.

The final part of this review briefly discussed various controlled islanding methods that have been developed. Much of the work relies on offline analysis which is not truly adaptive. This is still an on-going topic of research, as much of the previous developments can be computationally heavy or require offline analysis which then needs to be updated for every new operating point. The chapter concludes with a discussion on the SPS designs reported in literature.

Chapter 3

Wide Area Synchrophasor Measurement-based Remedial Action Scheme for Overload Prevention

In this chapter, a measurement based Remedial Action Scheme (RAS) for Manitoba Hydro Grid with multiple HVdc infeeds and multiple HVac interconnections is proposed to prevent overloading issues that occur when a tie-line exporting power is tripped. The proposed scheme includes three stages. The first stage involves identification of the events, the second stage checks for thermal limit violations, and the third stage determines the emergency control action. The remedial action considered is the fast reduction of HVdc power by modifying the converter set points. The proposed Remedial Action Scheme prevents cascaded tripping and ensures maximum power exports under a given contingency situation. Simulation results are presented to demonstrate the effectiveness of the proposed method.

3.1 Background and Problem Description

HVdc transmission plays an important role in the modern power system by delivering bulk power over long distances and facilitating interconnection between asynchronously operated ac systems [35]. Manitoba Hydro grid in Manitoba, Canada, is an example of a power system where two asynchronously operated ac systems are interconnected with multiple HVdc links transmitting bulk power terminating in close proximity. In this section, the relevant geographical features and the structure of the selected test system; Manitoba Hydro Grid, including the tie-line interconnections to the neighboring provinces are explained. The section concludes with a detailed description about the problems identified in the selected test system.

3.1.1 General Features of Manitoba Hydro Power System

Electricity generation in Manitoba is primarily based on hydro power plants (over 98%). Major power generation is contributed by three generating stations: Kettle, Long Spruce and Limestone located on the Nelson River in the north-end of Manitoba. These generating stations are known as Northern Collector System (NCS) and operates isolated from the main ac grid. Power generated from the NCS is delivered to the load centers in the south through three HVdc lines: Bi-pole I, Bi-pole II, and Bi-pole III. Bi-pole III is a new addition to the Manitoba grid commissioned in 2018 to improve system reliability and power transmission capacity. Bi-pole I and Bi-pole II are terminated at the Dorsey converter station and Bi-pole III is terminated at the Riel convertor station, both close to the Winnipeg area.

The loads at the north side are supplied by the other generating units, located at Kelsey, Jenpeg, and Grand Rapids. The remaining power from these small generating units is delivered to the southern load points via 230 kV and 138 kV ac transmission lines operating synchronously to the main ac grid which constitutes the Northern ac System. Moreover, small hydro generating stations on River Winnipeg located at the southern region of Manitoba connects the ac grid by 115 kV lines. The geographical map of the MH grid is shown in Figure **3.1**.

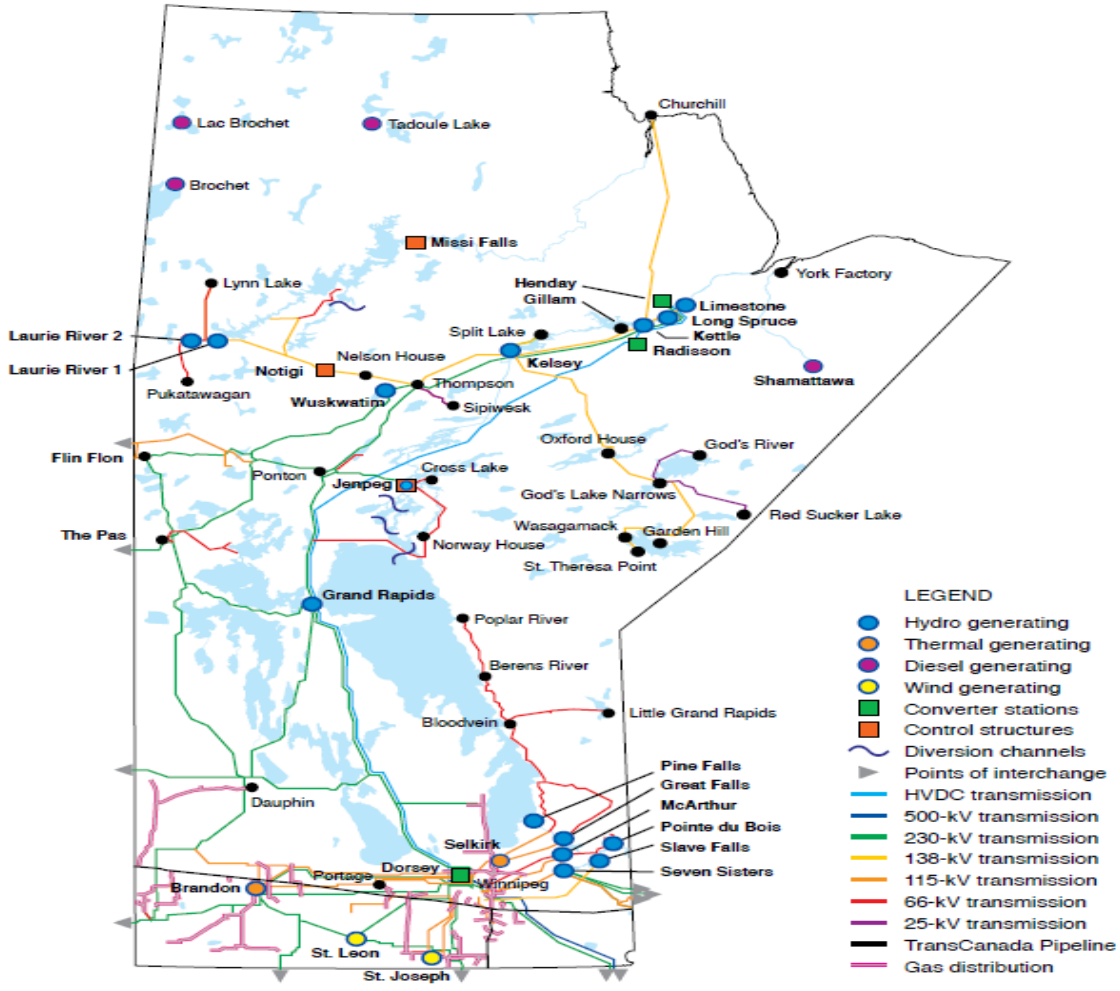

Figure 3.1 Geographical representation of Manitoba Hydro-Grid

The large inertia of the generating units in the NCS which operates isolated from the main ac grid, does not account for the system stability. However, these isolated generating units are allowed to operate over a broad range of frequency as they do not supply any load directly. These features of the generators in the NCS assist the system in tolerating sudden large power variations in the HVdc links. This unique feature of the Manitoba grid can be used for implementing control actions in the form of rapid changes in HVdc power injected to the main ac grid.

3.1.2 Interconnections with Other Power Utilities

The power delivered through HVdc links are exported to the USA and other provinces via multiple HVac lines. The Manitoba Hydro southern ac system is interconnected with Saskatchewan to the west with four 230 kV ac lines and with Ontario to the east via two 230 kV ac lines. These two long lines are supplied via phase shifting transformers [36]. Manitoba power system is interconnected to Midwest Independent System Operator (MISO), USA, in the South end through 500 kV and 230 kV tie-lines. These interconnections and dc infeeds are schematically shown in Figure **3.2**.

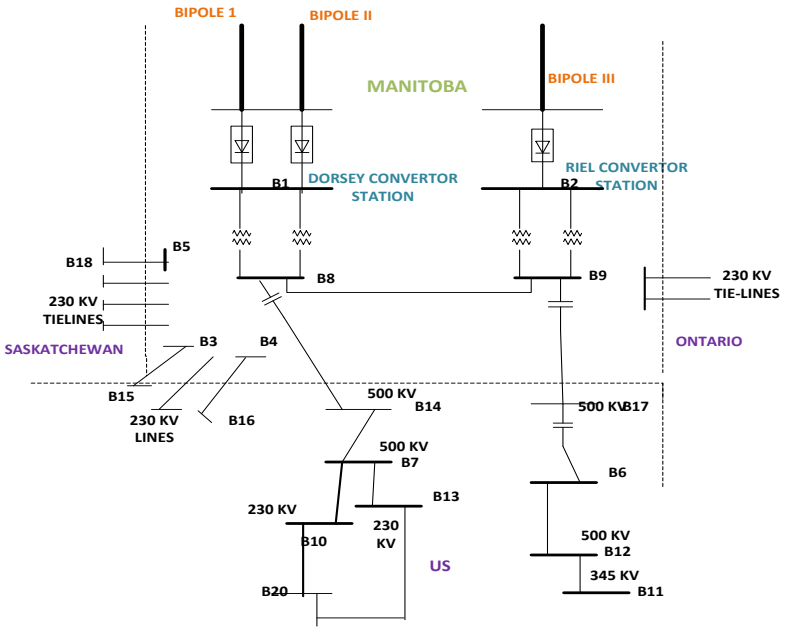

Figure 3.2.Manitoba grid and interconnections

3.1.3 Problem Description

Manitoba Hydro exports its surplus generation to the neighboring utilities, mainly to the USA. The total exports could exceed 3000 MW at peak conditions. Under high export conditions, if any one of the tie-lines connecting to US region is tripped, the excess power will cause overloading of the remaining tie-lines, some transformers and some remote lines in the Manitoba and the USA. The absence of remedial action during such conditions will result in cascaded tripping of all the remaining ties between Manitoba Hydro system and the neighboring provinces, resulting in the total isolation of the Manitoba Hydro system. Manitoba Hydro currently employs an event based remedial action scheme, which quickly act to reduce the excess power by reducing the power coming through the HVdc links to prevent the system overloading (Koch, Krüger, & Tenbohlen, 2009). This event-based RAS monitors various network elements in the power system via telecommunication links

for occurrence of pre-identified contingencies and initiate the control action if a contingency occurs [37]. Changes in the system status help in identifying the contingencies and the RAS has logic designed to identify a particular contingency based on the status signals [38]. The amount of HVdc power reduction is determined as a percentage of the pre-fault power flow in the affected lines, and this percentage amount is predetermined based on the system studies. The RAS does not take into account the actual loading on the affected lines, and therefore the reduction in power may be more than that is required. This could translate into loss of power export revenues.

This thesis investigates the possibility of developing a measurement-based overload prevention approach which reduces only the minimum amount of dc power that needs to be curtailed to avoid overloading. The intention is to utilize the fast power controllability of the HVdc converters as in the existing RAS while using the synchrophasor measurements [39] from selected locations to detect overloading and corrective actions. As major outages causing the system overloading are due to tripping of the interconnecting lines in the US region, the events selected for implementing the control scheme mainly focussed around the interconnection to US. The scheme can be implemented using the system-wide synchrophasor communication infrastructure or using dedicated communication channels, depending on the reliability requirements.

Addition of new Bipole III HVdc scheme and the proposed new 500 kV HVac tie line to the USA will require redesigning of the current RAS. This is a good opportunity to examine the possibility of using a measurement-based scheme. Often, a RAS becomes more complex after system expansions; although the opposite may also happen if the system modifications help to alleviate the issues dealt with by the RAS.

3.2 Existing Remedial Action Scheme

The existing HVdc reduction controller in the Manitoba grid consists of three main parts; a tie-line monitoring system, a reduction controller and an allocator. The structure of the existing RAS design is shown in Figure **3.3**.

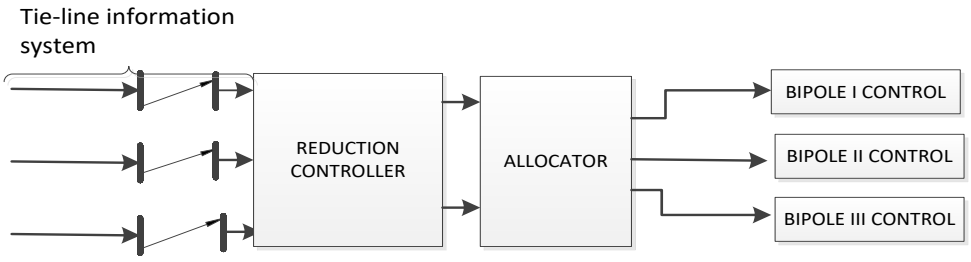

Figure 3.3 Existing remedial action scheme in Manitoba Hydro system

Tie-line monitoring system monitors the breaker status signals of all the tie-lines. Measurement units are also placed on all the tie-lines for detecting the power flow. The line trip signals and the power flow of all the lines are transferred to reduction controllers located at Dorsey converter station using communication channels. Following a tie-line tripping event, when a trip signal is received from the faulted line to the reduction controller, the controller calculates the amount of power to be reduced. The reduction amount is equal to the power transmitted through the tripped line prior to the fault with an additional 15% to account for the losses in the HVdc system since the HVdc power orders are referred to the rectifiers. The controller will send the calculated power reduction amount to the allocators. The function of the allocator is to distribute the reduction amount among the Bipoles based on certain calculations. The reduction amount calculated by the allocator is sent to individual bipole controls and the system control center. The allocator

also generates a 'Trigger' signal to the HVdc controls and the system control center. In order to obtain high redundancy, the tie-line information system is duplicated, i.e. two communication channels are used for carrying the same information signal. The reduction controller and allocator are also triplicated to achieve very high-reliability.

3.3 Structure of the Proposed WAC System

The components of the remedial action scheme proposed for determining the HVdc power order reduction is illustrated in Figure **3.4**. Near real-time synchrophasor measurements of specific bus voltages and selected line currents are delivered to a phasor data concentrator, which provides the time aligned aggregated data to the proposed RAS. The HVdc power reduction controller consists of three functional stages:

(i) Event detection mechanism,

(ii) Overload violations identification, and

(iii) Determination of emergency HVdc power reduction amounts.

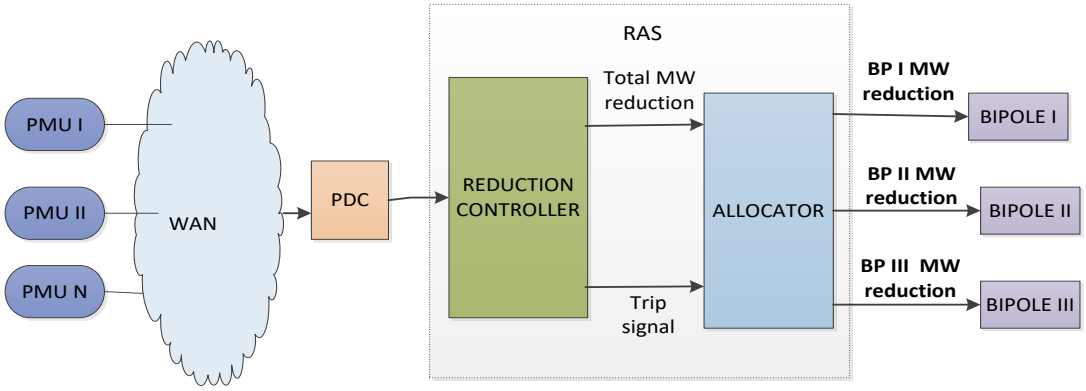

Figure 3.4. Components of PMU based remedial action scheme

Using the synchrophasor measurements, RAS continuously monitors the power flow through some selected branches. A disturbance detector detects the occurrence of a

disturbance and identifies the element that is removed from the system. If the RAS observes overloading of any of the monitored branches, it calculates the amount of dc power to reduce to bring the line flows below their normal ratings. The amount of HVdc reduction is computed using the sensitivity of power flow in a particular line to the reduction in HVdc power, which will be explained in Section 3.4.4. The estimated amount of HVdc power to be reduced is input to the allocator to divide the amount among the three HVdc inverter stations. The operation of the proposed scheme is explained in Figure **3.5**.

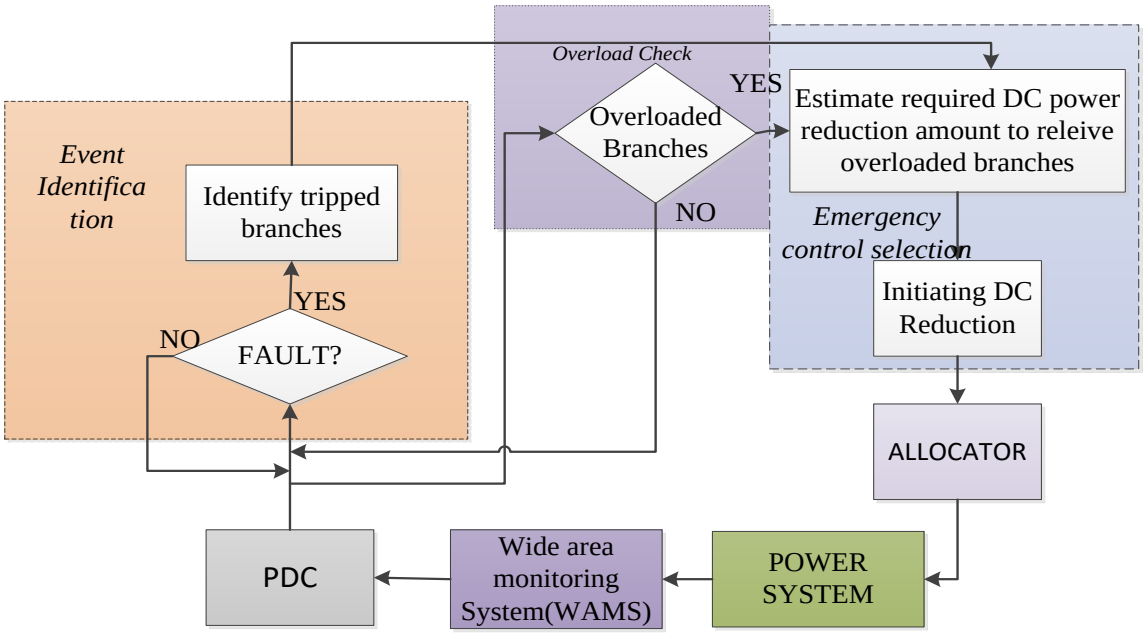

Figure 3.5. Functional structure of the proposed measurement based RAS

3.4 RAS Design Methodology

The proposed RAS is discussed in this section. The PMU location setting, the faulty event detection technique and the power order calculation for the contingencies is explained in detail.

3.4.1 PMU Location

Considering the general topology of the Manitoba Hydro power system, and knowledge acquired from load flow and stability studies, eight locations were selected for installing phasor measurement units (PMUs) for monitoring of overload conditions. As the RAS is implemented for preventing overloading of HVac lines of the interconnected system, several PMUs are installed on the locations in the US side. This is important, as some of the lines that are subjected to overloading are inside the US region. It is assumed that the synchrophasor network covers all selected locations. The PMU locations are listed below in Table **3.1**. The PMUs measure bus voltages and selected branch currents, so that power flow in these branches can be calculated. Power calculations can be done at the PMU level and transmit with the synchrophasor data frame as an analog quantity or computed at the controller using the voltage and current phasors.

Table 3.1 Selected PMU Locations

PMU Location	Nominal Voltage	Features
BUS 3	230	Line monitoring
BUS 4	230	Line monitoring
BUS 6	500	Line monitoring
BUS 7	230	Line monitoring
BUS 8	500	Line monitoring
BUS 9	500	Line monitoring
BUS 12	345	Line monitoring
BUS 5	230	Line monitoring

3.4.2 Event Detection

Although the proposed measurement-based RAS responds only when the overload conditions are detected, the method of determining the amount of HVdc power reduction depends on the contingency. There is a set of pre-identified events that cause overload situations. These include tripping of 500 kV and 230 kV lines and the loss of transformers in the US and Manitoba region. The contingency corresponding to the fault condition can be identified by observing the relevant branch power flows using the algorithm presented in the flowchart of Figure **3.6.**

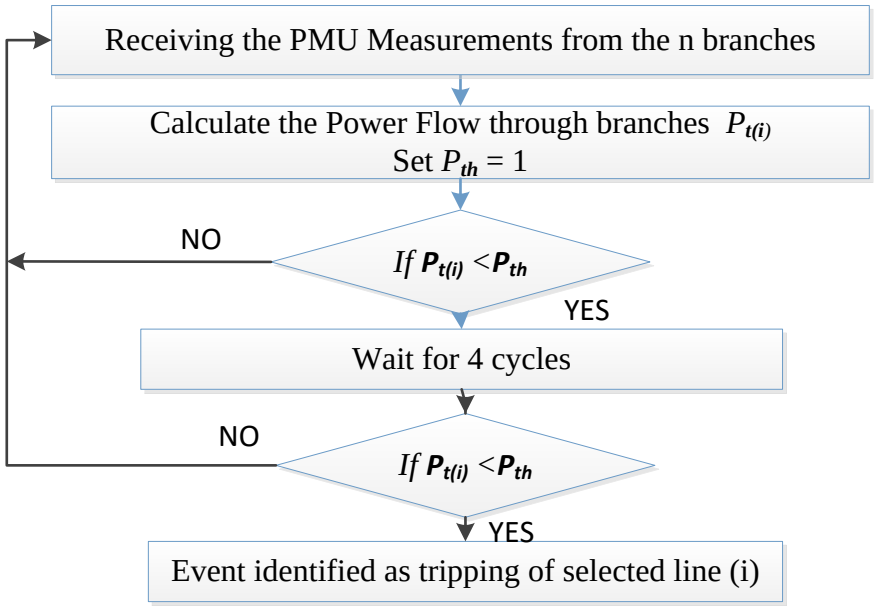

Figure 3.6. Event detection and recognition logic

The line outages can be determined when the power flow through the lines suddenly drops below a pre-set threshold power for a reasonable time. Here the threshold magnitude of power is set as 1 MW and the power flow variation is observed for 4 cycles to identify it as a permanent change in the line state before initiating the trip signal. When the line is tripped, a trip signal is initiated from the particular location which helps in identifying the

event. In the disturbance detection logic in Figure **3.6**, $P_{t(i)}$ is the power flow through the i^{th} branch and P_{th} is the threshold power, which is set to 1 MW in the logic.

The controller calculates the steady state power flow through the line by computing the average over a sliding window, during the pre-contingency period. The dc power reduction scheme is implemented only after an overload violation is observed and an event or contingency that leading to tripping of one of the monitored line is identified. The normal and emergency MVA ratings of the critical lines are provided to the RAS as data. When an overloading is identified from the PMU measurements, a trigger signal is sent to the power flow controller to calculate the required HVdc power reduction to prevent or remedy the overloading of the violated line.

3.4.3 Relationship between HVdc Power Reduction and Change in Line Power Flows

The control action proposed here is the reduction of HVdc power in the bipoles when an overloading is observed on the remaining lines after a critical line is tripped. After performing stability studies, the branches prone to overloading are selected for monitoring and are shown in Table **3.2** with their normal and emergency ratings.

The HVdc power reduction scheme to prevent the overloading of the lines are pre-designed for each event. For the i^{th} branch which can be either a transmission line or a transformer, the normal MVA rating, $S_{nR,i}$ and the emergency MVA ratings, $S_{eR,i}$, which can be maintained for 30 minutes under emergency situations, are given.

Table 3.2 Critical lines selected for monitoring overload conditions

Branch	Voltage (kV)	Normal rating S_{nR} (MVA)	Emergency Rating S_{eR} (MVA)
B8 to B14	500	2730.6	3003.6
B9 to B17	500	1732.1	2165.1
B8 to B9	500	1732.1	1905.3
B3 to B15	230	430	478
B4 to B16	230	207	229.9
B7 to B10	230	470.5	517.5
B7 to B13	230	370	407
B6 to B12	500	1732.1	2165.1
B12 to B11	345	1173.6	1195.1
B5 to B18	230	227.5	250

In order to develop an approach to determine the proper amount of HVdc power that needs to be reduced under a given situation, dynamic simulation studies were performed with different contingencies. The contingencies simulated are faults that lead to tripping of some critical branches, selected based on the experience of planning engineers. For each contingency, multiple scenarios were simulated with different amounts of HVdc reductions (ΔP_{dc}) following the contingency, and the amount of power flow on each line was recorded.

Consider the example of fault on a 500 kV line B8-B14. The line was removed four cycles after the fault, and the simulations were repeated with different amounts of HVdc power reduction. The power flow variations in all the selected lines were recorded. An example of the data recorded for a particular line (B9-B17) for a given contingency (tripping of line B8-B14 after a fault) is shown in Table **3.3**.

Table 3.3 Relationship between HVdc power reduction and line power flows (Line B9-B17)

$\Delta P_{dc\ (MW)}$	$S_{i\ (MVA)}$	$\Delta S_{i\ (MVA)}$	$\Delta S_{\%,\ i}$
0	2309.79	-577.69	-33.35
97.16	2190.09	-457.99	-26.44
242.91	2088.96	-356.86	-20.60
291.49	2055.54	-323.44	-18.67
485.81	1930.11	-198.01	-11.43
631.55	1839.28	-107.18	-6.19
728.72	1777.27	-45.17	-2.61
825.88	1716.30	15.8	0.92
971.62	1626.73	105.37	6.08

The power flow values are taken after the system is stabilized following the dc power reduction. Similar tables can be created for all monitored branches, excluding the tripped branch as shown in Appendix A. Overloading on the i^{th} line, ΔS_i, can be normalized based on the line's normal MVA rating $S_{nR,i}$ as:

$$\Delta S_{\%,i} = \frac{(S_{nR,i} - S_i)100}{S_{nR,i}}\% \tag{3.1}$$

where S_i is MVA flow in line i. The values of $\Delta S_{\%,i}$ computed for different lines for the event of tripping of 500 kV line B8-B14 after a fault are presented in the form of a ΔP_{dc} vs. $\Delta S_{\%,i}$ graph in Figure **3.7.**

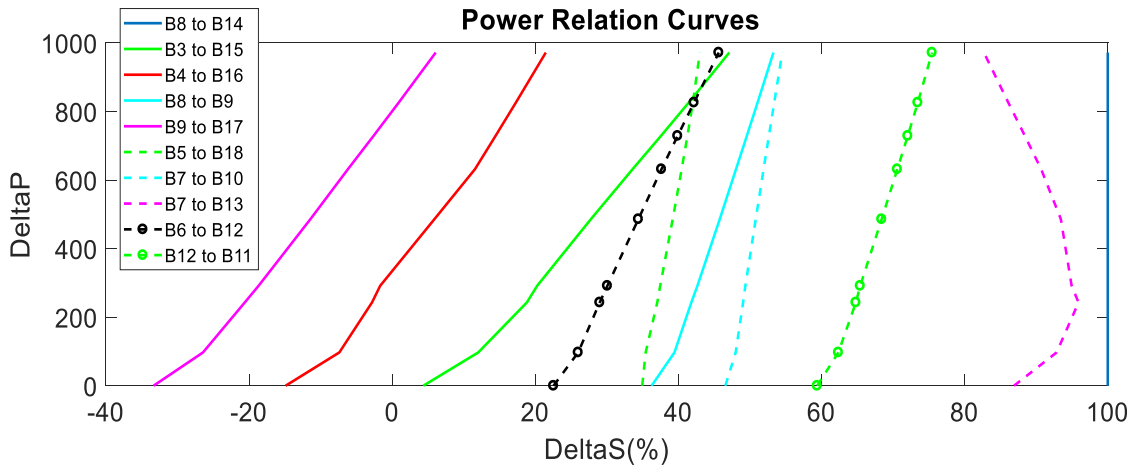

Figure 3.7. Relationship between the HVdc power reduction and the resulting change in overloading on different lines following the tripping of line B8-B14.

For example, 500 kV line from B9-B17 gets heavily overloaded after this contingency (tripping of 500 kV line B8-B14). If no HVdc power reduction is applied, this line is about 33% overloaded (based on the line's normal MVA rating). This is above the line's emergency rating, $S_{eR,i}$, which corresponds to about 25% overload. Overloading on this line can be reduced to about 10%, if the total output of three Bipoles is reduced by 500 MW. For this contingency, only two lines (B9-B17 and B4-B16) get overloaded. All other lines will remain within their normal limits, which correspond to $\Delta S_{\%,i} = 0$.

As another example, for the case of tripping 230 kV line B7-B10, the response of the selected branches for HVdc power reduction is shown in Figure **3.8**. The sensitivity table is given in Appendix A.

These relationships are slightly nonlinear but can be approximately represented using linear functions in the form of:

$$\Delta P = m_i \cdot \Delta S_{\%,i} + C_i \qquad (3.2)$$

for most cases. There are a few cases such as B7-B13 in Figure **3.7**, where the curve cannot be approximated by a linear function due to change of power flow direction under different HVdc power reduction amounts. However, this line is not going to be overloaded and can be ignored.

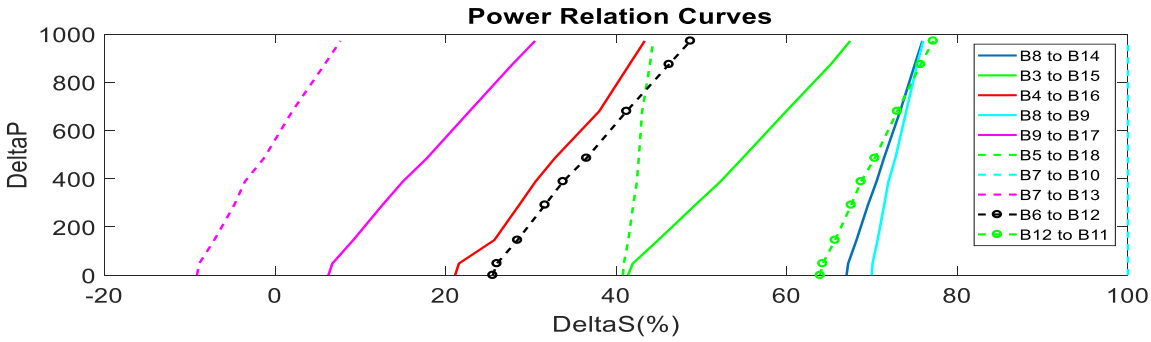

Figure 3.8. Relationship between the HVdc power reduction and the resulting change in overloading on different lines following the tripping of line B7-B10

For this case, line B7-B13 is observed to be crossing the overload rating when there is no HVdc power reduction. The HVdc power reduction and the corresponding line rating of the overloaded line B7-B13 are shown in Table **3.4**.

Table 3.4 Relationship between HVdc power reduction and line power flow (Line B7-B13)

$\Delta P_{dc\ (MW)}$	$S_{i\ (MVA)}$	$\Delta S_{i\ (MVA)}$	$\Delta S_{\%,\ i}$
0	403.901	33.901	-9.16
48.58	402.920	32.92	-8.89
145.74	396.404	26.404	-7.14
291.49	387.749	17.749	-4.8
388.65	383.101	13.101	-3.54
485.81	374.806	4.806	-1.3
680.14	362.561	7.439	2.01
874.46	348.499	21.501	5.81
971.62	341.673	28.327	7.66

A sensitivity of the power flow for a selected branch to HVdc power changes can be approximately obtained from the slope of ΔP_{dc} vs. $\Delta S_{\%,i}$ curves (ex. Figure **3.7** and Figure **3.8**). The sensitivity factor of the i^{th} branch, $S_{F,i}$ can be defined as the slope m_i of the fitted curves.

3.4.4 Calculation of the Amount of HVdc Power Reduction

In order to determine the sensitivities, a set of curves which relate the amount of HVdc power to reduce with the percentage overload for each monitored line were developed using dynamic studies. If an overload exceeds the branch emergency limit, it first attempts to bring the line flow below the 30-minute emergency rating, and then act progressively to bring the power level below normal rating.

For calculating the HVdc power to be curtailed to prevent the chances of overloading only the line with highest percentage overload is considered. For example, in Figure **3.7** it is observed that two branches are crossing the normal rating after tripping the 500-kV line B8-B14. The branch B9-B17 has the highest percentage overload, and the curve corresponding to that line is considered for calculating the required reduction of HVdc power (ΔP_{dc}^{*}). For the tripping of 230 kV line B7-B10 shown in Figure **3.8**, only one branch (B7-B13) is overloaded, the curve corresponding the that branch is used for calculating ΔP_{dc}^{*}.

To determine the level of HVdc power reduction, two cases are considered. If the line power flow goes above the emergency rating during the transient period following the line trip, HVdc power reduction is immediately activated and the reduction amount is computed with the aim of bringing the power flow down to a level midway between the emergency

and normal ratings. This step is taken to avoid tripping of lines by protection, but at the same time not to reduce too much power in the dc links during the transient period. This operation is referred to as Mode-1. The second case, which is referred to as Mode-2, is when the overload for a particular line is above the normal ratings, but still below the emergency rating. In this case, a delay of 1 second is allowed after the contingency is recognized before an action is taken. The target operating point after HVdc power reduction, in this case, is the normal rating.

The HVdc power to be reduced in the bipoles can be computed using the sensitivity factors:

$$\Delta P_{dc}^{*} = S_{F,i} \cdot \Delta S_{\%,i} \tag{3.3}$$

The process of determining the level of HVdc power reduction is explained in Figure **3.9**. Suppose point 'Y' is the observed percentage of overload after the tripping event. The aim is to bring the operating point to 'Z', which is assumed as the mid-point between normal and emergency ratings. The required reduction is ΔP_{dc1}^{*} illustrated in Figure **3.9**. A period of about 2 s is allowed for the system to settle, before applying one more step of reduction to bring the power to nominal ratings. The amount of HVdc power to be reduced is ΔP_{dc2}^{*} shown in Figure **3.9**.

All branches are monitored continuously and if further overload is present after a delay of 1 s, HVdc power is further reduced. This iterative process is required due to linear approximation of ΔP_{dc} vs. $\Delta S_{\%,i}$ relationships and the differences in the pre-contingency operating points. Also note that data for the examples shown in Figure **3.7** and Figure **3.8** are obtained considering the steady operation after a HVdc power change, while RAS may

take action while overload conditions are changing. Thus, subsequent changes may be needed in some cases, and the amount of reduction is computed in an equivalent manner considering the observed operating point on the $\Delta S_{\%,i}$ axis. This process is continued until all monitored line power flows are below the corresponding normal ratings. If a different branch shows a higher percentage of overload during the process, the sensitivity corresponding to that line is used for calculating the amount of HVdc power reduction. Flowchart explaining the operations of the HVdc power reduction control is shown in Figure **3.10**.

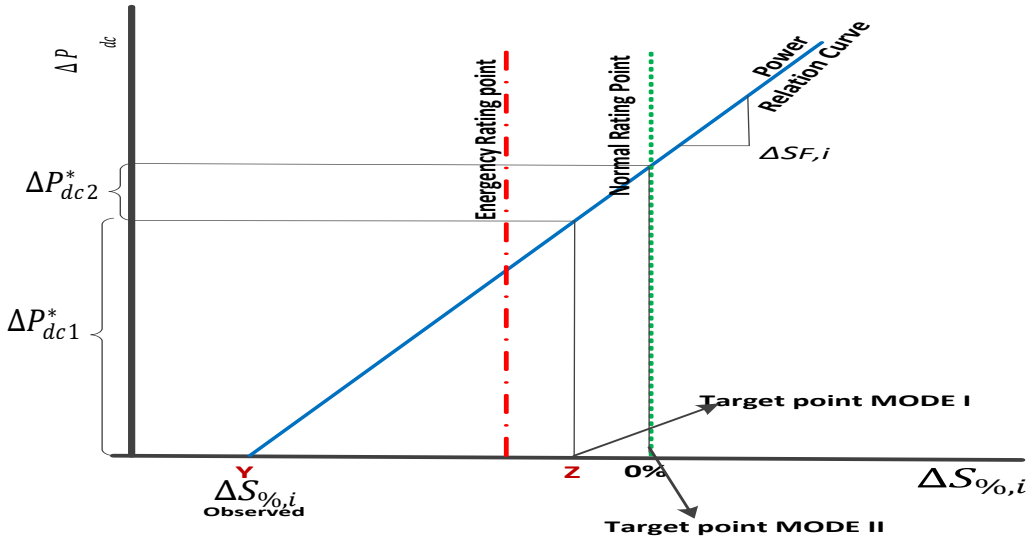

Figure 3.9. Process of calculating HVdc power reduction

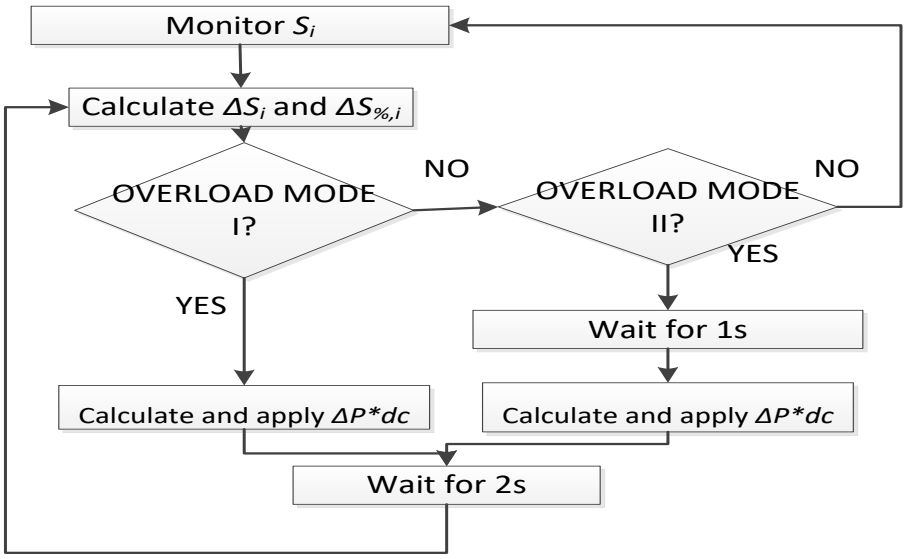

Figure 3.10. Flow chart for calculating HVdc power reduction

The control logic of the proposed HVdc reduction scheme is shown in Figure **3.11**.

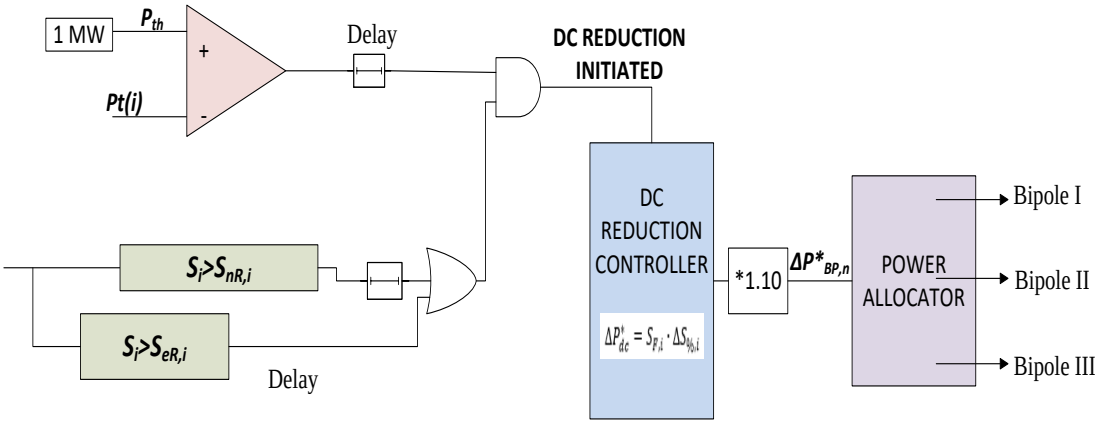

Figure 3.11. Control logic

The power to be reduced at the rectifier side is calculated by increasing the amount of ΔP^*_{dc} by 10% to account for possible errors in the logic. Finally, the estimated power is proportionally allocated to each bipole using (3.4), where *n* is the bipole number (*n* =I, II, or III).

$$\Delta P_{BP,n} = \frac{1.1\Delta P_{dc}^{*} \cdot P_{BPrated,n}}{P_{BPrated,I} + P_{BPrated,II} + P_{BPrated,III}} \quad (3.4)$$

3.5 Case Study

In this section, the performance of the proposed dc power control scheme is evaluated for some selected contingencies. Summer off-peak cases are selected for the study as they corresponds to highest export and considered to be the worst case for line overloading. Dynamic simulations of the Manitoba Hydro power system and adjacent areas were performed using PSS/E software. The simulation model included dynamic models of HVdc systems and user-defined models to implement remedial action schemes.

3.5.1 Case1- Loss of 230kV Line from B7 to B10

A three-phase fault is applied on the 230 kV tapping from B7 to B10 around 0.1 s. This 230 kV line was transferring about 359.84 MW of pre-fault power, and the line was tripped four cycles after the fault. The variation of power flowing through the key branches are observed. In a real-time implementation, these power flows are observed using synchrophasor measurements. It was observed that the power flow in 230 KV line B7-B13 shows the highest percentage overload for this contingency. The variation of power flow in line B7-B13 is shown in Figure **3.12**. Power flow exceeds the emergency overload rating immediately after clearing the fault by tripping line B7-B10. Although the power flow drops below the emergency rating for a short period during the subsequent power oscillations, this is clearly a Mode-1 overloading event. Therefore, immediate action is

needed to reduce the power flow through the particular line below its emergency rating. According to the algorithm described in Section 3.4.4, the target power flow for the first step is the mid-point between emergency rating (407 MVA) and the normal rating (370 MVA), that is 388.5 MVA. The required HVdc power reduction ΔP^*_{dc1} was estimated to be 286 MW using the slope of ΔP_{dc} vs. $\Delta S_{\%,i}$ relationship for line B7-B13. Based on the calculations, a signal was sent to initiate the control actions to reduce 383 MW of HVdc power.

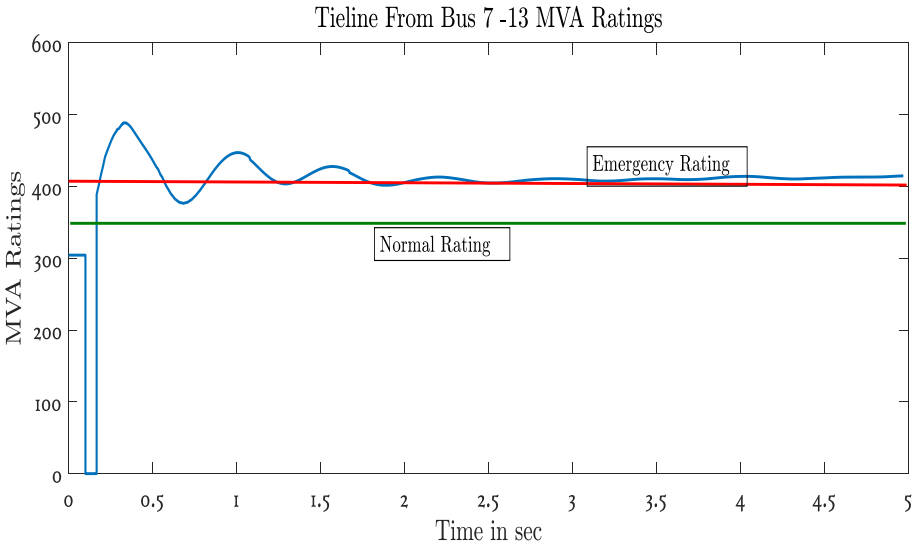

Figure 3.12. Variation of power flow in line B7-B13 after tripping line B7-B10 for clearing the fault. The normal and emergency ratings of the line are also indicated.

The variation of power flow in line B7-B13 after this remedial action is shown in Figure **3.13**. It was assumed that control action was applied after a delay of 500 ms, taking into account the latency involved in measurement, communication and identifying the contingency. The power flow settles slightly above the target.

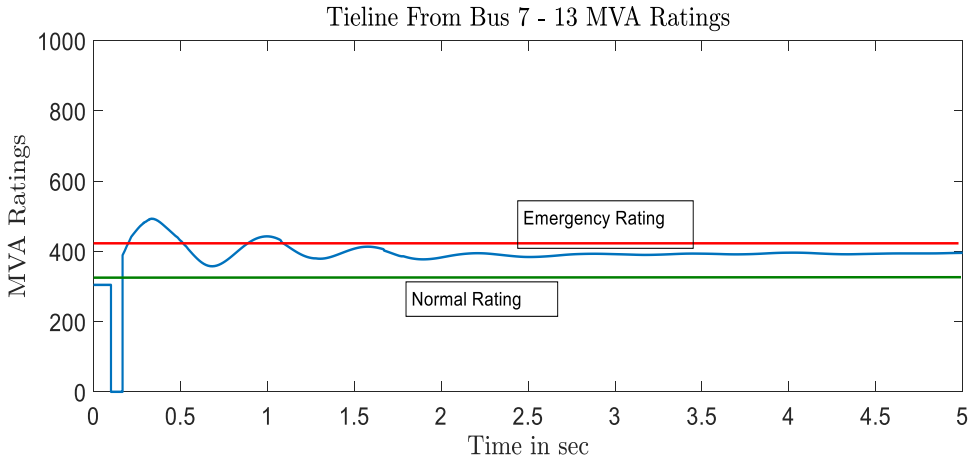

Figure 3.13. Variation of power flow in line B7-B13 after the first step of HVdc power reduction.

After 2 s, the measurement-based RAS will recognize this as a Mode-2 overload condition and activate another 383 MW of HVdc power reduction. The power rating of the overloaded line after implementing the 2-step reduction is shown in Figure **3.14**. Further reduction steps may be taken if the overload remains higher than the normal rating.

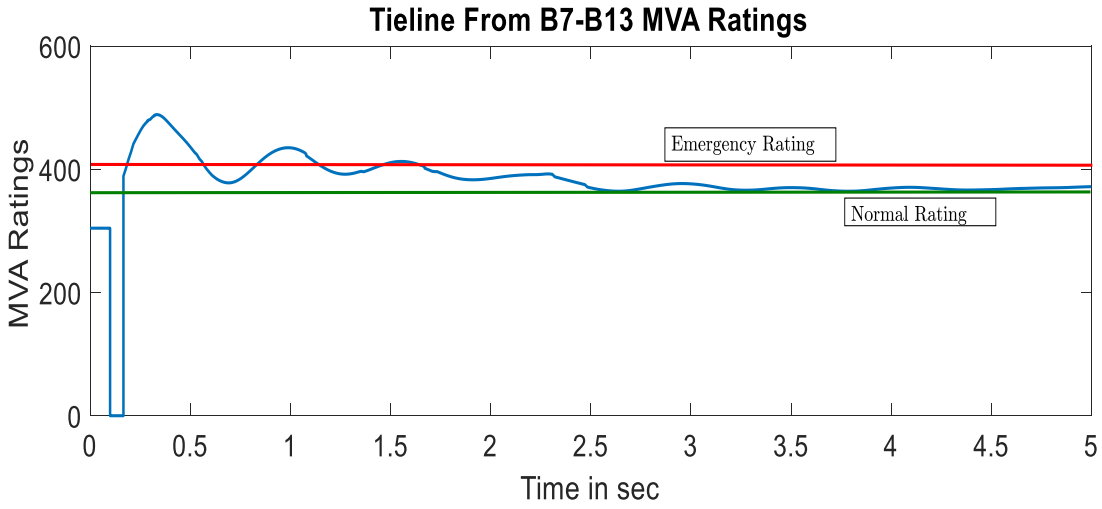

Figure 3.14. Variation of power flow in line B7-B13 after the second step of HVdc power reduction

3.5.2 Case 2-Loss of 500KV Line from B8 to B14

A three-phase fault is applied on 500 kV tie-line from B8 to B14. The fault occurs at 0.1 s and it lasts for 4 cycles. The fault is cleared by tripping the line. The 500 kV line B9-B17 is the branch that has the highest percentage overload for this contingency. After the fault is cleared, it is observed that the 500 KV line B9-B17 exceeds its emergency MVA rating, 2165.1 MVA, around 0.45 s. Thus, the action is to bring down the power flow to between emergency and normal ratings, 1732.1 MVA. The required reduction in HVdc power is computed using the slope of ΔP_{dc} vs. $\Delta S_{\%,i}$ relationship for the line B9-B17 and was found to be 421 MW. By adding 10% to incorporate the losses, a command is sent to reduce 518 MW of power from the three bipoles. In the second step, RAS reduces further 365 MW of HVdc power to bring the line flow below normal rating. The power flows in the line with proposed scheme, existing scheme and without implementing HVdc power reduction are shown in Figure **3.15**.

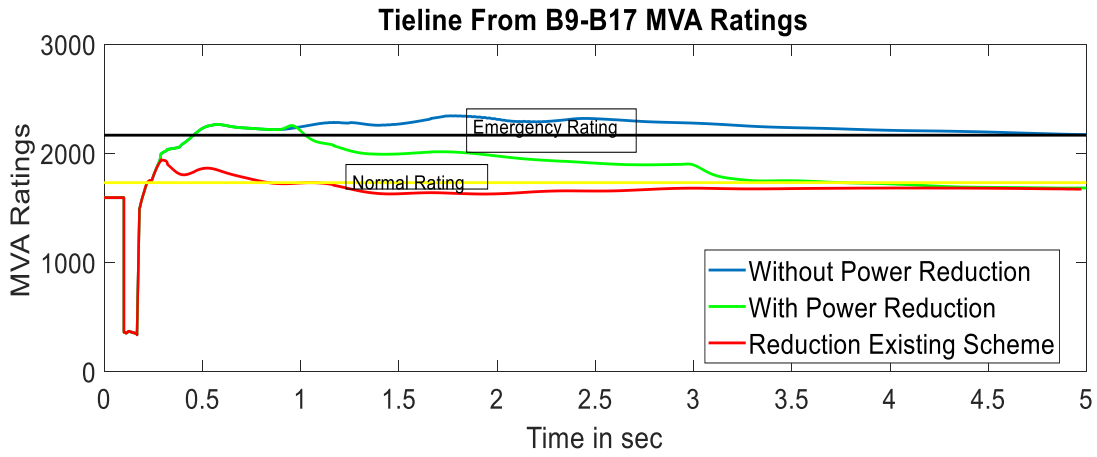

Figure 3.15. Variation of power flow in line B9-B17 with proposed scheme, existing scheme and without HVdc power reduction

With the event-based RAS designed for this system, 972 MW of HVdc power reduction would have applied for this case, however, only 883 MW of HVdc power is reduced with the proposed measurement-based RAS. From Figure **3.15**, it can be seen that even with a less amount of HVdc power reduction in the Bipoles, the power flow variation in the overloaded line can be brought down to the level achieved with the existing HVdc power reduction scheme.

3.6 Concluding Remarks

The Manitoba Hydro power system which has three HVdc infeeds experiences overload conditions when a major tie-line or any other line associated with power export is tripped. A synchrophasor measurement based remedial action scheme was proposed to prevent the overloading of lines and transformers by rapidly reducing HVdc power injection during some critical contingencies. The amount of HVdc power reduction is computed using a pre-identified relationship between the HVdc power reduction and resulting power flow change in a given line. Their relationships are identified using offline dynamic simulations under different contingency scenarios. As this scheme curtails only the minimum required amount of HVdc based on the measured overload, and there is a potential for economic and reliability benefits.

Also, compared to the present reduction scheme used by the Manitoba Hydro, the proposed scheme completely avoids the chances of overloading while reducing the amount of HVdc power shed for some events. If the scheme can use a common corporate PMU network, the need for specially dedicated communication channels for implementing RAS can be

avoided. However, practical aspects such as measurement and communication latencies, cyber security etc. need to be carefully studied.

Chapter 4

Synchrophasor Measurements Based Controlled Islanding

In this Chapter, an emergency control system is proposed to perform controlled islanding to rescue a power system from impending transient instabilities. The proposed method includes identification of coherent group of generators, splitting the power grid into several stable islands after determining the boundaries of each island, and post-islanding load-generation balancing. The major contribution of the controlled islanding method proposed in this chapter is a method to determine the number of islands and their boundaries in real-time using synchrophasor data.

4.1 Background and Problem Statement

Controlled islanding is often considered as the final resort to solve power system stability problems. The main aim of system islanding is to preserve as many stable areas in a power system that is becoming unstable. Controlled islanding operations are system dependent and there is no standard operation pattern applicable to all power system. Several factors

can assist the designing of islanding scheme other than the geographical proximity of the generators in the system. The type, location and the dynamic performance of the system against the fault are some among them.

Typical islanding schemes in practice are developed completely off-line. The geographical boundaries of the islands are predetermined for a set of critical events in the system [40]. This type of planned schemes defines the lines that need to be opened when certain situations arise. These scenarios are selected after extensive system studies. The major issue with these kinds of schemes is that the control scheme needs to be rebuilt when the system is subjected to changes which indeed requires more time and efforts. Also, there is a possibility of uncontrolled islanding or system collapse due to a rare event that is not considered in the predetermined event set.

Wide area synchrophasor measurements can be used to develop improved controlled islanding algorithm as they will provide accurate real-time measurements which can be used for the stability assessment, identification of coherent generator groups and island boundaries based on the prevailing system conditions. Real-time measurements from PMUs such as voltage, current, phase angle, frequency, and rate of change of frequency help observe the system conditions and track the abnormalities [6]. These measurements can help in making crucial decisions about the implementation of system separation. The real-time application of controlled islanding based on synchrophasor measurements is not much explored in the published literature.

Generally, the application of control islanding schemes for smaller systems are relatively simpler than large systems. Implementing a reliable controlled islanding scheme requires a sufficient number of PMUs installed to cover different areas of the system. The PMU

placement in the system is important and requires extensive system studies and sound engineering judgement. The measurements from these PMUs need to be communicated to the central control center, and therefore, a reliable communication infrastructure that can support transferring a large amount of data with acceptable latency is required. The control system should also be capable of processing data from hundreds of PMUs in real-time to make islanding decisions. Therefore, development of efficient methodologies for making controlled islanding decisions is necessary.

The proposed controlled islanding methodology deals with two main questions: when to island the system and where to island the system. Considering that the generator coherency is determined in the prior stage of analysis, controlled islanding can be identified as one of the last resort remedial actions to rescue a power system declared to be transiently unstable. Identification of feasible islands and determination of separating points are performed in two steps. First the loads are allocated to a group of coherent generators that will form an island and then the physical boundary of each island is determined. The question of where to island become crucial in obtaining the generator load balance of the island and in maintaining an acceptable network topology. Proper splitting of islands considering the power generation and load balance will reduce the requirements for post-islanding load shedding and generator tripping to restore the frequency stability of islands. Besides, when considering the network topology for island creation and separation of the islands, the transmission lines interconnecting the islands need to be identified.

4.2 Structure of the Controlled Islanding Scheme

The proposed controlled islanding technique use the voltage, and current phasor measurements obtained from PMUs for determining the islands and for implementing post-islanding protection schemes. It is assumed that PMUs are available on all the generator and load terminals in the power system considered for the study. The proposed method is designed considering the transient stability prediction and coherent generator group identification algorithms proposed in [41] . These algorithms use the post-fault generator terminal voltage magnitudes as inputs.

An abstract representation of the proposed emergency control scheme is shown in Figure **4.1**. The proposed emergency control scheme consists of four main functional blocks: event detection, transient stability prediction, coherent generator groups identification, and emergency control. When an event is detected, the transient stability prediction algorithm and the coherent generator group identification functions are initiated. If the system is declared as transiently unstable, a signal is sent to emergency control block to enable the control islanding algorithm. Once the feasible islands are determined, trip signals are sent to the relevant breakers to open the boundary lines. After the system is islanded, the frequency in each island is monitored and frequency-based generator and load tripping is activated to maintain the frequency of islands if necessary. Main assumption considered in the proposed control islanding method is that the coherent generator groups are identified by the time of predicting the transient instability.

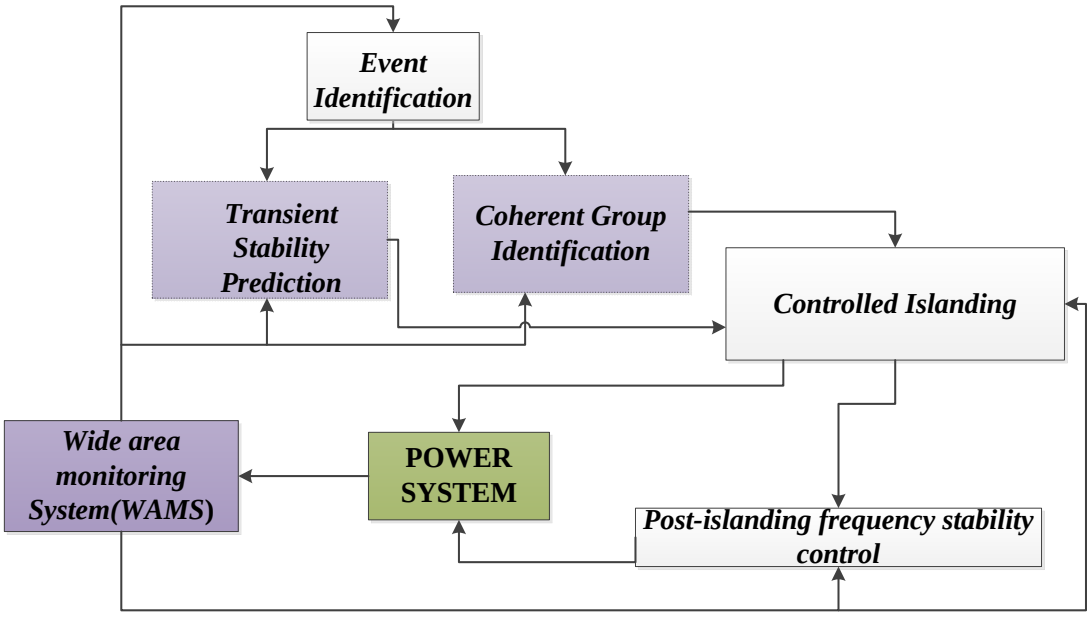

Figure 4.1.Structure of proposed emergency control scheme

4.3 Power System Used for Experimentation

The proposed emergency control scheme is validated offline using the IEEE New England test system [42]. This system includes 39 buses, 10 generators, 19 loads and 34 transmission lines as shown in Figure **4.2**. The generator at bus-39 represents an aggregated large system.

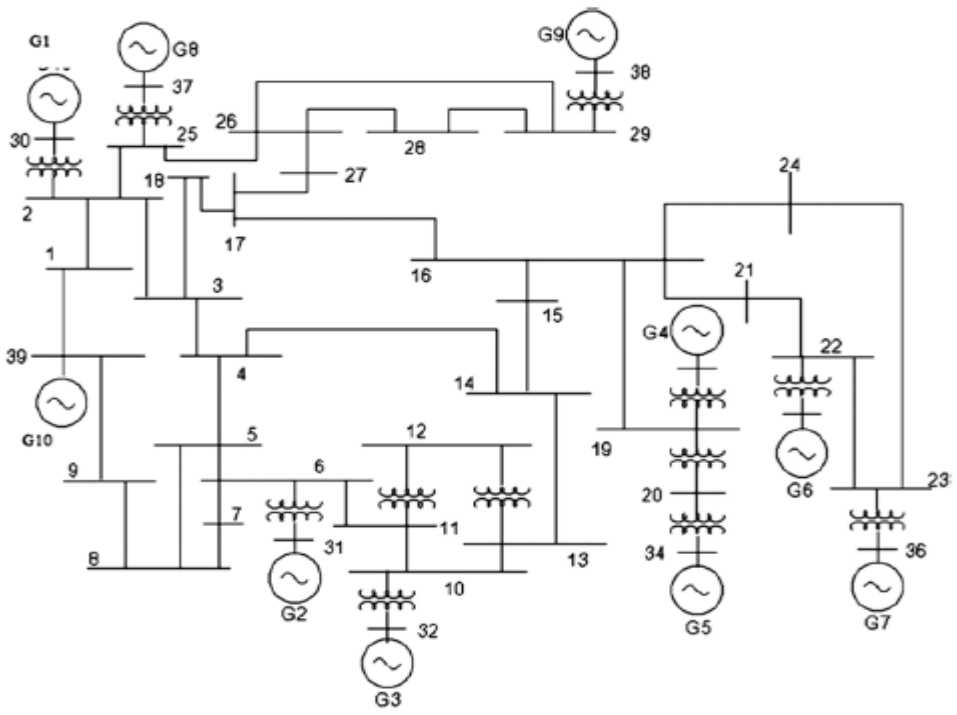

Figure 4.2. IEEE New England Test system(adapted from [42]

It is assumed that each generator represents a generating station comprising of several small generator units, so that complete shut down of generating stations is avoided when activating frequency-based generator tripping to achieve power balance within islands. No governor controls are modeled for the generators in the system, assuming that controlled islanding is accomplished in a short period of time. Although having governor controls modelled is more realistic, in terms of balancing the load and generation in islands, not having governor controls is the worst case. Therefore, lack of governor models leads to more conservative results. The system parameters are given in Appendix B. The generator stations and the corresponding number of units are shown in Table **4.1**. The required simulations are conducted in dynamic simulation software TSAT [43]. TSAT software is efficient in simulating a substantial number of fault scenarios using batch mode operation

during the offline study. All the contingencies and required operations are simulated in the TSAT software using a contingency file.

Table 4.1.No of generating units

Generator station	No of units	Per generating unit capacity
Gen 30	4	62.5
Gen 31	3	174
Gen 32	3	217
Gen 33	3	211
Gen 34	5	101.5
Gen 35	4	162.5
Gen 36	4	140
Gen 37	4	135
Gen38	4	207.5
Gen39	4	250

4.4 Transient Stability Prediction in Power systems

A simple and effective way of predicting impending transient instabilities through monitoring the generator voltage magnitudes trajectories after clearing a fault was proposed in [44]. For the transient stability prediction function of the proposed control islanding scheme, the algorithm proposed in [44] is used. The voltage deviation at a generator terminal, ΔV, and the rate of change of ΔV, which is equal to the rate of change of voltage, $ROCOV$, after clearing a fault are the transient stability indicators used in this

algorithm. The voltage measurements for the transient stability prediction are obtained from synchronized phasor measurement units located at the generator terminals of the considered system. The values of ΔV and the rate of change of ΔV are calculated as:

$$\Delta V = V_{mag} - V_{mag,ref} \tag{4.1}$$

$$\frac{d}{dt}\Delta V = \frac{d}{dt}V_{mag} = ROCOV \tag{4.2}$$

where V_{mag} is the terminal voltage measured at the generator end, $V_{mag,ref}$ = 1.0 p.u. and $ROCOV$ is the rate of change of generator terminal voltage (pu/s). The $ROCOV$ at the n^{th} measurement can be determined as:

$$\text{ROCOV}(n) = \left(V_{mag}(n) - V_{mag}(n-1)\right) \cdot F_s \tag{4.3}$$

where F_s is the reporting rate of PMU in frame/s or fps.

The algorithm declares an instability condition if the locus of the generator on a $ROCOV$ -ΔV plane crosses a pre-set boundary as illustrated in Figure **4.3**. For the stable cases, the operating point moves in a circular trajectory and converges on the ΔV axis, as $ROCOV$ becomes zero. For the unstable cases, the operating point deviates away from the origin. The system is declared as unstable when the post-disturbance operating point moves away from the stable area of operation to the unstable region. A method to determine the stability boundary, which is specified using the coordinates of points B and C, is also described in [44].

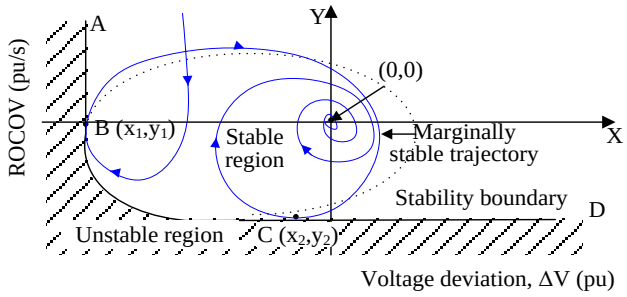

Figure 4.3. Stability boundary on $\boldsymbol{ROCOV}$–$\boldsymbol{\Delta V}$ plane (adapted from [44])

The selected technique is easier to implement and predicts the instabilities in shorter time which is important in emergency control. The technique also identifies the generators that are first to become out-of-step. This piece of information is important for the emergency control scheme proposed in this research as it helps in identifying the critical group of generators and the critical island in the power system which includes those generators.

A method to determine the stability boundary, which is specified using the coordinates of points B and C, is also described in the selected method. According to this method, the marginally stable contingencies need to be identified for defining the stability boundaries of the generators. Determination of the marginally stable cases and stability boundary for each generator in includes the following steps:

a) The marginally stable case can be identified by applying a three-phase short circuit at the terminal of the generator and increasing the fault duration till the generator reaches the unstable point. The marginally stable case can be recognised by decreasing the fault duration of the unstable case by one cycle.

b) Plot the $ROCOV$-ΔV curve for the marginally stable case.

c) Locate point B (x1, y1) shown in Figure **4.3** at the left end of the plot and connect a line joining A and B as parallel to the Y axis. The area on the right of the parallel line

corresponds to the stable region of operation and is identified as the first section of the stability determination boundary on the $ROCOV$ -ΔV plane as in Figure **4.3**.

d) The point C (x2, y2) is located just below the lowest end of the plot and joined by a line CD which is parallel to the X axis. The region on top of the line CD, is identified as the stable region and considered to be the third section of the stability determination boundary.

e) Create an ellipse passing through points B and C such that left end of the ellipse passes through point B and the lower end of ellipse cuts point C. The ellipse segment BC is identified as the second section of the stability determination boundary through which the unstable trajectories cut the stability region.

The stability boundary of Gen 30 in the IEEE 39 Bus system selected for the study is determined using the described method. A three-phase fault is applied on the generator terminal and the fault duration is increased in steps until the generator got unstable.

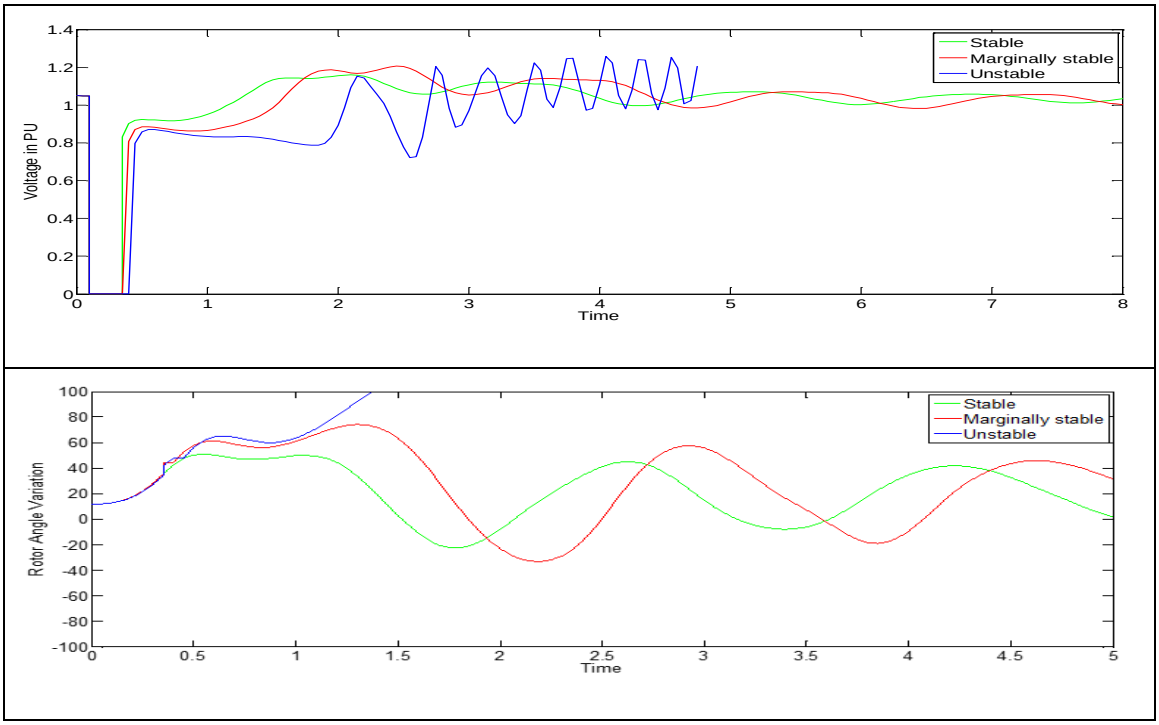

Figure 4.4. Voltage and Rotor angle variation of Gen 30 for stable, unstable and marginally stable operation

The voltage and phase angle variations of the generator for stable, marginally stable and unstable operation is shown in Figure **4.4**.

The stability boundary of the generator can be identified by plotting the post fault voltage variation of the generator in the $ROCOV$ -ΔV for the marginally stable case. The stability boundary of Gen 30 is shown in Figure **4.5** along with the voltage variation of the particular generator for unstable, marginally stable, and stable cases. From Figure **4.5**, it is clear that the generator voltage variation crosses the stability margin when the generator is unstable.

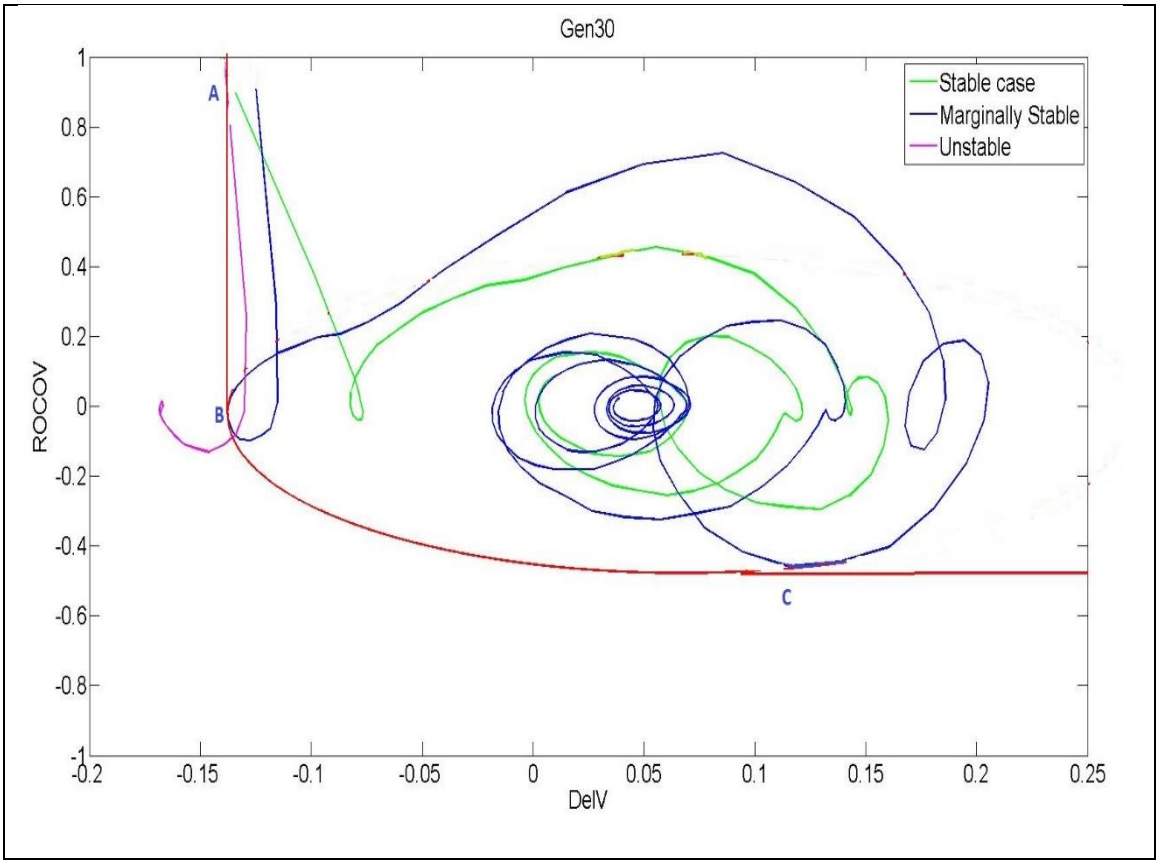

Figure 4.5. Stability boundary on $\boldsymbol{ROCOV}$–$\boldsymbol{\Delta V}$ plane for Gen 30

The B and C coordinates of each generators identified based on the above method is shown in Table **4.2**.

Table 4.2. Stability boundary points

Generator	B(x1 pu,y1 pu/s)	C(x2 pu,y2 pu/s)
Gen 30	-0.137, 0	0.115, -0.4578
Gen 31	-0.5,0	-0.36, -1.29
Gen 32	-0.475,0	-0.361,-1.002
Gen 33	-0.310,0	-0.264,-0.935
Gen 34	-0.315,0	-0.248,-0.5
Gen 35	-0.23,0	0.1007,-0.318
Gen 36	-0.322,0	-0.29,-1.11
Gen 37	-0.363,0	-0.347.,-0.608
Gen 38	-0.372,0	-0.263,-0.837

4.5 Coherent Group Identification

It is important to determine the coherent groups of generators prior to islanding. The coherent cluster recognition technique implemented in this research uses the differences in the rate of voltage recovery during the post-disturbance period as proposed in [41]. The generators exhibiting slow voltage recovery following the clearance of a fault has the tendency to accelerate faster and swing together. In [41], the early post-disturbance voltage magnitudes obtained from PMUs at the generator terminals have been used to identify the critical cluster that includes the generator(s) predicted to be out of step first.

In order to determine coherent groups, generator terminal voltage magnitudes in an observation data window of k consecutive measurements are collected for each generator in the system. The distance between the trajectories of the post disturbance terminal voltages of two generators can be measured by

$$I_{pq} = \sum_{t=t_{cl}}^{t_{cl}+k\Delta t} \left[V_{magG}^{(p)}(t) - V_{magG}^{(q)}(t)\right]^2 \quad ; \quad \text{for } p, q = 1, 2, \ldots, n_g \tag{4.4}$$

where $V_{magG}^{(p)}(t)$ and $V_{magG}^{(q)}(t)$ are the voltage magnitudes of p^{th} and q^{th} generators at time t, Δt is the reporting time interval of PMUs given in (4.5) and n_g is the number of generators.

$$\Delta t = \frac{1}{F_s} \tag{4.5}$$

A matrix of I_{pq}values is computed considering all the generator pairs to identify the generators that swing together. The distance I_{pq} will be smaller than the distance I_{pr}, when generators p and q belong to the same coherent cluster and generator r belongs to a different cluster. The classification is done according to the routine prescribed in [45] considering the minimum distance between two generators. The original algorithm given in [45] is based on rotor angle trajectories, but in [41], it has been adapted to use considering the distance between voltage magnitude trajectories.

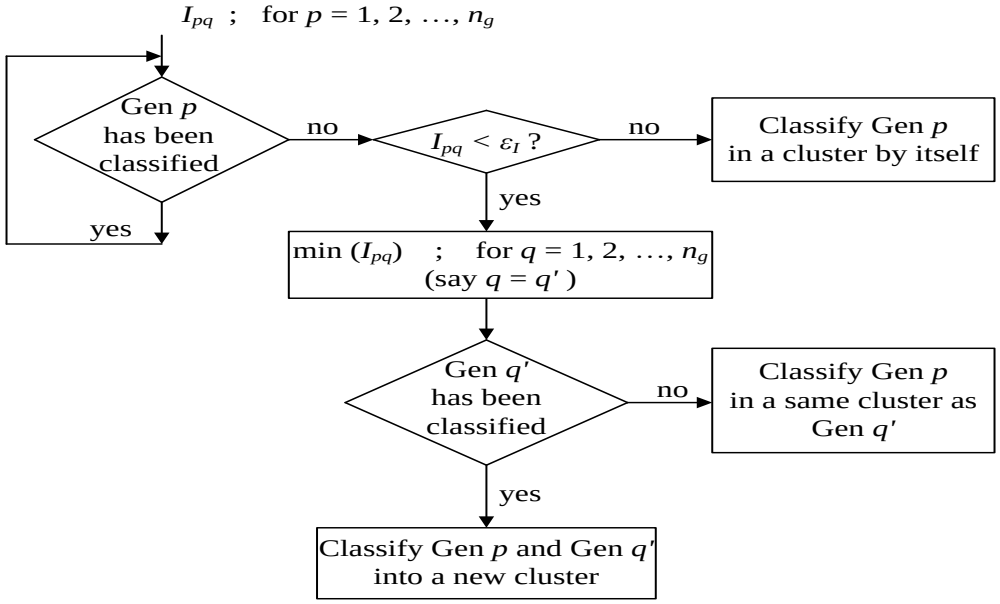

Figure 4.6. Coherent generator clusters recognition routine [41]

As shown in Figure **4.6** the distance values of each generator pair are compared with a pre-specified threshold ε_I obtained through studies. If the distance from generator p to all other generator is greater than the threshold, the generator p is classified in a cluster by itself; otherwise the closest generator (say generator q') to the generator p is identified. Generator p is classified into the same cluster as generator q' if it is already classified. Both generators p and q' are classified into a new cluster if generator q' is unclassified. This process is continued until all the generators are grouped. If I_{pq} value between any two generators, say for generator p and generator r in the same cluster is greater than the threshold ε_I then I_{pr} values are compared with ε_I and the generator r is assigned to a different cluster, which has more I_{pr} values that are smaller than the threshold ε_I.

In order to determine the exact data window k and threshold value ε_I for identifying the coherent group of generators, analysis was conducted using different data window lengths for calculating the I_{pq}. The threshold value ε_I was selected based on the observed I_{pq} distance matrix under different scenarios for the selected test system. The threshold value should be between the maximum distance between the generators in the same coherent group and the minimum distance between the generators in different coherent group. Here the threshold was selected in the range of 0.2 to 0.1 for each set of data frame; the suitable threshold value within the above range was identified through a search process.

The post-fault voltage variation for a scenario of three-phase fault on Line 2-25 is considered for illustration of the process. Table **4.3** - Table **4.6** show I_{pq} distance matrices for different data window lengths (k = 10, 15, 20, and 25 cycles). It is clear from Table **4.3** that for a data window with k =10 cycles, it is not possible to identify a coherent group

when the threshold is higher. Gen 37 alone forms a group when the threshold is reduced to 0.14.

Table 4.3. Matrix of distances between generator voltage trajectories for 10 cycle data window

	G30	G31	G32	G33	G34	G35	G36	G37	G38	G39
G30	0.0000	0.0278	0.0267	0.0311	0.0196	0.0044	0.0011	0.1453	0.0276	0.0038
G31	0.0278	0.0000	0.0002	0.0006	0.0014	0.0102	0.0191	0.0464	0.0015	0.0453
G32	0.0267	0.0002	0.0000	0.0015	0.0020	0.0094	0.0186	0.0489	0.0008	0.0426
G33	0.0311	0.0006	0.0015	0.0000	0.0014	0.0127	0.0212	0.0422	0.0038	0.0514
G34	0.0196	0.0014	0.0020	0.0014	0.0000	0.0060	0.0119	0.0587	0.0043	0.0369
G35	0.0044	0.0102	0.0094	0.0127	0.0060	0.0000	0.0018	0.0998	0.0103	0.0131
G36	0.0011	0.0191	0.0186	0.0212	0.0119	0.0018	0.0000	0.1233	0.0201	0.0086
G37	0.1453	0.0464	0.0489	0.0422	0.0587	0.0998	0.1233	0.0000	0.0518	0.1829
G38	0.0276	0.0015	0.0008	0.0038	0.0043	0.0103	0.0201	0.0518	0.0000	0.0416
G39	0.0038	0.0453	0.0426	0.0514	0.0369	0.0131	0.0086	0.1829	0.0416	0.0000

For a data window with k =15 cycles as shown in Table **4.4**, it is observed that from thresholds in the range of 0.2 to 0.1, only generator 37 swings differently from the other generators.

Table 4.4. Matrix of distances between generator voltage trajectories for 15 cycle data window

	G30	G31	G32	G33	G34	G35	G36	G37	G38	G39
G30	0.0000	0.0475	0.0460	0.0493	0.0301	0.0080	0.0014	0.2543	0.0716	0.0049
G31	0.0475	0.0000	0.0002	0.0007	0.0028	0.0166	0.0338	0.0824	0.0064	0.0750
G32	0.0460	0.0002	0.0000	0.0015	0.0033	0.0157	0.0330	0.0855	0.0059	0.0719
G33	0.0493	0.0007	0.0015	0.0000	0.0024	0.0183	0.0346	0.0803	0.0095	0.0793
G34	0.0301	0.0028	0.0033	0.0024	0.0000	0.0079	0.0188	0.1105	0.0159	0.0551
G35	0.0080	0.0166	0.0157	0.0183	0.0079	0.0000	0.0034	0.1728	0.0327	0.0216
G36	0.0014	0.0338	0.0330	0.0346	0.0188	0.0034	0.0000	0.2199	0.0564	0.0113
G37	0.2543	0.0824	0.0855	0.0803	0.1105	0.1728	0.2199	0.0000	0.0664	0.3141
G38	0.0716	0.0064	0.0059	0.0095	0.0159	0.0327	0.0564	0.0664	0.0000	0.1001
G39	0.0049	0.0750	0.0719	0.0793	0.0551	0.0216	0.0113	0.3141	0.1001	0.0000

With a data window of 20 cycles, distance matrix in Table **4.5** can be obtained. It is possible to identify two coherent groups with a threshold of 0.14. The distance matrix shown in Table **4.6** was observed with a data window of 25 cycles, and the identified coherent groups

remains the same as the groups obtained with 20 cycles data window. Again, the threshold setting of 0.14 was used. After testing with some other contingencies, it was found that a 20 cycle data window is sufficient to correctly identify coherent groups of generators. The generator clustering information is critical for the determination of islanding boundaries, and therefore must be reliable. Although use of long data windows increases the reliability of coherent group identification, it at the same time reduces the time available for taking emergency control actions. Therefore, a data window of 20 cycles and a threshold value of 0.14 deemed the best compromise.

Table 4.5. Matrix of distances between generator voltage trajectories for 20 cycle data window

	G30	G31	G32	G33	G34	G35	G36	G37	G38	G39
G30	0.0000	0.0890	0.0845	0.0879	0.0554	0.0175	0.0025	0.4779	0.1947	0.0131
G31	0.0890	0.0000	0.0003	0.0007	0.0049	0.0279	0.0631	0.1549	0.0280	0.1612
G32	0.0845	0.0003	0.0000	0.0015	0.0047	0.0254	0.0597	0.1622	0.0299	0.1536
G33	0.0879	0.0007	0.0015	0.0000	0.0038	0.0281	0.0615	0.1568	0.0333	0.1613
G34	0.0554	0.0049	0.0047	0.0038	0.0000	0.0116	0.0348	0.2093	0.0527	0.1171
G35	0.0175	0.0279	0.0254	0.0281	0.0116	0.0000	0.0076	0.3139	0.0969	0.0569
G36	0.0025	0.0631	0.0597	0.0615	0.0348	0.0076	0.0000	0.4140	0.1578	0.0264
G37	0.4779	0.1549	0.1622	0.1568	0.2093	0.3139	0.4140	0.0000	0.0815	0.6304
G38	0.1947	0.0280	0.0299	0.0333	0.0527	0.0969	0.1578	0.0815	0.0000	0.2944
G39	0.0131	0.1612	0.1536	0.1613	0.1171	0.0569	0.0264	0.6304	0.2944	0.0000

Table 4.6. Matrix of distances between generator voltage trajectories for 25 cycle data window

	G30	G31	G32	G33	G34	G35	G36	G37	G38	G39
G30	0.0000	0.1091	0.1030	0.1068	0.0689	0.0234	0.0033	0.5674	0.2487	0.0191
G31	0.1091	0.0000	0.0003	0.0007	0.0055	0.0322	0.0758	0.1797	0.0363	0.2093
G32	0.1030	0.0003	0.0000	0.0015	0.0051	0.0289	0.0712	0.1888	0.0392	0.1992
G33	0.1068	0.0007	0.0015	0.0000	0.0043	0.0318	0.0733	0.1830	0.0424	0.2075
G34	0.0689	0.0055	0.0051	0.0043	0.0000	0.0132	0.0425	0.2427	0.0662	0.1547
G35	0.0234	0.0322	0.0289	0.0318	0.0132	0.0000	0.0099	0.3634	0.1212	0.0807
G36	0.0033	0.0758	0.0712	0.0733	0.0425	0.0099	0.0000	0.4869	0.1991	0.0378
G37	0.5674	0.1797	0.1888	0.1830	0.2427	0.3634	0.4869	0.0000	0.0859	0.7722
G38	0.2487	0.0363	0.0392	0.0424	0.0662	0.1212	0.1991	0.0859	0.0000	0.3905
G39	0.0191	0.2093	0.1992	0.2075	0.1547	0.0807	0.0378	0.7722	0.3905	0.0000

4.6 System Islanding Based on the Phase Angle Difference and Relative Electrical Distance Concept

The key objective of the proposed controlled islanding scheme is to identify the loads belonging to each coherent group of generators for the proper splitting of power system into islands. Loads are assigned to a particular island based on the phase angle difference between the load points and the generator cluster in the island. The phase angle difference between two locations in a power system can be considered as an indicator which represents the network stress [46]. Phasor measurement units placed at strategic locations in the network can provide phase angle information for calculating the phase angle differences as in [47]. Here the post-fault phase angle magnitude difference between a generator and a load point in the system are monitored to identify the loads belonging to different islands. Phase angle difference is obtained as:

$$\Delta\delta = |\delta_{gen} - \delta_{load}| \tag{4.6}$$

The load points with smaller phase angle differences with the generators in a selected coherent group are clustered together to form an island. However, consideration of phase angle difference alone is not sufficient to determine whether a load point belong to a given generator cluster. This is because a load point with the minimum phase angle difference with respect to a generator cluster can be located far away form the generators in the cluster considered. Therefore, it is necessary to consider the electrical (or physical) distance between the load point and the generator group, in addition to the phase angle difference.

The concept of relative electrical distance(RED) was introduced by [48] to represent the relative distance between the generators and the load buses. The RED concept is used for

real power generation rescheduling in [49].Considering the RED values, the load points with smaller RED values with respect to a particular generator cluster are identified as geographically closer to each other. Both the phase angle difference $\Delta\delta$ and RED criteria are considered when assigning a particular load bus to an island consisting of a group of coherent generators.

Consider a power system consisting of *n* number of buses with *g* number of generator buses and the remaining *(n-g)* buses being load buses. The system equation can be written as:

$$\begin{bmatrix} I_G \\ I_L \end{bmatrix} = \begin{bmatrix} Y_{GG} & Y_{GL} \\ Y_{LG} & Y_{LL} \end{bmatrix} \begin{bmatrix} V_G \\ V_L \end{bmatrix} \tag{4.7}$$

where $[I_G], [I_L],$ and $[V_G], [V_L]$ represent current and voltage vectors at the generator and load points. $[Y_{GG}], [Y_{GL}], [Y_{LL}],$ and $[Y_{LG}]$, are the separated sections of system Y-bus matrix.

$$[I_G] = [Y_{GG}][V_G] + [Y_{GL}][V_L] \tag{4.8}$$

$$[I_L] = [Y_{LG}][V_G] + [Y_{LL}][V_L] \tag{4.9}$$

From (4.9),

$$\begin{gathered} [Y_{LL}]^{-1}[I_L] = [Y_{LL}]^{-1}[Y_{LG}][V_G] + [V_L], \\ [V_L] = [Y_{LL}]^{-1}[I_L] - [Y_{LL}]^{-1}[Y_{LG}][V_G] \end{gathered} \tag{4.10}$$

Substitution of $[V_L]$ in (4.8) gives

$$[I_G] = [Y_{GG}][V_G] + [Y_{GL}][Y_{LL}]^{-1}[I_L] - [Y_{LL}]^{-1}[Y_{LG}][V_G] \tag{4.11}$$

Representing the equations in matrix form we get,

$$\begin{bmatrix} V_L \\ I_G \end{bmatrix} = \begin{bmatrix} Z_{LL} & F_{LG} \\ K_{GL} & Y_{GG} \end{bmatrix} \begin{bmatrix} I_L \\ V_G \end{bmatrix} \tag{4.12}$$

Where $$[F_{LG}] = -[Y_{LL}]^{-1}[Y_{LG}] \tag{4.13}$$

The columns of $[F_{LG}]$ matrix correspond to the generators while the rows corresponding to the load buses. Thus, $[F_{LG}]$ matrix provides the connection between load and generator bus voltages. It can be used for calculating the electrical distance between a particular load and a generator bus, which is also known as the relative electrical distance. Relative electrical distance, RED, is often related to the geographical distance and can be obtained from the expression:

$$[RED] = [I] - |[F_{LG}]| \tag{4.14}$$

where $[I]$ is a unity matrix having the same dimensions as $[F_{LG}]$.

When applying controlled islanding to the test system selected for demonstration, it is assumed that only two islands are formed. Therefore, only the critical generator cluster i.e. the group of generators which includes the generator that moves to instability first, is allowed to select the loads, until approximate load-generation balance is achieved. The remaining loads are assigned to the other island. This makes the load selection process faster and thereby reduces the islanding decision time. Proceeding in this way will help in obtaining the power flow balance in the island containing the critical generators to certain extent. But still, load shedding and generator unit tripping may be necessary for securing stable islands.

A search algorithm is developed considering the phase angle difference and RED. In each depth of search, the loads with minimum phase angle difference corresponding to the critical island generators are identified and grouped together. Operation of the load searching process is illustrated in Figure **4.7**. The termination criteria for the load searching algorithm are:

1. The power imbalance in the critical island is less than a threshold.

2. No more load points with RED less than the threshold value.

The matrix containing RED values can be computed off-line considering the prevailing network topology and can be updated in regular intervals.

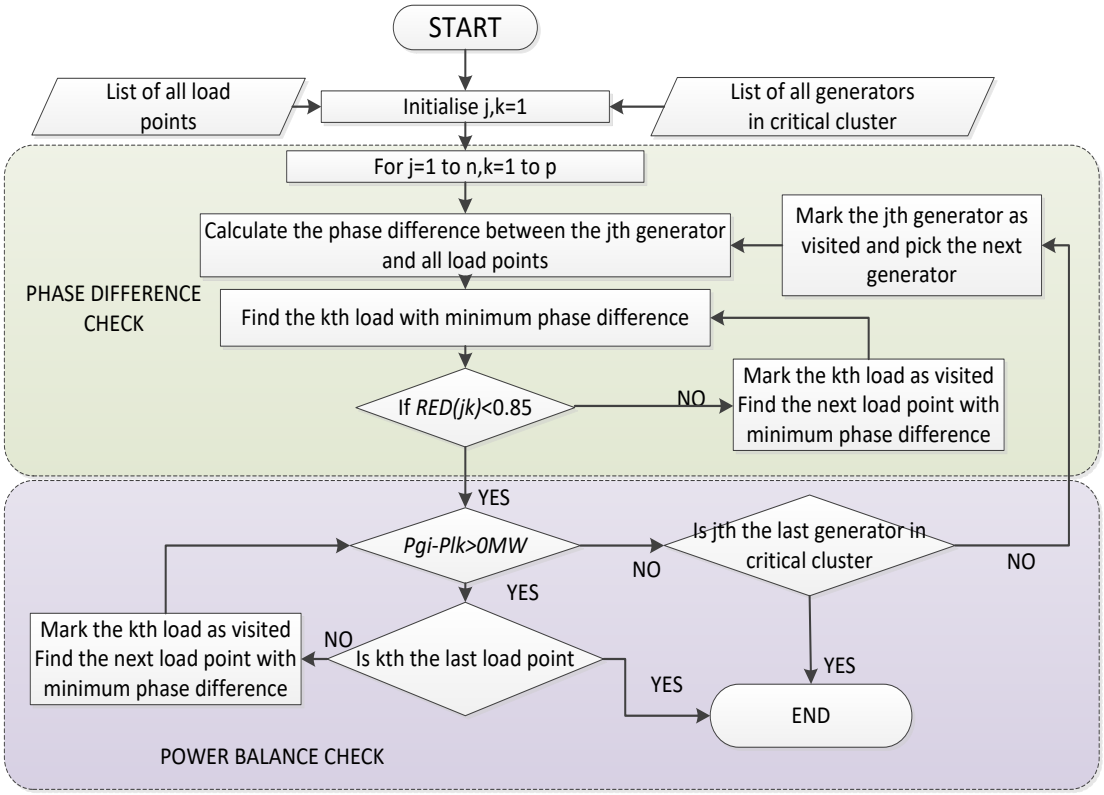

Figure 4.7.Load searching algorithm

However, during a disturbance event, the network configuration is subjected to changes with the removal of lines and transformers to clear faults, thus quick updating of the admittance matrix and thereby the matrix of RED values is necessary.

4.6.1 Updating the RED Matrix using Sparse Factor Updating Technique

With the changes in the network configuration caused due to tripping of branches, the system admittance matrix need to be updated by updating its factor matrices. This approach is much easier than reconstructing the updated matrix from the beginning. This will reduce the computation time and increase the efficiency of the algorithm. Sparse factor updating technique explained in [50][51] which use the property of the compensation method and partial matrix factorization can be considered as a straight forward approach for updating the admittance matrix. This approach is used in the controlled islanding method for the RED matrix updation as it can reduce the computation time and complexity of the algorithm. In the compensation technique [50], the new admittance matrix after including the network changes can be reconstructed by introducing a modification of the form

$$[\Delta Y] = [M] \cdot [\delta y] \cdot [M]^T \tag{4.15}$$

to the normal admittance matrix *Y*. Consider an example of a single line outage between buses *p* and *q*. The updated admittance matrix after the line removal can be obtained by subtracting, δy, representing the tripped line admittance, from the diagonal element Y_{pp} and adding the tripped line admittance to the off-diagonal elements Y_{pq} and Y_{qp}. The equation of the updated matrix, Y_{new} can be shown as:

$$\begin{aligned} [Y_{new}] &= [Y] + [\Delta Y] \\ [Y_{new}] &= Y + [M] \cdot [\delta y] \cdot [M]^T \end{aligned} \tag{4.16}$$

where M is a $(n \times l)$ matrix showing the network connection which is sparse in nature and M^T is the transpose of M, δy is a $(l \times l)$ diagonal matrix including the new updating

factor of *Y*, where *l* is the number of lines tripped resulting in the updation of the main matrix and *n* represents the number of buses in the network. *M* compose of 0s with the $p^{th}\ and\ q^{th}$ elements as +1 and -1 respectively. For example in the case of a 5 bus system, if a single line connecting bus 3 and bus 5 is tripped we can write the $[M]^T$matrix as [0 0 +1 0 -1].

4.7 Selection of Lines for System Splitting

Splitting of the islands is an important challenge, as the search space of line cut-sets grows considerably higher when the network becomes large and in satisfying the system constraints [52]. For example, for an *n*-bus system having *l* lines, total there will be 2^l possible choices for system splitting [53]. As a result, the search space becomes too large. Other than that speed and correctness of the search algorithm is important for implementing islanding. In literature, there are several methods proposed for identifying the boundaries of islands, i.e. selecting the transmission lines to be tripped for islanding the power network. Methods include exhaustive search (You,Vittal, Wang, 2004), minimal-flow minimal-cut set determination using search algorithms [55], heuristic methods [56][57], graph simplification and partitioning [53], and power flow tracing [58].

The systematic methods address the network separation problem based on mathematical principles. Those are not system bounded as it does not utilize the particular system information and experience. Moreover, the splitting strategy proposed by analytical methods doesn't fit the whole system and are specific for some critical lines. When compared to the systematic methods, the heuristic methods are considered to be more reliable and simpler for the network splitting problem. In the heuristic methods, proper

system knowledge and operational experience are needed for identifying the islands in the system. These kinds of search processes consider the generator capacity, line and load characteristics while planning the islands. The heuristic method has the advantage of lesser online calculation requirement for splitting. Due to time constraints, the lines to be tripped are decided by observation of the network and identified buses in the two islands.

4.8 Post-islanding Generator and Load Shedding

The simple generator and load shedding scheme proposed in this research relies on the frequency measurements at the generators and the load centers, and is sufficient to demonstrate the proposed controlled islanding concept. The main aim is to achieve load-generation balance, immediately after islanding the power system. Frequency of the island can be properly restored when the governor controls come into action. Furthermore, it is assumed that PMUs are installed at all major load centres enabling accurate frequency measurements. The over frequency generator tripping and under frequency load shedding algorithm is triggered immediately after the system is islanded when a frequency limit violation is observed. As the proposed scheme is centralized and time-critical, it is assumed that a dedicated communication network is available for sending signals to trip generators and loads.

A flow chart describing the frequency-based load and generator shedding scheme is shown in Figure **4.8**. The average frequency f_{isl}, of each island is determined from the frequency measurement obtained from the PMUs located at the generator and load terminals as

$$f_{\text{isl}} = \frac{1}{n'} \sum_{k=1}^{n'} f_k(t) \tag{4.17}$$

where $f_k(t)$ is the frequency of the k^{th} generator or load point in the island at time t and n' is the number of generators and loads in the island.

The algorithm recognizes that severe situations need extreme actions, and the severity is classified based on the average frequency f_{isl} into several levels. Three severity levels are recognized through three frequency settings defined such that $f_{set1} > f_{set2} > f_{set3}$ for generation rich islands. Likewise, another set of frequency thresholds is identified for the load rich islands denoted as $f_{set4} > f_{set5} > f_{set6}$.

For the generation rich islands, if the average system frequency is higher than the highest threshold f_{set1}, two units of generation will be tripped from all the generator stations in the island. For frequency setting higher than f_{set2}, one unit of generation will be tripped from all the generating stations in the island. And one unit of generation with the highest frequency variation will be tripped if the average frequency of the island goes above f_{set3}. A timer with pre-set duration is initiated after the first stage of tripping, to prevent further generator tripping until it is expired. The delay time is chosen to allow the power system to have enough time to respond the corrective action. After the first stage of tripping, if the island frequency is not recovered within the delay time, further generator tripping is performed as a second stage of operation, and the action is selected based on the observed average frequency of the island. The waiting-times associated with different frequency thresholds for generator tripping are different and are $t_{set1,}$ $t_{set2,}$ and t_{set3} respectively. These time settings are decided through offline studies and are highly dependent on the selected system. In the second stage of operation if the average frequency of the island remains in the same range following to the first stage of generator tripping one unit of generation from the generator with highest frequency variation is tripped.

The load shedding is also implemented considering three severity levels, defined by three low frequency thresholds: f_{set4}, f_{set5}, and f_{set6}. The locations for load shedding are selected based on the local frequency values reported by PMU's located at load centres ($f_l(t)$ at the l^{th} load). If the average frequency goes below f_{set6}, the locations with the three lowest frequencies are selected for shedding, and 50% of load at each of the three locations is shed under this severe frequency depression. If $f_{set5} < f_{\text{isl}} \leq f_{set6}$, two load centres with the lowest frequency are selected and only 50% of the load at each location is shed. If $f_{set4} < f_{\text{isl}} \leq f_{set5}$ only 50% of the load at the load centre with the lowest frequency is shed. As in the case of generator tripping, a time delay is introduced after each stage of load shedding to allow the power system to respond to the load shedding action before taking further control actions. The time delays are $t_{set4,}$ $t_{set5,}$ and t_{set6} respectively. The number of loads, frequency thresholds, and the time delay settings need to be selected system studies, as these settings are highly system dependent. The flow chart explaining the principle of the under-frequency load shedding scheme is shown in Figure **4.8**.

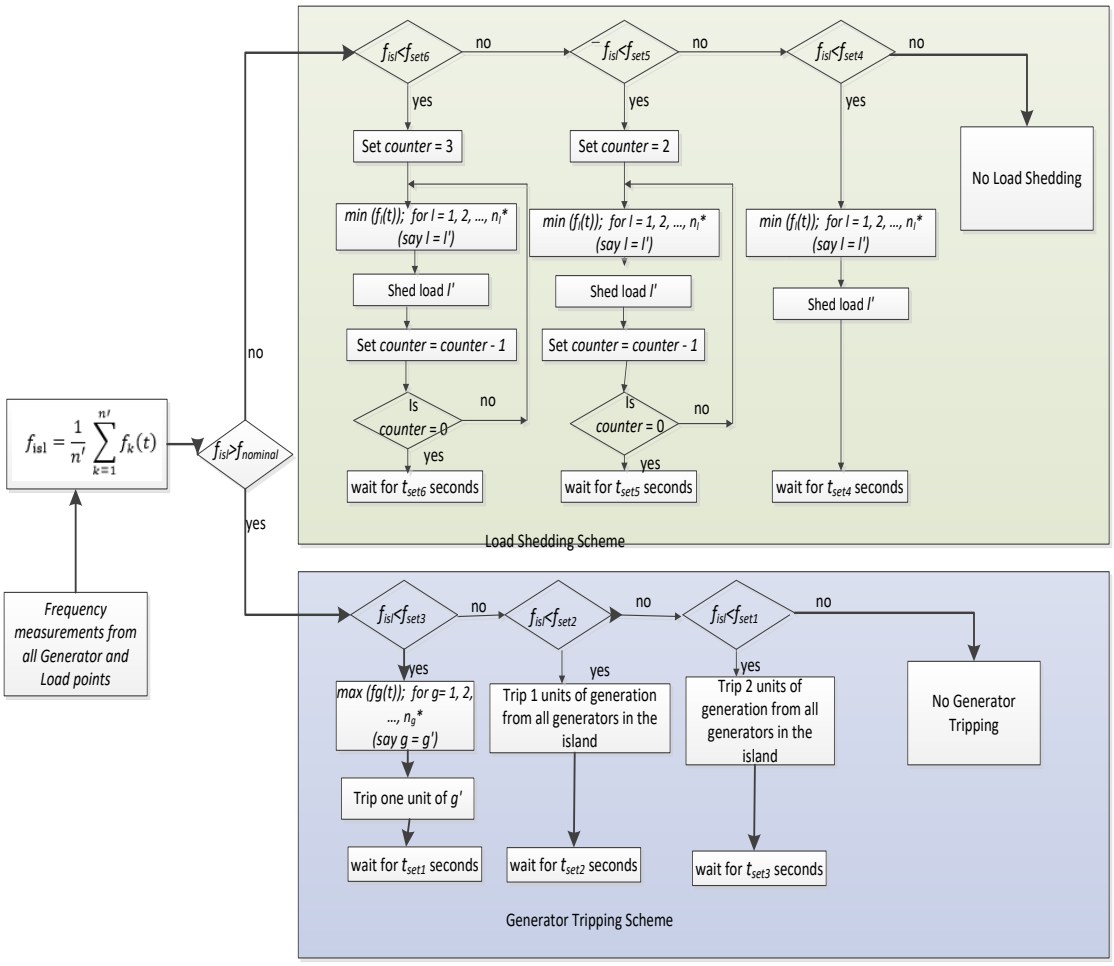

Figure 4.8. Over frequency Generator Tripping and Load shedding scheme

4.9 Case Study

An offline study was conducted for demonstrating the algorithm using the modified IEEE 39 bus test system introduced in Section 4.3. Different scenarios were simulated using the TSAT software, adopting a step-by-step approach to simulate the actions of the controlled islanding scheme. The simulated power system variables were entered to the emergency cotrollers, and then the system was re-simulated incorporating the responses of the control

scheme (actions and their timings) after every control action. Frequency settings and the corresponding waiting times of the scheme are given in Table **4.7** and Table **4.8** .

Table 4.7. Frequency settings of the generator tripping and load shedding scheme

Over Frequency Threshold range(Hz)			Under Frequency threshold range(Hz)		
f_{set1}	f_{set2}	f_{set3}	f_{set4}	f_{set5}	f_{set6}
62.5	61.5	60.5	59.75	59.5	59

Table 4.8.Waiting time settings

Over Frequency Waiting time(ms)			Under Frequency Waiting time(ms)		
t_{set1}	$t_{set2,}$	t_{set3}	t_{set4}	t_{set5}	t_{set6}
1000	800	500	1000	800	500

4.9.1 Scenario 1-Fault on Line 2-25 (at 50% from bus 2)

In Scenario 1, Line 2-25 (at 50% of the length) was subjected to a three-phase to ground fault at t = 0.1 s and cleared by tripping the faulted line after 6 cycles. The post-fault variations of the rotor angle and generator terminal voltage are shown in Figure **4.9**. Using the generator terminal voltage magnitude data following the fault clearance, the coherent generator clusters identification technique recognized two clusters of generators. The first coherent generator cluster comprised of the generators Gen 37 and Gen 38; and the second coherent generator cluster comprised of the remaining seven generators.

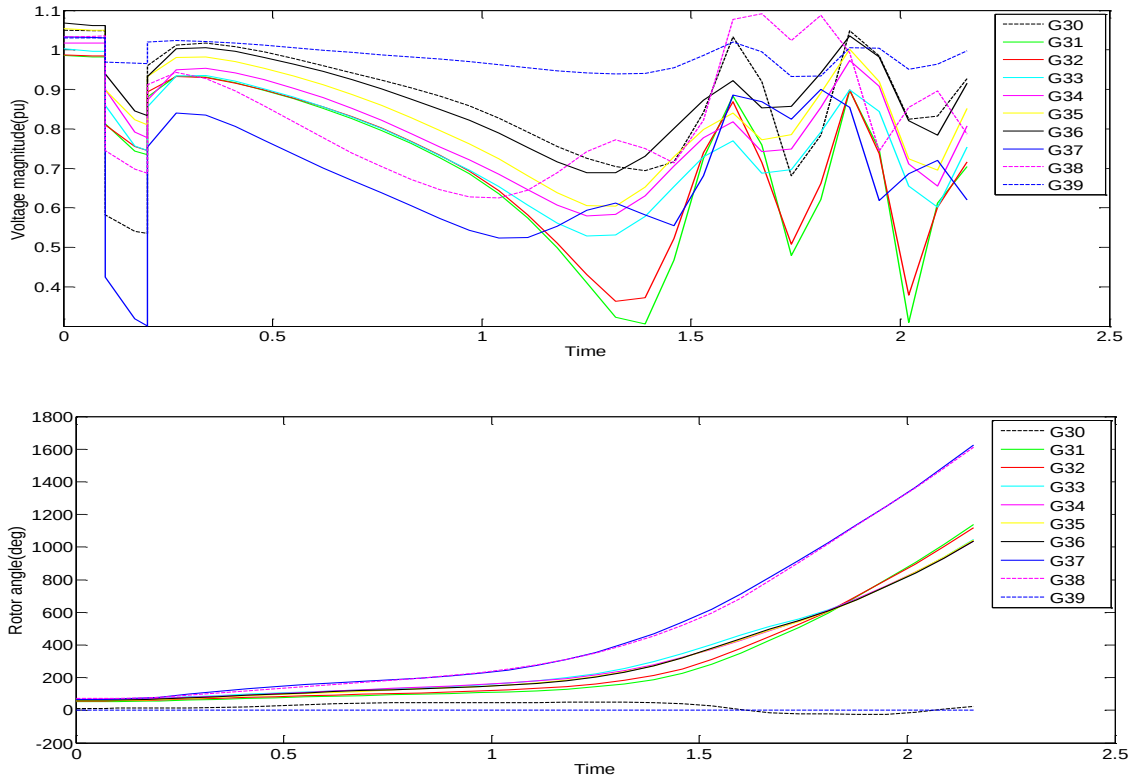

Figure 4.9 Post fault voltage and rotor angle variations of the generators for fault on line 2-25

The distance matrix elements, I_{pq} for this case are given in Table **4.9**. These values clearly show that the generators Gen 37 and Gen 38 are in a different group.

Table 4.9.Matrix of distances between generator voltage trajectories for Scenario 1

	G30	G31	G32	G33	G34	G35	G36	G37	G38	G39
G30	0	0.089011	0.08446	0.08789	0.05536	0.01751	0.00250	0.47792	0.19465	0.01305
G31	0.08901	0	0.00025	0.00070	0.00487	0.02794	0.06311	0.15490	0.02802	0.16123
G32	0.08446	0.00025	0	0.00152	0.00474	0.0254	0.05973	0.16220	0.02989	0.15362
G33	0.08789	0.00070	0.00152	0	0.00384	0.02810	0.06152	0.15684	0.03333	0.16129
G34	0.05536	0.00487	0.00474	0.00384	0	0.01162	0.03482	0.20934	0.0527	0.11705
G35	0.01751	0.02794	0.02543	0.02810	0.01162	0	0.00764	0.31392	0.09690	0.05689
G36	0.00250	0.06311	0.05973	0.06152	0.03482	0.00764	0	0.41403	0.15777	0.02641
G37	0.47792	0.15490	0.16220	0.15684	0.20934	0.31392	0.41403	0	0.08151	0.63037
G38	0.19465	0.02802	0.02989	0.03333	0.05274	0.09690	0.15777	0.08151	0	0.29436
G39	0.01305	0.16123	0.15362	0.16129	0.11705	0.05689	0.02641	0.63037	0.29436	0

The transient stability prediction module, which use the same input data as the coherent generator group identification algorithm, detected an impending instability around 0.8 sec and determined that the generator at bus 37 will become out-of-step first. The plots of the

trajectories of generators 37 and 38 on ROCOV−ΔV plane shown in Figure **4.10** illustrates this.

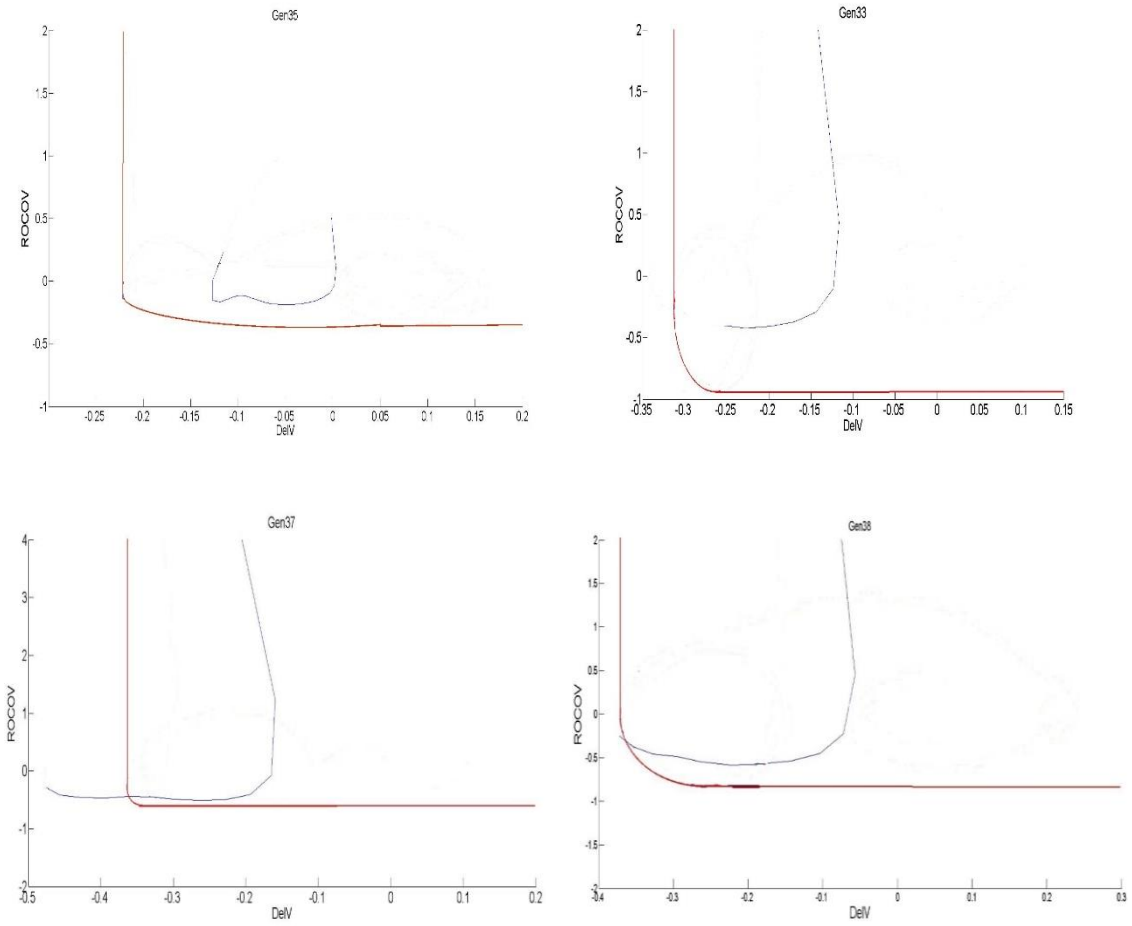

Figure 4.10 ROCOV-ΔV trajectory of Gen 37 and Gen 38 for fault on line 2-25

Since the system is going to be unstable, the emergency controller decided to separate the system into two islands, involving the two coherent generator groups. The generator at bus-37, which is becoming unstable first, belonged to the first coherency cluster, and therefore, this coherency cluster was categorized as the critical cluster.

The next step is to allocate the load buses into two islands, considering the phase angle differences and the relative electrical distances (REDs). The phase angle differences

between the load points and the generators in the critical island (immediately after detecting the instability) are shown in Figure **4.11**. The matrix containing RED values was updated to reflect the topology change due to removal of line to clear the fault before starting the search. The threshold value of RED that is used to determine whether a load bus belonging to a given coherency cluster was set as 0.85 based on the system studies. The load points with RED values with respect to Gen 37 and Gen 38 are shown in Table **4.10**.

From the RED values we can observe that the relative electrical distance from the generator points are higher for some load points even though their phase difference values are in a smaller range like as for Load 19.

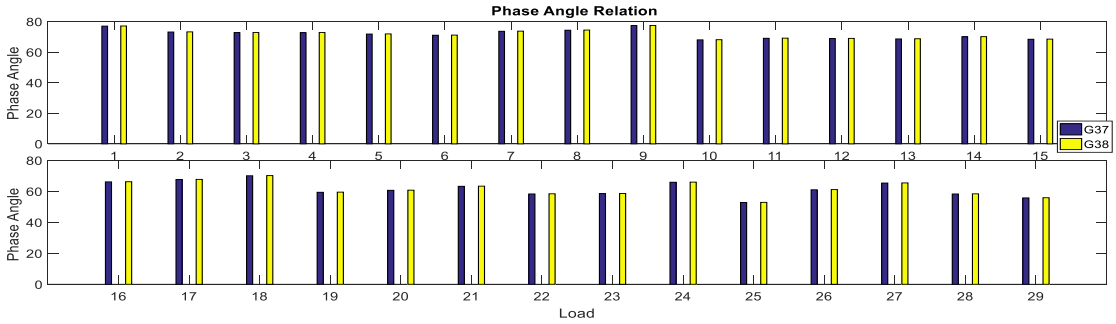

Figure 4.11 Phase angle differences between load points and the critical generators for a fault on line 2-25

Table 4.10. RED values of load points with critical generators for a fault on line 2-25

Load (RED to Gen 37)	Load (RED to Gen 38)
Load 25 (0.287)	**Load 29(0.203)**
Load 26(0.696)	**Load 28(0.304)**
Load 27(0.793)	**Load 26(0.636)**
Load 28(0.848)	**Load 27(0.752)**
Load 29(0.897)	**Load 25(0.847)**
Load 19(0.977)	Load 19(0.973)

The load selection process was implemented based on the depth searching algorithm explained in Section **4.6**. The whole process can be explained with this example. In this case, load 25 and load 29 are added in the first level of search since those loads are having

the minimum phase angle difference with respect to Gen37 and Gen38. In the second search level, load 28 and load 26 were included. Load 27 was added in the third depth. After three depths of load searching, loads 25, 29, 28, 26 and 27 were grouped with Gen 37 and Gen 38 to form Island 1. The critical island is shown in Figure **4.12**.

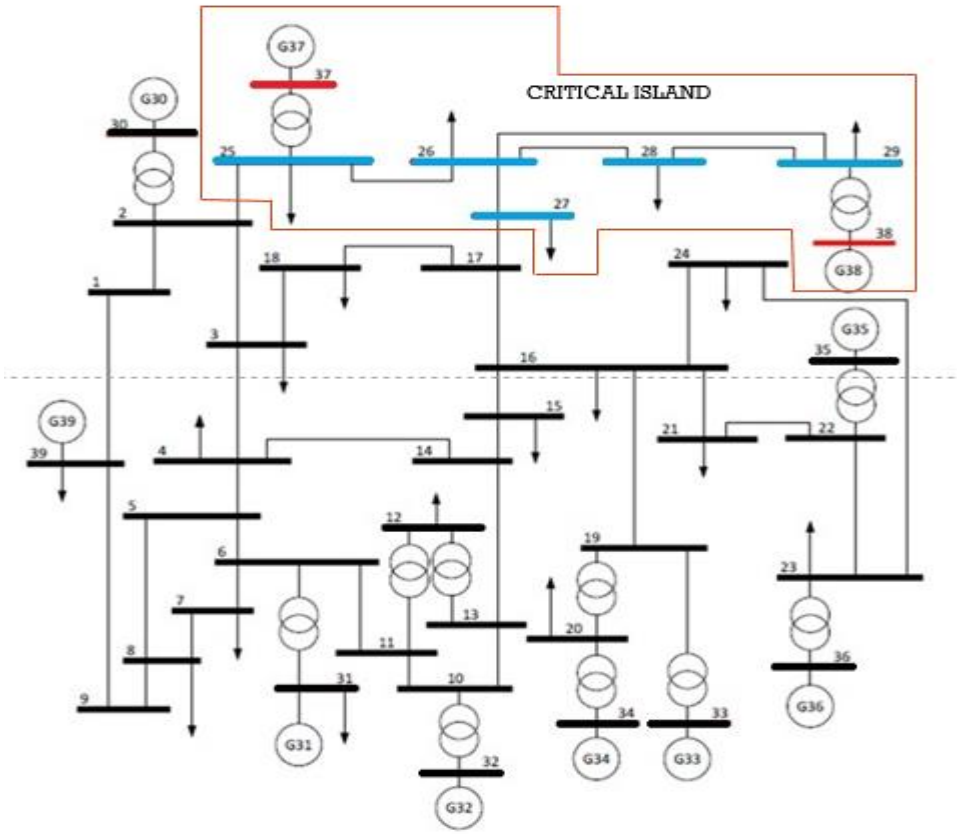

Figure 4.12. Critical island identified after clearing fault on line 2-25

The rest of the generators and the load buses formed Island 2. With the help of the search algorithms, we can identify the transmission lines that are required to be tripped to separate the system into two islands. In this research, the lines were selected from observations. Line 27-17 and Line 27-17 were identified as the lines to be tripped for islanding the power system. Lines were tripped at t = 0.88s to form the islands.

The frequency variations of the buses in islands 1 and 2 after splitting the system is shown in Figure **4.13**. The frequencies in both islands are increasing, if no further action is taken.

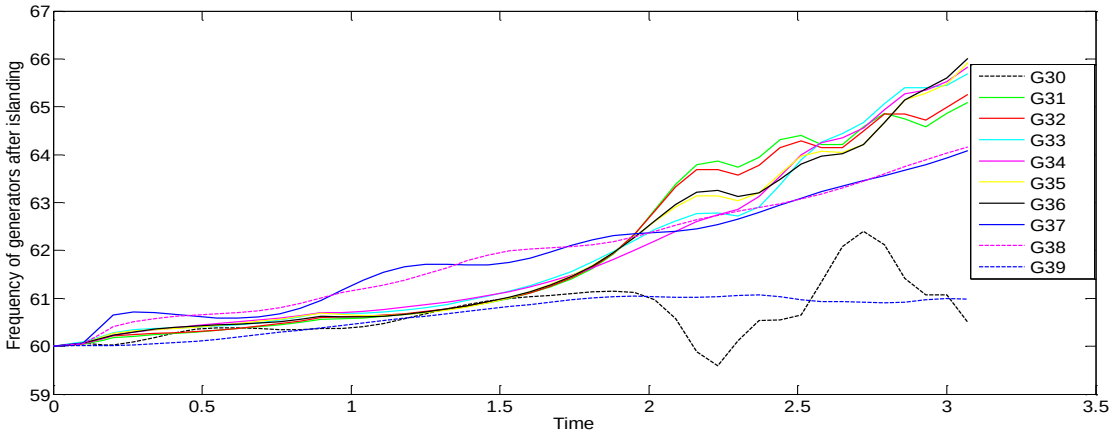

Figure 4.13. Frequency variation after islanding for a fault on line 2-25

At t = 0.91 s the system frequency rose above 60.5 Hz for both islands 1 and 2 and consequently, a signal was issued to trip one unit of generation at Gen 38, Gen 36, Gen 34, Gen 35 and Gen 33, as these generator frequencies were greater than the average island frequency. After the waiting time, t_{set3}, the frequency of island 1 was still above 60.5 Hz; hence, a signal was issued to trip another unit of generation at Gen 38. As the system frequency did not improve after the second generator tripping the third signal was issued to trip another unit of generation at Gen 38. After the generator tripping in island 1, it was observed that the frequency of island 1 drops below 59.75 Hz around t = 5.2 s. In order to maintain the generation and load demand balance, and to restore the island frequency, 50% of load at Bus 25, which had the lowest frequency, was tripped. Further load shedding was initiated in island 1 by reducing 50% load at Bus 28 and Bus 26 around t = 5.7sec as the frequency dropped below 59.5Hz. After the load tripping, the frequency of island 1 was observed as recovering as shown in Figure **4.14**.

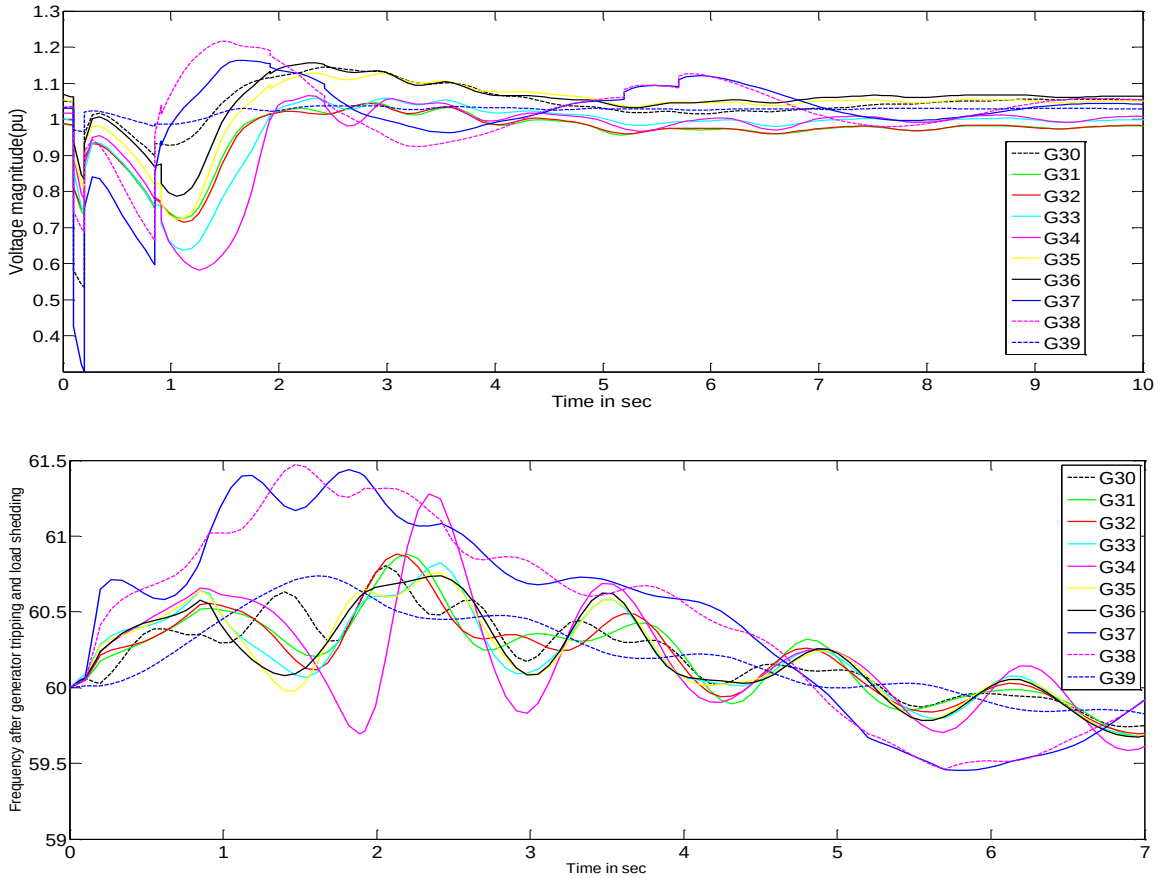

Figure 4.14. Voltage and the frequency variation of generators after implementing generator tripping and load shedding scheme for a fault on line 2-25

For island 2, after the first step of generator tripping it is observed that after the waiting time of t_{set3}, the generator frequency was still above 60.5Hz. Further generator tripping was initiated around t = 1.91sec by tripping one unit of generation at Gen 35. One unit of generation from the highest frequency generator, Gen 34 was tripped as a final step resort to recover the frequency at t = 2.42sec. After the generator tripping, it was observed that the frequency of island 2 drops was recovered. The voltage and the frequency variations of generators in the system followed by the process is shown in Figure **4.14**. It was expected that generator governor control can stabilize the system frequency after these generator

tripping and load shedding steps. The sequence of events and control actions followed by the fault are summarized in Table **4.11**.

Table 4.11. Sequence of emergency control operation for Scenario 1

Time	Event/Control Action
t = 0.1 s	Fault occurrence
t = 0.2 s	Fault clearance
t = 0.2 s	Initiate Transient stability prediction and coherent group identification algorithm
t = 0.533 s	Coherent generator groups identified
t = 0.8 s	System declared as unstable, Initiated islanding operation
t = 0.91 s	Generator tripping in Island 1 and 2
t = 2.42 s	Generator tripping in Island 2
t = 5.2 s	Load tripping island 1
t = 5.7 s	Load tripping island 1

4.9.2 Scenario 2 - Fault on Line 26-29 (at 25% from bus 26)

Line 26-29 (at 25% of the length) was subjected to a three-phase to ground fault at 0.1 seconds. After 6 cycles the fault was cleared by tripping the line. The post-fault variations of the generator rotor angles and the terminal voltage are shown in Figure **4.15**. After the fault was removed by tripping the line, the proposed coherent generator clusters recognition algorithm recognized two clusters: the first coherent generator cluster comprised the generators at bus 38 and the second cluster comprised of the remaining eight generators as can be seen from $\mathbf{I_{pq}}$ values shown in

Table 4.12. The transient stability prediction module detected an impending instability at t = 0.8 s and determined that the generator at bus 38 will become out-of-step first. A plot showing the trajectory of the generator at bus-38 on **ROCOV**–**ΔV** plane is shown in

Figure 4.16. The generator at bus-38 belonged to the first coherency cluster, and therefore, this coherency cluster was categorized as the critical cluster.

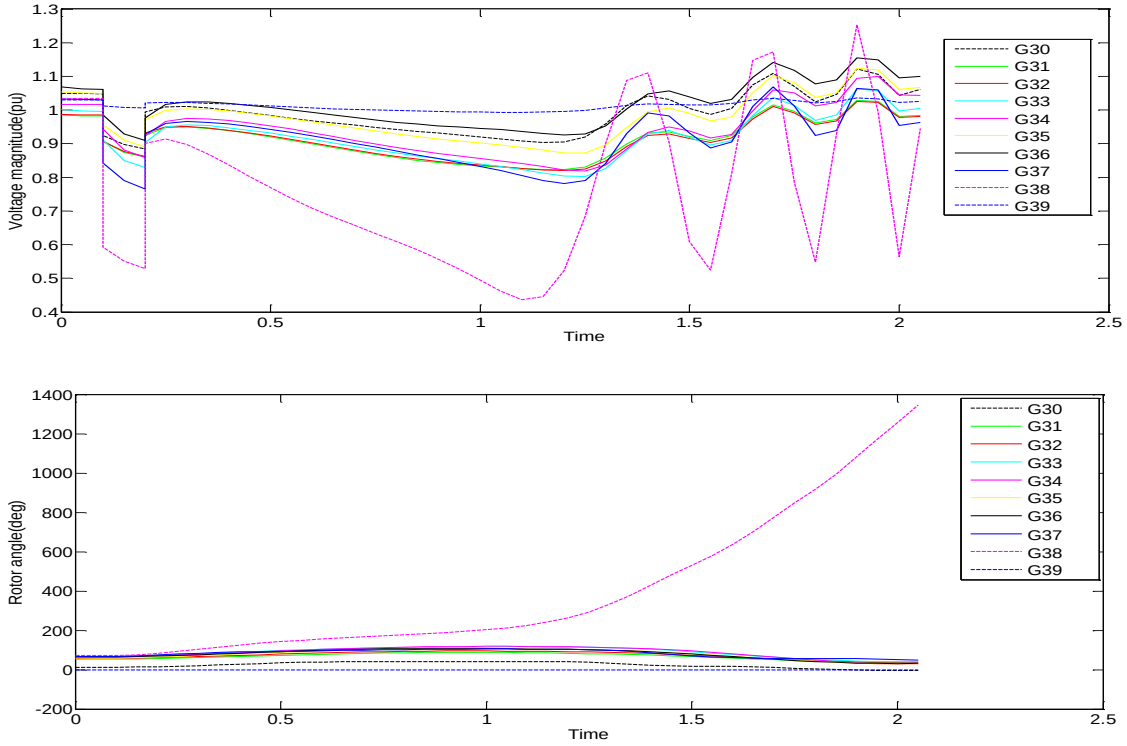

Figure 4.15 Post fault voltage and rotor angle variations of generators for fault on line 26-19

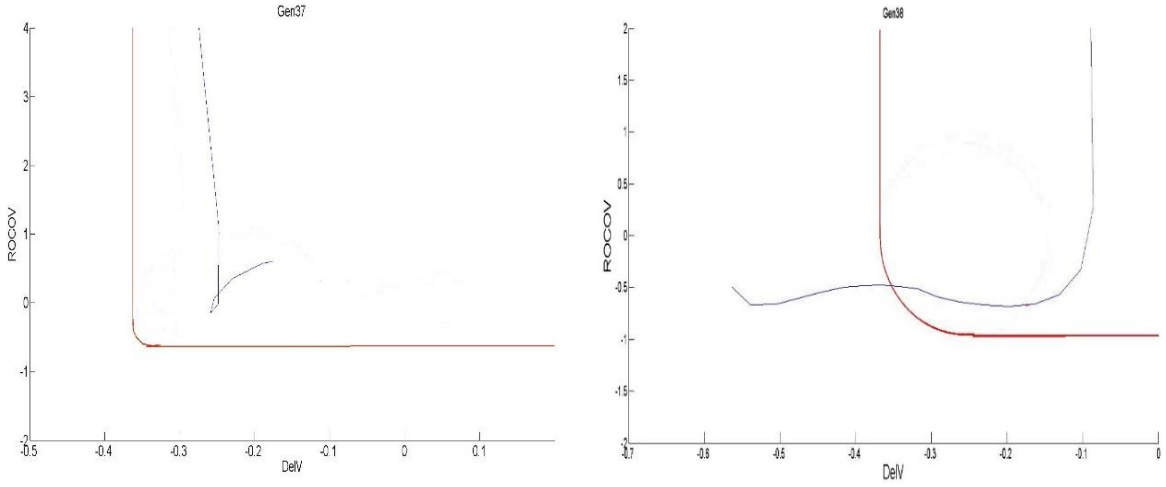

Figure 4.16 ROCOV-Δ*V* trajectory of Gen 38 for fault on line 26-29

Table 4.12. Matrix of distances between generator voltage trajectories for Scenario 2

	G30	G31	G32	G33	G34	G35	G36	G37	G38	G39
G30	0	0.048172	0.044607	0.04213	0.01872	0.0008	0.00535	0.03922	0.57602	0.0240
G31	0.04817	0	9.94E-05	0.00242	0.00897	0.04012	0.07891	0.01328	0.32778	0.1184
G32	0.04460	9.94E-05	0	0.00257	0.00794	0.03702	0.07465	0.01301	0.33594	0.1126
G33	0.04213	0.00242	0.002573	0	0.00520	0.03428	0.06933	0.00598	0.3394	0.1148
G34	0.0187	0.00897	0.007945	0.00520	0	0.01308	0.03692	0.00990	0.42032	0.072
G35	0.00085	0.04012	0.037023	0.03428	0.01308	0	0.00671	0.03415	0.55947	0.0271
G36	0.00535	0.07891	0.074655	0.06933	0.03692	0.00671	0	0.06636	0.68238	0.0124
G37	0.03922	0.01328	0.013018	0.00598	0.00990	0.03415	0.06636	0	0.33642	0.1206
G38	0.57602	0.32778	0.335943	0.3394	0.42032	0.55947	0.68238	0.33642	0	0.8141
G39	0.02401	0.11840	0.112616	0.11480	0.0724	0.02713	0.01245	0.12062	0.81413	0

The phase difference between the critical generator and the load points, which were used for allocating the loads to islands are shown in Figure **4.17**. After recognizing the loads with lower phase angle with the generator in critical cluster, RED values were updated to reflect the change in topology due to faulted line. The REDs between Gen 38 and load points is given in Table **4.13**.

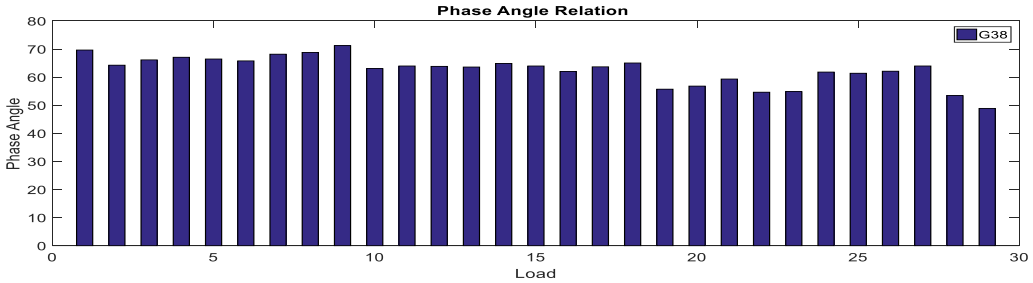

Figure 4.17 Phase angle differences between the load points and critical generator for a fault on line 26-29

Table 4.13. RED values of load points with critical generators for a fault on line 26-29

Gen 38(RED to Gen38)
Load 29(0.147)
Load 28(0.293)
Load 26(0.765)
Load 27(0.837)

Load 22(0.984)
Load 19(0.9812)

Then the depth search process was applied to select the loads for the two islands.After four steps in the search process, loads 29, 28, 26 and 27 were grouped with Gen 38 to form Island 1. It is observed that the load points 19 and 22 are also having smaller phase angle difference but their RED values are higher than the threshold. This island, which is the critical island for this case, is shown in Figure **4.18**. The rest of the generators and the load buses will form Island 2. Lines 27-17 and 26-25 were identified as the lines needed to be tripped for separating system in to two islands.

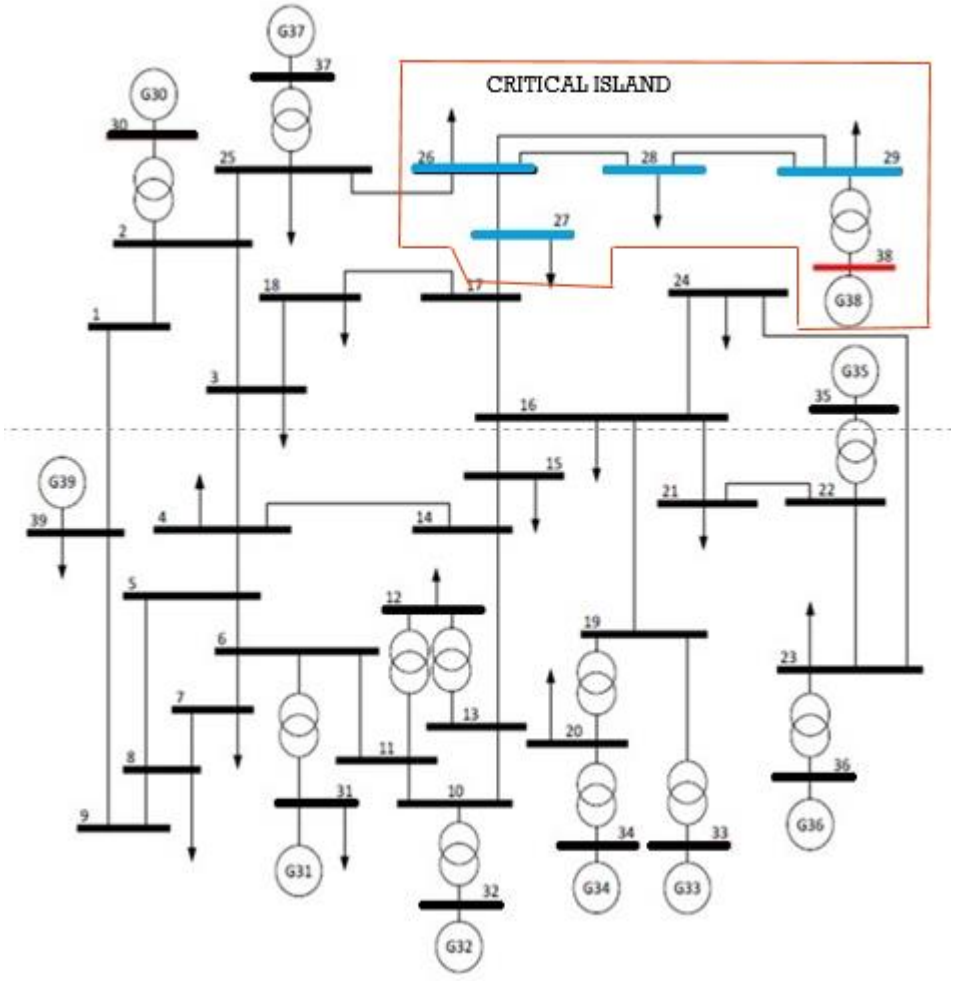

Figure 4.18.Critical island formed after clearing fault on line 26-29

The frequency variations of the generators after splitting the system are shown in Figure **4.19**.

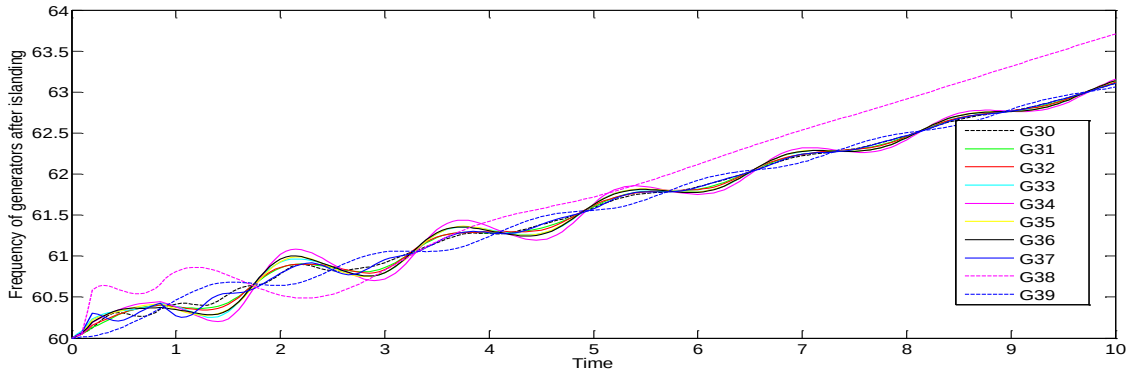

Figure 4.19.Frequency variation after islanding for fault on line 26-29

At t = 0.91 s, it was detected that the system frequency rised above 60.5 Hz for Island 1, a signal was issued to trip one unit of generation at Gen 38, as the generator frequency was higher than the average frequency of the island. After the tripping of the generator unit, it was observed that the frequency of island 1 drops below 59.75 Hz around t = 1.65 s. Therefore, to balance the generation and demand, and to restore the frequency, 50% of Load 27, which has the lowest frequency was shed. After the waiting time, t_{set4} it was observed that the system frequency of island 1 has dropped further, below 59.5Hz. Hence, a signal was issued to shed load 27 completely and 50% of load 26. However, the island frequency went further down, falling below 59 Hz. At this point, a signal was issued to shed load 26 completely and 50% of loads 28 and 29.

For island 2, it was observed that around t = 1.6 s, the generator frequency was above 60.5Hz. One unit of generation from the generators with the highest frequency values, Gen 30, Gen 39 and Gen 37, was tripped at that point. After the waiting time of t_{set3}, the frequency was observed to be recovering. Further generator tripping was initiated at t = 3.1 s as the frequency started to move above 60.5 Hz. One unit of generation from Gen 34 was

tripped at that time, as it was observed to have a frequency higher than the average frequency of the island. At t =3.9 s the average frequency of island 2 remained around 60.5 Hz initiating further generator tripping. One unit of generation from Gen 39 was reduced at this point to restore the island frequency. The voltage magnitude and the frequency of the generators in the system after the implementation of frequency-based generator tripping and load shedding scheme is shown in Figure **4.20**.

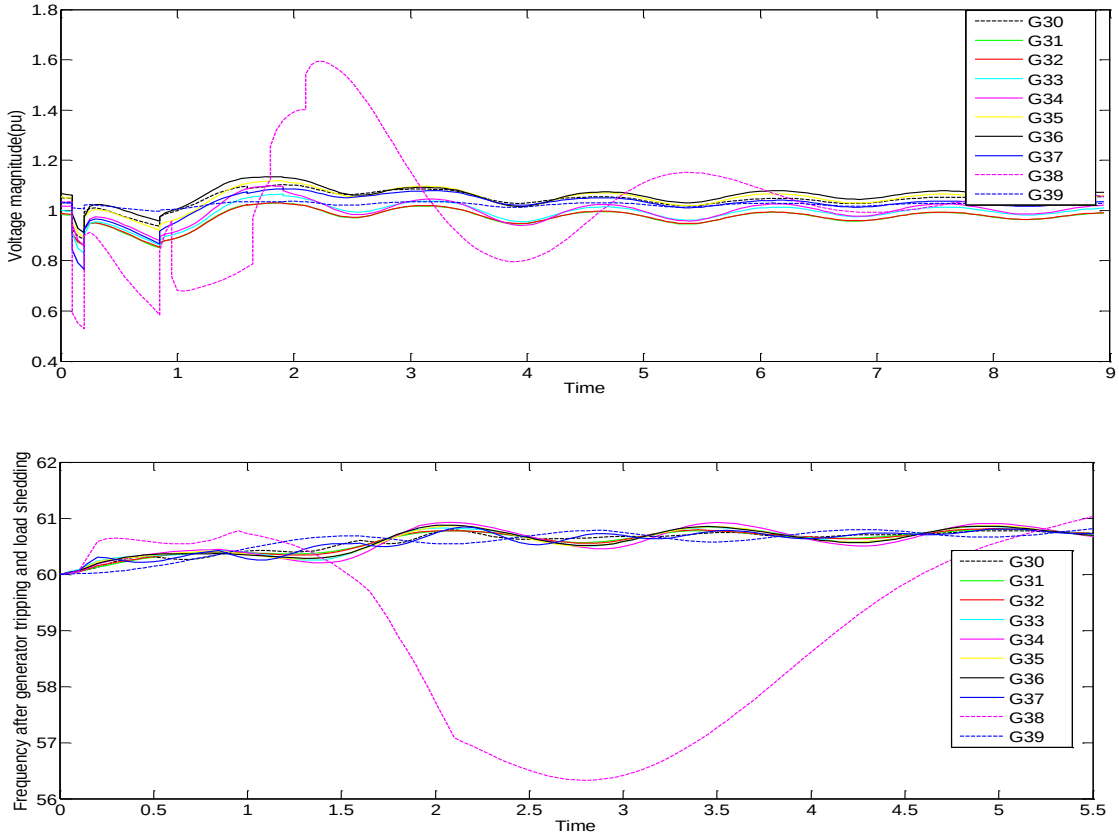

Figure 4.20. Voltage magnitude and frequency variations after implementing generator tripping and load shedding for a fault on line 26-29

4.9.3 Scenario 3 - Fault on Line 16-17 (near bus 16)

A three-phase to ground fault was applied on line 16-17 at t = 0.1 s and the fault is cleared by removing the line after 6 cycles. The post-fault variations of the generator rotor angles and voltage magnitudes are shown in Figure **4.21**.

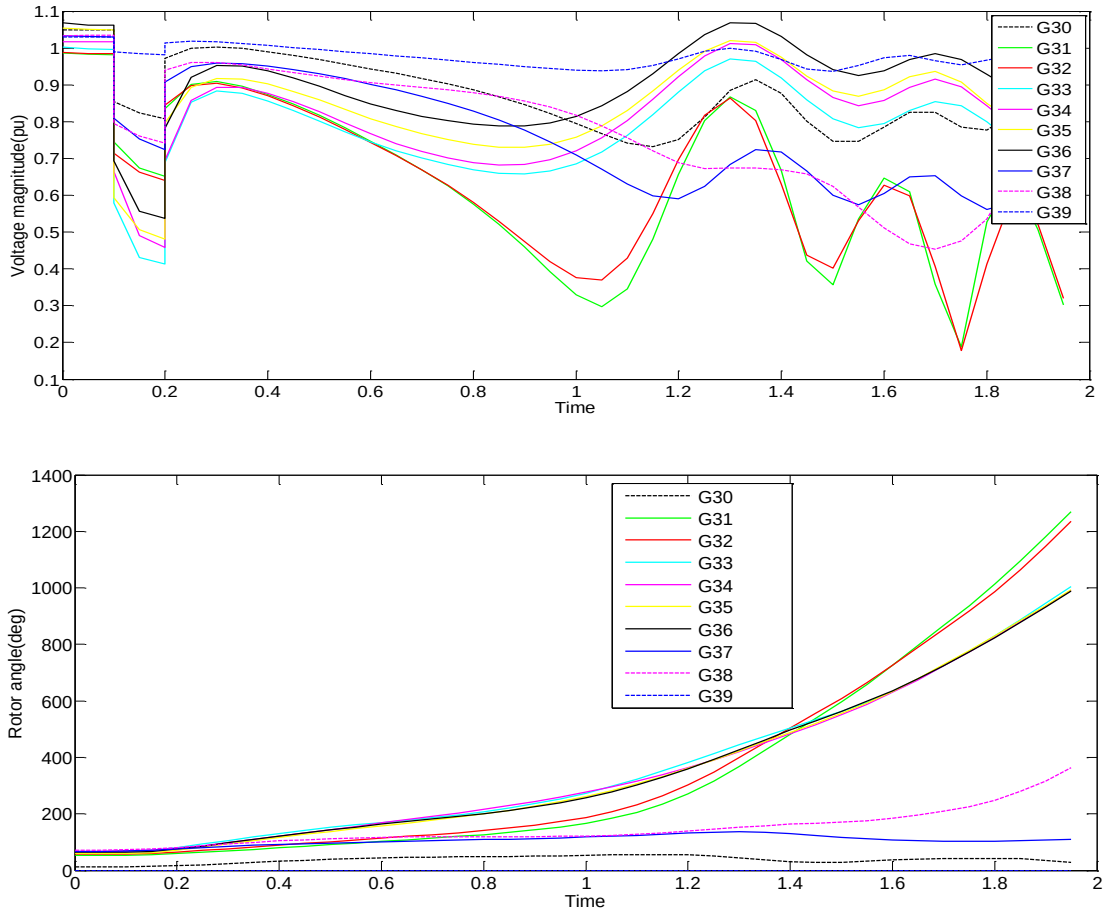

Figure 4.21 Post fault voltage and rotor angle variations of generators for fault on line 16-17

Many of the generators get disturbed due to the fault, and the coherent generator groups are not clearly visible as in the previous two cases, until the separation between rotor angles are very large. However, the proposed coherency cluster recognition technique recognized two clusters, at the time it predicted the impending instability, that is around t = 0.95 s. The first coherent generator cluster comprised of generators at bus 31, bus 32, bus 33, bus

34, bus 35 and 36 where as the second coherent generator cluster comprised of the remaining four generators. The corresponding I_{pq} values are given in Table **4.14**.

Table 4.14 Matrix of distances between generator voltage trajectories for Scenario 3

	G30	G31	G32	G33	G34	G35	G36	G37	G38	G39
G30	0	0.35812	0.36440	0.41217	0.33625	0.18538	0.14032	0.02495	0.01766	0.01639
G31	0.3581	0	0.00025	0.03028	0.03403	0.04331	0.08793	0.20543	0.24149	0.52571
G32	0.3644	0.00025	0	0.03235	0.03719	0.04634	0.09204	0.21031	0.24551	0.53266
G33	0.4121	0.03028	0.03235	0	0.00495	0.04533	0.08173	0.23725	0.27696	0.58627
G34	0.3362	0.03403	0.03719	0.00495	0	0.02400	0.05269	0.18089	0.21757	0.49423
G35	0.1853	0.04331	0.04634	0.04533	0.02400	0	0.01280	0.07604	0.10025	0.30803
G36	0.1403	0.08793	0.09204	0.08173	0.05269	0.01280	0	0.05162	0.06734	0.24359
G37	0.0249	0.20543	0.21031	0.23725	0.18089	0.07604	0.05162	0	0.00358	0.07859
G38	0.0176	0.24149	0.24551	0.27696	0.21757	0.10025	0.06734	0.00358	0	0.06038
G39	0.0163	0.52571	0.53266	0.58627	0.49423	0.30803	0.24359	0.07859	0.06038	0

The transient stability prediction module predicted an impending instability after clearing the fault and determined that the generators at bus 31 and 32 will become out-of-step first. The generator at bus-31 and bus 32 belonged to the first coherency cluster, and therefore, this coherency cluster was categorized as the critical cluster.

As the system is becoming transiently unstable, it was decided to split the sysem into islands. The loads were assigned to the two identified generator clusters as in the previous cases, using phase angle differences and RED values. The phase angle differences between the load points and critical group of generators are shown in Figure **4.23**. The load points with RED values for Gen 31, Gen 32, Gen 33, Gen 34, Gen 35 and Gen 36 are shown in Table **4.15**.

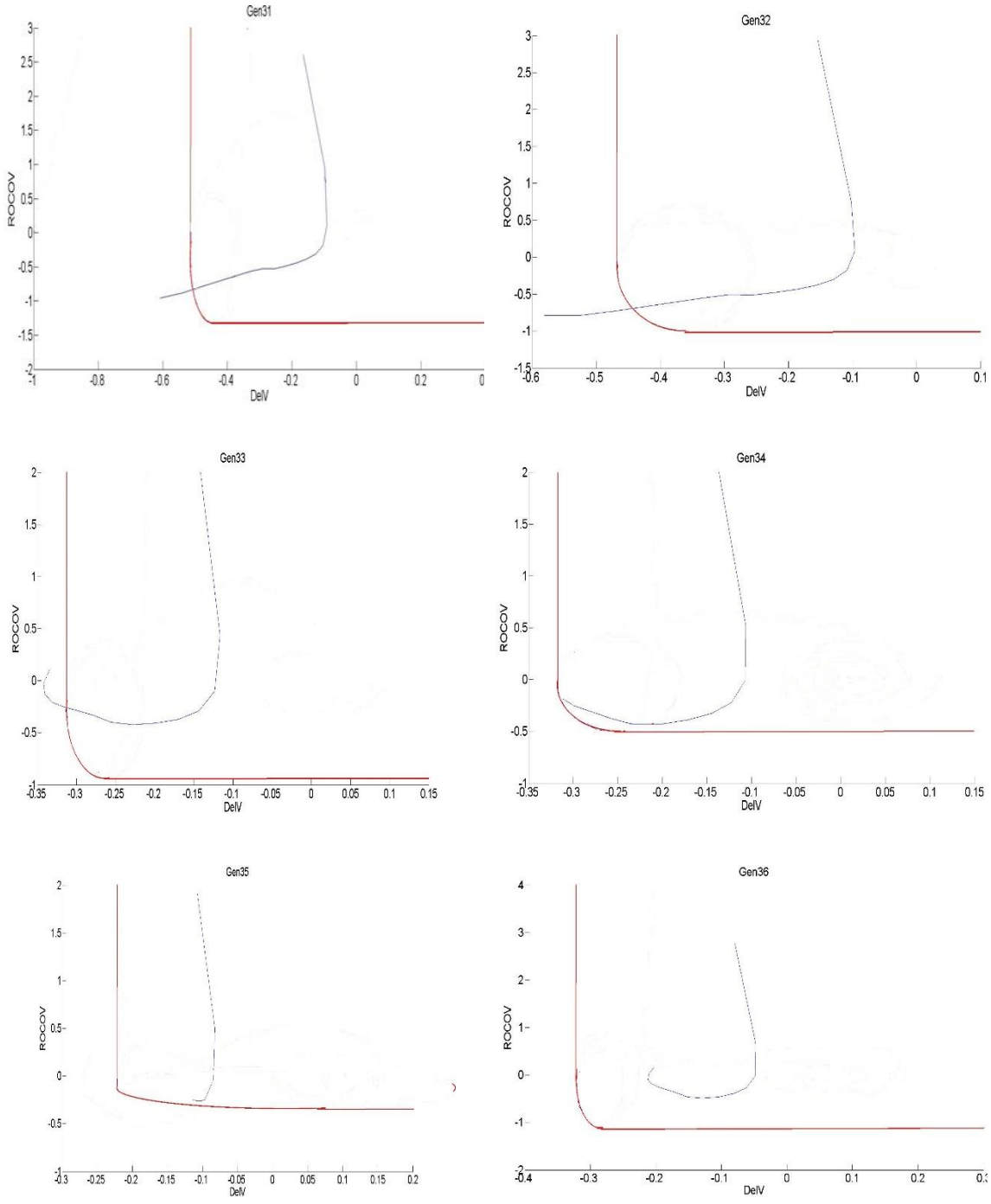

Figure 4.22 ROCOV-Δ*V* trajectory of Gen 31, Gen 32, Gen 33, Gen 34, Gen 35 and Gen 36

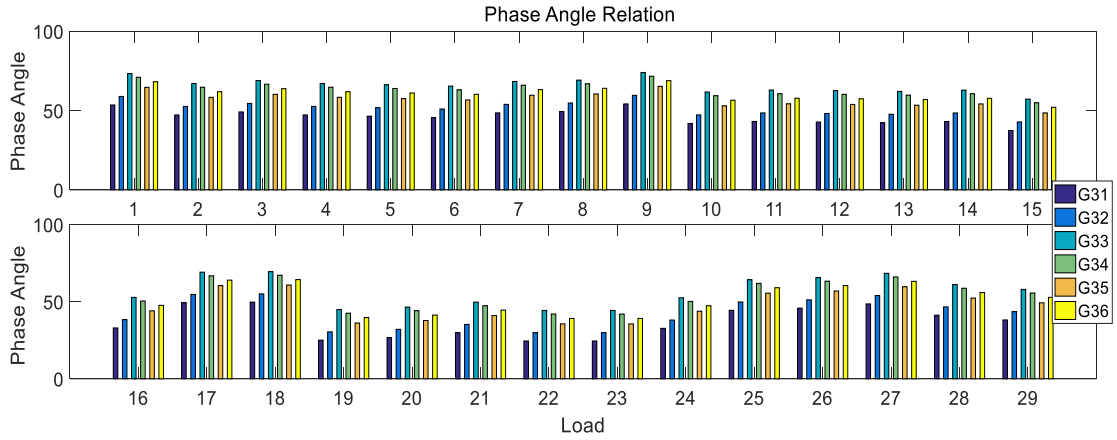

Figure 4.23 Phase angle difference between load points and critical generators for a fault on line 16-17

Table 4.15.RED values of load points with critical generators for a fault on line 16-17

Gen 31	Gen 32	Gen 33	Gen 34	Gen 35	Gen 36
Load 10(0.784)	**Load 15(0.839)**	**Load 19(0.280)**	**Load 20(0.000)**	**Load 23(0.588)**	**Load 23(0.617)**
Load 13(0.787)	**Load 10(0.534)**	**Load 21(0.77)**	Load 21(1.00)	**Load 22(0.413)**	**Load 22(0.783)**
Load 12(0.761)	**Load 13(0.583)**	**Load 24(0.694)**	-	**Load 21(0.567)**	**Load 21(0.814)**
Load 11(0.7344)	**Load 12(0.592)**	**Load 16(0.665)**	-	**Load 24(0.6978)**	**Load 24(0.8116)**
Load 14(0.802)	**Load 14(0.650)**	**Load 15(0.731)**	-	**Load 16(0.716)**	**Load 16(0.8445)**
Load 6(0.6344)	**Load 11(0.600)**	Load 23(0.874)	-	**Load 15(0.773)**	Load 14(0.9041)
Load 5(0.6604)	**Load 6(0.730)**	Load 28(0.993)	-	Load 27(0.983)	Load 12(0.97)
Load 4(0.7669)	**Load 5(0.740)**	Load 25(0.982)	-	Load 29(0.996)	Load 10(0.9729)
Load 7(0.6647)	**Load 4(0.754)**		-	Load 9 (0.984)	Load 28(0.996)
Load 8(0.680)	**Load 7(0.750)**		-	Load 5(0.957)	Load 27(0.99)
Load 15(0.90)	**Load 8(0.0.758)**		-	Load 19(0.88)	Load29(0.998)

According to the load search algorithm here the search process terminated after 5 depths as the no more load points with RED value below the threshold value was identified. The load points; load10, load 15, load 19, load 20, load 23, load 22, load 13, load 12, load 21, load 24, load 16, load 11, load 14, load 6, load 5, load 4 and load 7 were grouped with Gen 31,Gen 32,Gen 33,Gen 34,Gen 35 and Gen 36 to form Island 1. This was the critical island, because the generators at buses 31 and 32 were the first to become out-of-step. The critical island is identified is shown in Figure **4.24**.

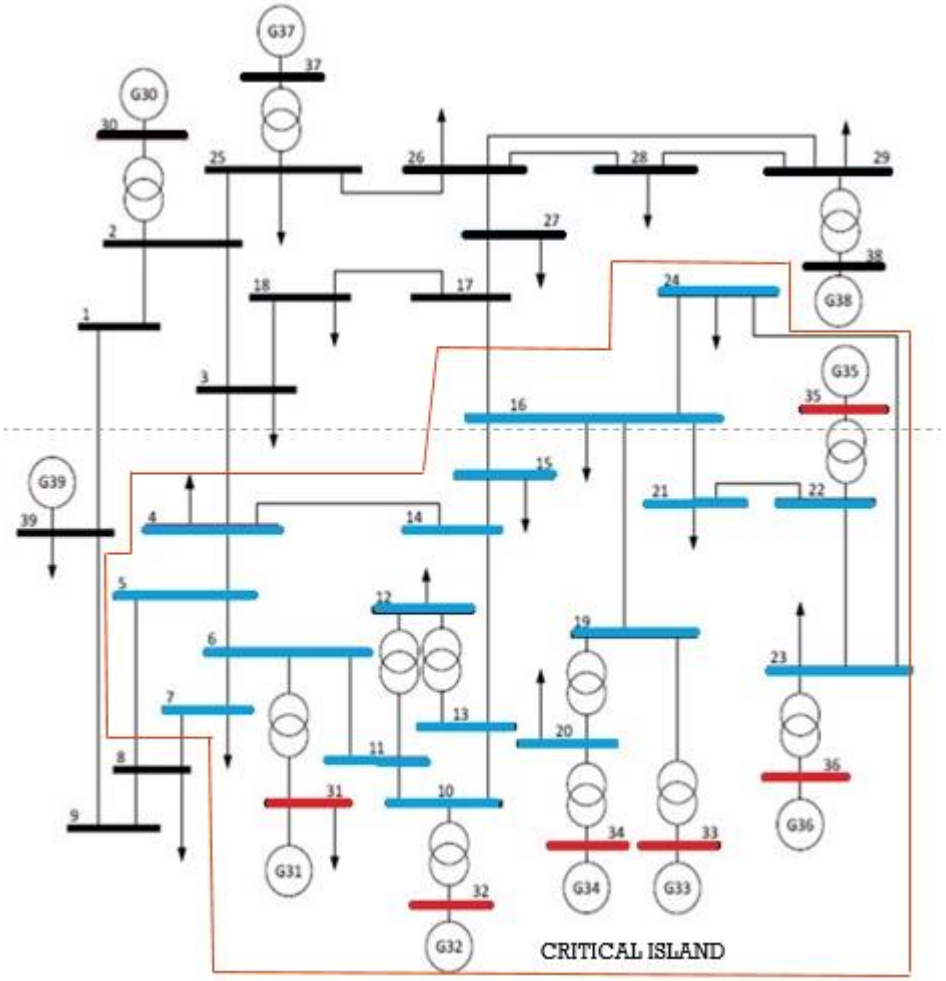

Figure 4.24. Critical island formed after clearing fault on line 16-17

Island-2 consisted of the rest of the generators and the load buses. Lines 7-8, 8-5 and 3-4 were identified as the lines to be tripped for islanding the power system. The variations of frequency of the generators is shown in Figure **4.25**.

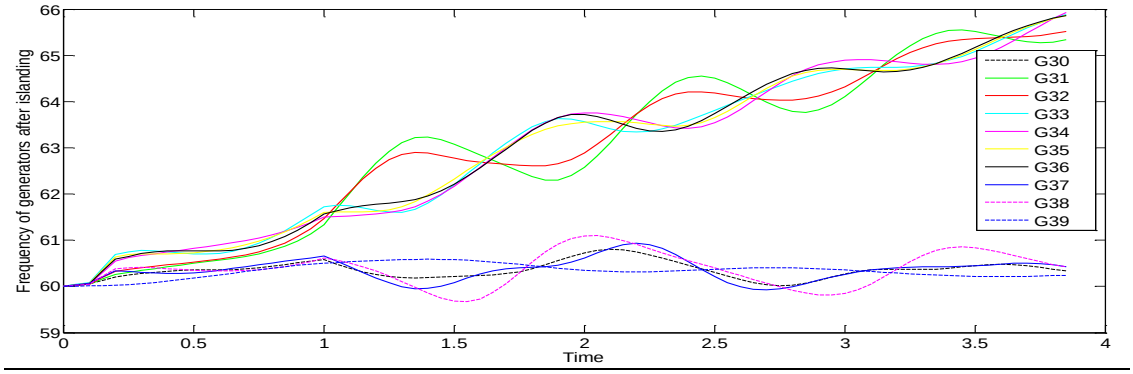

Figure 4.25. Frequency variation after islanding for a fault on line 16-17

At t = 1.25 s it was detected that the system frequency rose above 61.5 Hz for Island 1, and as a result, a signal was issued to trip one unit of generation from all the generators in the island (Gen 31, Gen 32, Gen 33, Gen 34, Gen 35, Gen 36). After a waiting time of t_{set2}, it is identified that the average frequency of the island was still remaining above 61.5 Hz. Therefore, a trip signal was initiated to trip one unit of generation from the generator with the highest frequency deviation, which is Gen 34. The third step of generator tripping were implemented in island 1 at t = 2.55 s for reduction the frequency in the island. One unit of generation each from the stations Gen 31 was reduced during the third step of operation. After the third step of operation, the system frequency in island 1 dropped below 59.75 Hz around t = 6.2 s. Therefore, in order to restore the frequency, 50% of Load 20, which had the lowest frequency was tripped. After the waiting time, t_{set4} the average frequency of island 1 remained below 59.75Hz; hence, a signal was issued to shed 50% of load 12, which had the minimum frequency value at this time and that action helped stabilizing island 1.

For island 2, it was observed that around t = 1.9 s, the average generator frequency was above 60.5Hz. One unit of generation from the generator with the highest frequency, Gen 38, was tripped to restore the frequency. The frequency variations of island 1 and 2 after implementing the generator tripping and load shedding scheme is shown in Figure **4.26**.

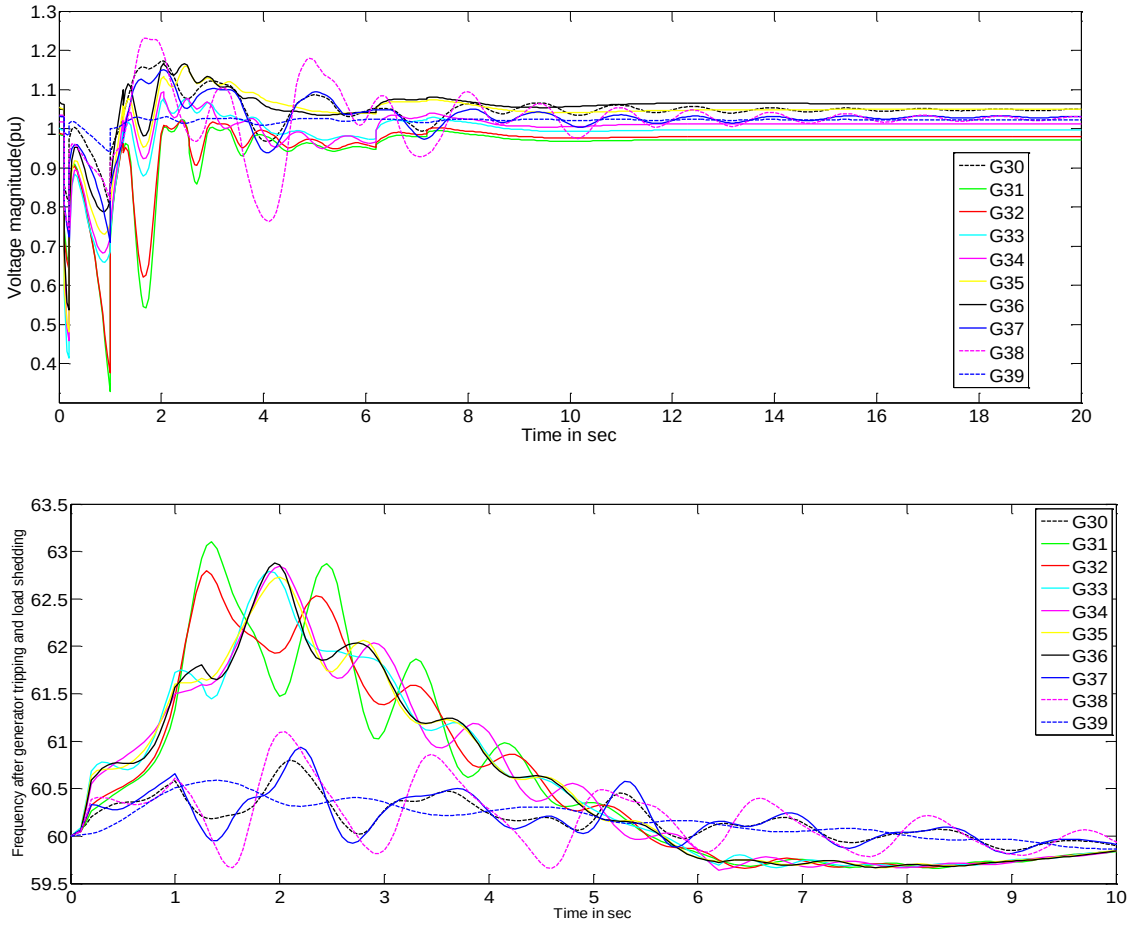

Figure 4.26.Voltage Magnitude and frequency variations after implementing generator tripping and load shedding for a fault on line 16-17

4.10 Concluding Remarks

A synchrophasor measurement-based controlled islanding method was developed in this Chapter. The application of the proposed controlled islanding method was demonstrated using the IEEE-39 bus system, offline simulations. The proposed controlled islanding scheme based on PMU measurements, is fast and can be implemented, when controlled islanding is the only way to save a system from transient stability. The load selection process, which is the most time-consuming search procedure, need to be conducted only

for the critical group of generators. This helps in reducing the calculation resources and time of the algorithm. The updated RED matrix that is re-built after the contingencies will help in retaining the accurate configuration of the system as some lines are removed during a contingency. Moreover, the load selection in this scheme based on phase angle difference and electrical distance helps in incorporating the system conditions and the network topology. The online measurements of the generator parameters make the coherency identification and load selection more accurate.

Unintentional islanding of the network is avoided as the controlled islanding scheme is implemented right after the transient stability prediction. The frequency-based generator tripping and load shedding procedure helps in restoring the power balance in each island. The addition of governors can help in reducing the amount of required load shedding in the proposed scheme. The governor controls are not designed for the selected test system as the main purpose of the research is to propose a control islanding scheme based on wide area measurement. It can be said that the proposed method based on PMU measurements can be considered as a general and reliable method for real-time network splitting which can be extended for wide area networks.

Chapter 5

Conclusions and Future Works

This chapter concludes the thesis discussing the major contributions of the research and the future research areas, in the development of response based Remedial Action Schemes using synchrophasor based wide area measurement technology.

5.1 Conclusions

In this thesis, the design of two response-based RASs, one to prevent overloading of the transmission lines and the other to prevent uncontrolled islanding and blackouts due to transient instability, was studied. Both schemes use synchrophasors measurements as inputs and the emergency control actions are reduction of HVdc power injections and controlled islanding, respectively.

In Chapter 2, the literature on several types of special protection schemes and various emergency control actions such as under frequency generator tripping, over frequency load shedding, HVdc power reduction, FACT devices control, and controlled islanding methods was reviewed. The importance of wide area measurement technology based on PMUs in implementing emergency control schemes were discussed. The review showed that much of the published work on response-based emergency control relies upon offline analysis

which is not truly adaptive. This is still an on-going topic of research, as most of the previous developments can be computationally heavy or require offline analysis which then needs to be updated for every new operating point.

In Chapter 3 a methodology for overload protection of transmission lines during the tripping of power exporting tie-lines in Manitoba Hydro power system was proposed. The proposed approach uses synchrophasors data and the main remedial action considered was the rapid control of the power supplied from three HVdc converters. The main novelty of the proposed methodology is the method for determining correct amount of HVdc power to be curtailed. This measurement-based emergency control scheme was validated through offline simulations for several fault conditions. Based on the study, it can be concluded that:

- It is possible to establish an almost linear relationship between the extent of overload and the required amount of HVdc power reduction for a given line, for a given contingency.
- These relationships, established through offline studies, can be used to estimate the minimum amount of HVdc reduction in real-time during a contingency leading to line overloading, in an iterative manner.
- The proposed response-based overload prevention scheme can reduce the HVdc power curtailments during tie-line tripping, thereby providing economic benefits that could justify the deployment of such a response-based RAS.

In Chapter 4, an emergency control scheme that performs controlled islanding to prevent transient instability was proposed and applied for the IEEE 39-bus test system. The methodology incorporated a previously proposed transient instability prediction algorithm

and a generator coherency recognition method to detect impending instabilities and identify a critical coherent generator group. A combination of measures that include phase angle differences and relative electrical distances between the loads and the generators in a coherent group were used to assign the loads in the islands. A frequency-based generator tripping and load shedding scheme was designed to ensure post-islanding frequency stability in the islands. The simulation studies carried out on IEEE 39 bus test system demonstrated the effectiveness of the emergency controller for a variety of contingencies. A boundary line selection algorithm could not be implemented due to time limitations. Based on the study, it can be concluded that,

- The adopted voltage magnitude-based stability prediction, critical generator identification, and coherent generator groups recognition algorithms provide sufficient information in a timely manner to implement controlled islanding.
- The combination of voltage phase angle differences and relative electrical distances serve as a reliable measure for assigning loads to islands.
- Post islanding load shedding and generator tripping is required to ensure the frequency stability of islands.

5.2 Contributions

The main goal of the research was to explore the possibilities of using wide area measurement technology in implementing emergency control operations. In order to achieve the goal, the following contributions are made as a part of the research. The first contribution of this thesis is the synchrophasor measurement based remedial action scheme proposed to prevent the overloading of lines and transformers by rapidly reducing HVdc

power injection during some critical contingencies in the Manitoba grid. The amount of HVdc power reduction is computed using a pre-identified relationship between the HVdc power reduction and resulting power flow change in a given line. As pointed out earlier, this scheme curtails only the minimum required amount of power based on the measured overload, there is a potential for economic and reliability benefits.

The second contribution of the thesis is a PMU measurement-based controlled islanding scheme for transient stability protection. A post islanding frequency-based generator tripping and load shedding scheme is also proposed in the thesis. The identified coherent group of generators help in determining the number of islands in the system. The main contribution of the proposed controlled islanding method is a load searching algorithm for determining the loads within the island based on the phase angle and the relative electrical distance. The loads are sorted into different islands based on the minimum phase difference with the RED values of the selected loads remaining in the threshold range, until the imbalance between the generator capacity and the load demand is met. The proposed idea is computationally faster since the RED index are pre-calculated following to various contingencies using sparsity factor matrix. The phase angle relations are determined right after the fault clearance. Moreover, the phase difference values are more sensitive to the changes in load and the RED helps in identifying the geographical distribution of loads and generators in the network which indeed helps in proper determination of the islanding boundaries. In that way, the system conditions along with the network topology can be incorporated into the decision making of system separation.

5.3 Recommendations for Future Work

In the proposed emergency control scheme based on HVdc power control, instead of selecting the PMU locations through offline studies and experience, an optimal selection of PMU locations in the system can be conducted using some optimization methods. Future research can be conducted to include the measurement and communication aspects of the proposed method. Moreover, the proposed method should be implemented in a real-time simulator and verified.

Proposed controlled islanding method can be improvised in many ways: The developed controlled islanding method takes into account the generator coherency identification. Other methods like spectral clustering, power flow tracing, and minimal cutset identification can be used for designing the islanding scheme. In the proposed method the control islanding constraints are limited to the phase angle difference and the electrical distance, more parameters like voltage, current, power magnitude can be included in islanding the system considering the power transfer capacity within the island and the economic perspectives. The line selection for splitting the network is not designed in the current research. So further research can be conducted for the proper selection of transmission line to be tripped for islanding the network. Use of machine learning techniques can be explored for selecting the optimal islanding boundaries based on the system conditions. Furthermore, the post-islanding frequency stability control scheme should be tested with governor and excitation control models included in the simulation. The generator tripping and load shedding schemes can be improved considering other inputs such as rate of change of frequency measurements available from PMU measurements.

Appendix A

I. Relationship between HVdc power reduction and line power flow

Relationship between HVdc power reduction and line power flow for the case of fault on Line B8-B14

$\Delta P_{dc\ (MW)}$	B9 to B17	B8 to B9	B3 to B15	B4 to B16	B7 to B10	B7 to B13	B6 to B12	B12 to B11	B5 to B18
0	-33.3522	36.2511	-14.897	4.3497	46.5560	86.8942	22.5458	59.3964	34.9395
97.16	-26.4412	39.4471	-7.3874	12.0260	48.0008	92.8557	25.9911	62.3564	35.4226
242.91	-20.6027	41.8040	-2.8232	18.818	49.0385	95.9176	29.0036	64.8033	37.0422
291.49	-18.6730	42.6550	-1.6779	20.2578	49.3565	94.9519	30.0739	65.4100	37.4547
485.81	-11.4320	45.5621	5.8998	27.7668	50.8038	93.4480	34.4050	68.4044	39.2017
631.55	-6.1876	48.0473	11.5653	33.5957	51.9036	90.6929	37.6341	70.5954	40.4535
728.72	-2.6076	49.5621	14.4455	37.5645	52.6445	88.4179	39.8396	72.0531	41.2603
825.88	0.9125	51.0618	17.2850	41.4464	53.3911	86.1021	42.1836	73.4584	42.0224
971.62	6.0831	53.2797	21.4659	47.1062	54.5098	82.6912	45.6395	75.4526	42.9926

Relationship between HVdc power reduction and line power flow for the case of fault on Line B7-B10

$\Delta P_{dc\ (MW)}$	B9 to B17	B8 to B9	B3 to B15	B4 to B16	B8 to B14	B7 to B13	B6 to B12	B12 to B11	B5 to B18
0	6.2499	69.960	21.1078	41.376	67.002	-9.1624	25.5214	63.9098	40.7744
48.58	6.7093	70.0482	21.5468	41.9321	67.191	-8.8975	26.0103	64.2049	40.8868
145.74	9.1611	70.6391	25.7054	44.9216	68.168	-7.1363	28.4230	65.6646	41.4090
291.49	12.5879	71.4174	28.6199	49.2635	69.513	-4.7972	31.6443	67.5496	41.9906
388.65	14.9785	71.9183	30.5388	52.2191	70.517	-3.5409	33.7665	68.7086	42.4216
485.81	17.8070	72.7251	32.8035	54.816	71.389	-1.2991	36.5197	70.3204	42.6368
680.14	22.7958	74.0001	38.0064	59.931	73.285	2.0104	41.215	72.9577	43.0379
874.46	27.8177	75.2830	41.5500	65.149	75.012	5.8110	46.1926	75.6996	43.9470
971.62	30.480	75.9884	43.333	67.433	75.896	7.6558	48.6993	77.1716	44.3197

Appendix B

I. IEEE New England 39 Bus system

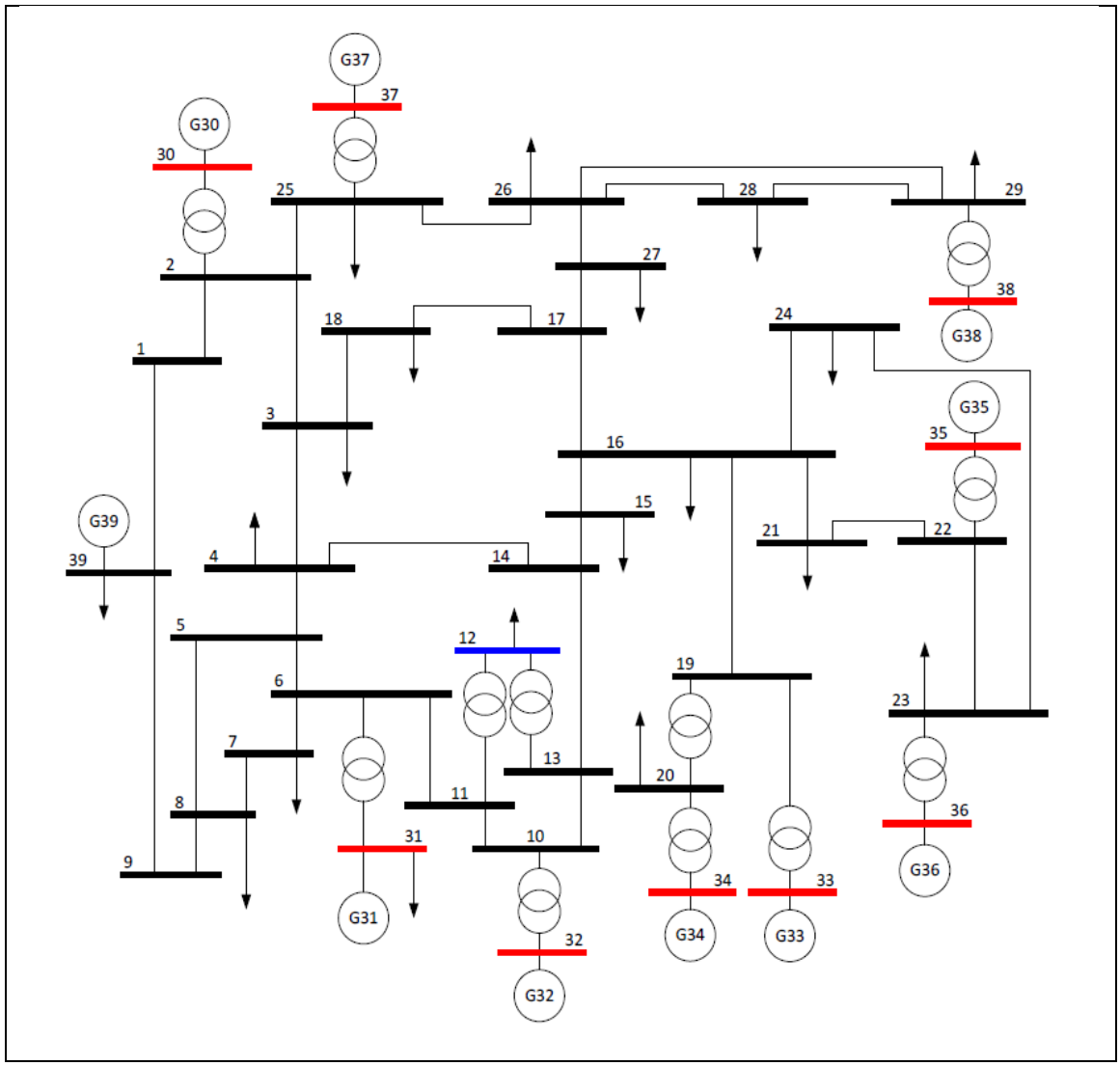

B.1 Generator Parameters

The synchronous generators are represented by the two-axis model whose parameters are given on the system base of 100 MVA.

Gen No	*Ra* (pu)	*Xl* (pu)	*Xd* (pu)	*Xq* (pu)	Xd' (pu)	Xq' (pu)	Xq'' (pu)	Xq'' (pu)	*H* (s)	T'_{do}(s)	T'_{qo}(s)	T''_{do} (s)	T''_{qo}(s)
30	0.00125	0.0125	0.1	0.069	0.031	0.028	0.025	0.025	42.0	10.2	1.5	0.05	0.06
31	0.00125	0.035	0.295	0.282	0.0697	0.170	0.05	0.05	30.2	6.56	1.5	0.05	0.06
32	0.00125	0.0304	0.2495	0.237	0.0531	0.0876	0.045	0.045	35.8	5.7	1.5	0.05	0.06
33	0.00125	0.0295	0.262	0.258	0.0436	0.166	0.035	0.035	28.6	5.69	1.5	0.05	0.06
34	0.00125	0.027	0.67	0.62	0.132	0.166	0.05	0.05	26.0	5.4	0.44	0.05	0.06
35	0.00125	0.0224	0.254	0.241	0.05	0.0814	0.04	0.04	34.8	7.3	0.4	0.05	0.06
36	0.00125	0.0322	0.295	0.292	0.049	0.186	0.04	0.04	26.4	5.66	1.5	0.05	0.06
37	0.00125	0.028	0.290	0.280	0.057	0.0911	0.045	0.045	24.3	6.7	0.41	0.05	0.06
38	0.00125	0.0298	0.2106	0.205	0.057	0.0587	0.045	0.045	34.5	4.79	1.96	0.05	0.06
39	0.00125	0.003	0.02	0.019	0.006	0.008	0.05	0.05	500.0	7.0	0.7	0.05	0.06

B.2 Exciter Parameters

Gen No	*TR*	*KA*	*TA*	V_{RMAX}	V_{RMIN}	*KE*	*TE*	*KF*	*TF*	*E1*	*SE(E1)*	*E2*	*SE(E2)*
30	0	5	0.06	1	-1	0	0.25	0.04	1	3.54	0.08	4.728	0.26
31	0	6.2	0.05	1	-1	0	0.405	0.057	0.5	3.036	0.66	4.049	0.88
32	0	5	0.06	1	-1	0	0.5	0.08	1	2.342	0.13	3.123	0.34
33	0	5	0.06	1	-1	0	0.5	0.08	1	2.868	0.08	3.824	0.314
34	0	40	0.02	10	-10	1	0.785	0.03	1	3.927	0.07	5.236	0.91
35	0	5	0.02	1	-1	0	0.471	0.075	1.2	3.587	0.064	4.782	0.251
36	0	40	0.02	6.5	-6.5	1	0.73	0.03	1	2.8	0.53	3.8	0.74
37	0	5	0.02	1	-1	0	0.528	0.085	1.26	3.191	0.072	4.255	0.282
38	0	40	0.02	10.5	-10.5	1	1.4	0.03	1	4.257	0.62	5.676	0.85

B.3 Transmission Line Parameters

The transmission line parameters for the IEEE 39-bus test system are given on the system base of 100 MVA.

From Bus	To Bus	R (pu)	X (pu)	B (pu)	From Bus	To Bus	R (pu)	X (pu)	B (pu)
1	2	0.0035	0.0411	0.6987	13	14	0.0009	0.0101	0.1723
1	39	0.0010	0.0250	0.7500	14	15	0.0018	0.0217	0.3660
2	3	0.0013	0.0151	0.2572	15	16	0.0009	0.0094	0.1710
2	25	0.0070	0.0086	0.1460	16	17	0.0007	0.0089	0.1342
3	4	0.0013	0.0213	0.2214	16	19	0.0016	0.0195	0.3040
3	18	0.0011	0.0133	0.2138	16	21	0.0008	0.0135	0.2548
4	5	0.0008	0.0128	0.1342	16	24	0.0003	0.0059	0.0680
4	14	0.0008	0.0129	0.1382	17	18	0.0007	0.0082	0.1319
5	6	0.0002	0.0026	0.0434	17	27	0.0013	0.0173	0.3216
5	8	0.0008	0.0112	0.1476	21	22	0.0008	0.0140	0.2565
6	7	0.0006	0.0092	0.1130	22	23	0.0006	0.0096	0.1846
6	11	0.0007	0.0082	0.1389	23	24	0.0022	0.0350	0.3610
7	8	0.0004	0.0046	0.0780	25	26	0.0032	0.0323	0.5130
8	9	0.0023	0.0363	0.3804	26	27	0.0014	0.0147	0.2396
9	39	0.0010	0.0250	1.2000	26	28	0.0043	0.0474	0.7802
10	11	0.0004	0.0043	0.0729	26	29	0.0057	0.0625	1.0290
10	13	0.0004	0.0043	0.0729	28	29	0.0014	0.0151	0.2490

B.4 Transformer Parameters

The transformer parameters for the IEEE 39-bus test system are given on the system base of 100 MVA.

From Bus	To Bus	R (pu)	X (pu)	B (pu)	Transformer Tap	
					Magnitude	Angle
12	11	0.0016	0.0435	0.0000	1.006	0.00
12	13	0.0016	0.0435	0.0000	1.006	0.00
6	31	0.0000	0.0250	0.0000	1.070	0.00
10	32	0.0000	0.0200	0.0000	1.070	0.00
19	33	0.0007	0.0142	0.0000	1.070	0.00
20	34	0.0009	0.0180	0.0000	1.009	0.00
22	35	0.0000	0.0143	0.0000	1.025	0.00
23	36	0.0005	0.0272	0.0000	1.000	0.00
25	37	0.0006	0.0232	0.0000	1.025	0.00
2	30	0.0000	0.0181	0.0000	1.025	0.00
29	38	0.0008	0.0156	0.0000	1.025	0.00
19	20	0.0007	0.0138	0.0000	1.060	0.00

B.5 Power Flow Data

Bus	Type	Voltage (pu)	Load		Generator	
			(MW)	(MVar)	(MW)	(MVar)
1	PQ	–	0.0	0.0	0.0	0.0
2	PQ	–	0.0	0.0	0.0	0.0
3	PQ	–	322.0	2.4	0.0	0.0
4	PQ	–	500.0	184.0	0.0	0.0
5	PQ	–	0.0	0.0	0.0	0.0
6	PQ	–	0.0	0.0	0.0	0.0
7	PQ	–	233.8	84.0	0.0	0.0
8	PQ	–	522.0	176.0	0.0	0.0
9	PQ	–	0.0	0.0	0.0	0.0
10	PQ	–	0.0	0.0	0.0	0.0
11	PQ	–	0.0	0.0	0.0	0.0
12	PQ	–	7.5	88.0	0.0	0.0
13	PQ	–	0.0	0.0	0.0	0.0
14	PQ	–	0.0	0.0	0.0	0.0
15	PQ	–	320.0	153.0	0.0	0.0
16	PQ	–	329.0	32.3	0.0	0.0
17	PQ	–	0.0	0.0	0.0	0.0
18	PQ	–	158.0	30.0	0.0	0.0
19	PQ	–	0.0	0.0	0.0	0.0
20	PQ	–	628.0	103.0	0.0	0.0
21	PQ	–	274.0	115.0	0.0	0.0
22	PQ	–	0.0	0.0	0.0	0.0
23	PQ	–	247.5	84.6	0.0	0.0
24	PQ	–	308.6	-92.0	0.0	0.0
25	PQ	–	224.0	47.2	0.0	0.0
26	PQ	–	139.0	17.0	0.0	0.0
27	PQ	–	281.0	75.5	0.0	0.0
28	PQ	–	206.0	27.6	0.0	0.0
29	PQ	–	283.5	26.9	0.0	0.0
30	PV	1.0475	0.0	0.0	250.0	–
31	PV	0.9820	9.2	4.6	521.0	–
32	PV	0.9831	0.0	0.0	650.0	–
33	PV	0.9972	0.0	0.0	632.0	–
34	PV	1.0123	0.0	0.0	508.0	–
35	PV	1.0493	0.0	0.0	650.0	–
36	PV	1.0635	0.0	0.0	560.0	–
37	PV	1.0278	0.0	0.0	540.0	–
38	PV	1.0265	0.0	0.0	830.0	–
39	PV	1.0300	1104.0	250.0	1000.0	–

II. Phase Angle difference between generators and load points

Table 0.1. Phase angle difference between the generator and load points for fault on line 2-25

	G30	G31	G32	G33	G34	G35	G36	G37	G38	G39
L1	10.33	54.13	59.13	70.51	69.21	61.95	65.86	77.01	77.10	3.57
L2	6.48	50.27	55.27	66.65	65.36	58.10	62.01	73.16	73.24	7.42
L3	6.06	49.86	54.86	66.24	64.94	57.68	61.59	72.74	72.83	7.84
L4	6.02	49.81	54.81	66.19	64.89	57.63	61.55	72.70	72.78	7.88
L5	5.14	48.94	53.94	65.32	64.02	56.76	60.67	71.82	71.91	8.76
L6	4.38	48.18	53.17	64.56	63.26	56.00	59.91	71.06	71.14	9.52
L7	6.96	50.76	55.76	67.14	65.84	58.58	62.49	73.64	73.73	6.93
L8	7.67	51.47	56.46	67.85	66.55	59.29	63.20	74.35	74.43	6.23
L9	10.68	54.48	59.48	70.86	69.56	62.30	66.21	77.36	77.45	3.22
L10	1.35	45.15	50.15	61.53	60.23	52.97	56.88	68.03	68.12	12.55
L11	2.38	46.17	51.17	62.55	61.25	53.99	57.91	69.06	69.14	11.52
L12	2.22	46.02	51.02	62.40	61.10	53.84	57.75	68.90	68.99	11.68
L13	1.95	45.75	50.75	62.13	60.83	53.57	57.48	68.63	68.72	11.95
L14	3.33	47.12	52.12	63.50	62.21	54.95	58.86	70.01	70.09	10.57
L15	1.74	45.53	50.53	61.91	60.62	53.36	57.27	68.42	68.50	12.16
L16	0.59	43.21	48.21	59.59	58.29	51.03	54.94	66.10	66.18	14.48
L17	0.93	44.73	49.73	61.11	59.81	52.55	56.46	67.61	67.70	12.97
L18	3.36	47.16	52.15	63.54	62.24	54.98	58.89	70.04	70.12	10.54
L19	7.30	36.50	41.49	52.88	51.58	44.32	48.23	59.38	59.46	21.20
L20	6.03	37.76	42.76	54.14	52.85	45.58	49.50	60.65	60.73	19.93
L21	3.45	40.35	45.35	56.73	55.43	48.17	52.08	63.23	63.32	17.34
L22	8.37	35.42	40.42	51.80	50.50	43.24	47.16	58.31	58.39	22.27
L23	8.20	35.59	40.59	51.97	50.68	43.41	47.33	58.48	58.56	22.10
L24	0.83	42.96	47.96	59.34	58.05	50.78	54.70	65.85	65.93	14.73
L25	13.90	29.90	34.90	46.28	44.98	37.72	41.63	52.78	52.87	27.80
L26	5.67	38.12	43.12	54.50	53.21	45.94	49.86	61.01	61.09	19.57
L27	1.34	42.45	47.45	58.83	57.53	50.27	54.19	65.34	65.42	15.24
L28	8.40	35.40	40.40	51.78	50.48	43.22	47.13	58.28	58.37	22.29
L29	10.92	32.88	37.88	49.26	47.96	40.70	44.61	55.77	55.85	24.81

Table 0.2. Phase angle difference between the generator and load points for fault on line 26-29

	G30	G31	G32	G33	G34	G35	G36	G37	G38	G39
L1	10.54	51.78	56.56	68.19	66.92	59.56	63.64	69.64	78.87	4.86
L2	5.15	46.39	51.16	62.80	61.53	54.17	58.25	64.25	73.48	10.25
L3	7.04	48.27	53.05	64.69	63.42	56.06	60.14	66.14	75.37	8.36
L4	7.97	49.20	53.98	65.62	64.35	56.99	61.07	67.07	76.30	7.43
L5	7.34	48.58	53.36	65.00	63.72	56.36	60.45	66.44	75.68	8.06
L6	6.67	47.91	52.69	64.33	63.06	55.70	59.78	65.78	75.01	8.72
L7	9.06	50.30	55.08	66.72	65.44	58.08	62.16	68.16	77.40	6.34
L8	9.69	50.93	55.71	67.35	66.07	58.71	62.80	68.79	78.03	5.71
L9	12.11	53.35	58.13	69.76	68.49	61.13	65.21	71.21	80.44	3.29
L10	3.93	45.17	49.95	61.58	60.31	52.95	57.03	63.03	72.27	11.47
L11	4.86	46.10	50.88	62.51	61.24	53.88	57.96	63.96	73.19	10.54
L12	4.73	45.97	50.74	62.38	61.11	53.75	57.83	63.83	73.06	10.67
L13	4.49	45.73	50.51	62.15	60.87	53.51	57.59	63.59	72.83	10.91
L14	5.77	47.01	51.79	63.43	62.16	54.80	58.88	64.88	74.11	9.63
L15	4.86	46.10	50.87	62.51	61.24	53.88	57.96	63.96	73.19	10.54
L16	2.92	44.16	48.94	60.57	59.30	51.94	56.02	62.02	71.25	12.48
L17	4.56	45.80	50.58	62.22	60.95	53.59	57.67	63.66	72.90	10.84
L18	5.93	47.16	51.94	63.58	62.31	54.95	59.03	65.03	74.26	9.47
L19	3.40	37.84	42.62	54.26	52.98	45.62	49.71	55.70	64.94	18.80
L20	2.30	38.94	43.72	55.36	54.08	46.72	50.81	56.80	66.04	17.70
L21	0.22	41.45	46.23	57.87	56.60	49.24	53.32	59.32	68.55	15.18
L22	4.47	36.77	41.55	53.18	51.91	44.55	48.63	54.63	63.86	19.87
L23	4.26	36.98	41.76	53.39	52.12	44.76	48.84	54.84	64.07	19.66
L24	2.70	43.94	48.71	60.35	59.08	51.72	55.80	61.80	71.03	12.70
L25	2.27	43.51	48.29	59.93	58.66	51.30	55.38	61.37	70.61	13.13
L26	3.00	44.24	49.02	60.66	59.38	52.02	56.10	62.10	71.34	12.40
L27	4.86	46.10	50.88	62.52	61.24	53.88	57.96	63.96	73.20	10.54
L28	5.68	35.56	40.33	51.97	50.70	43.34	47.42	53.42	62.65	21.08
L29	10.24	31.00	35.78	47.42	46.15	38.79	42.87	48.87	58.10	25.63

Table 0.3. Phase angle difference between the generator and load points for fault on line 16-17

	G30	G31	G32	G33	G34	G35	G36	G37	G38	G39
L1	11.70	53.48	58.87	73.28	70.95	64.58	68.12	70.29	75.84	5.53
L2	5.41	47.20	52.58	67.00	64.66	58.30	61.84	64.01	69.55	11.82
L3	7.32	49.10	54.49	68.91	66.57	60.21	63.74	65.92	71.46	9.91
L4	5.43	47.21	52.60	67.01	64.68	58.31	61.85	64.02	69.57	11.80
L5	4.63	46.41	51.80	66.21	63.88	57.52	61.05	63.23	68.77	12.60
L6	3.79	45.57	50.95	65.37	63.04	56.67	60.21	62.38	67.92	13.45
L7	6.71	48.50	53.88	68.30	65.96	59.60	63.14	65.31	70.85	10.52
L8	7.57	49.35	54.73	69.15	66.82	60.45	63.99	66.16	71.71	9.67
L9	12.38	54.16	59.55	73.96	71.63	65.26	68.80	70.97	76.52	4.85
L10	0.07	41.86	47.24	61.66	59.32	52.96	56.49	58.67	64.21	17.16
L11	1.32	43.11	48.49	62.91	60.57	54.21	57.74	59.92	65.46	15.91
L12	0.95	42.74	48.12	62.54	60.20	53.84	57.37	59.55	65.09	16.28
L13	0.46	42.24	47.62	62.04	59.71	53.34	56.88	59.05	64.59	16.78
L14	1.27	43.06	48.44	62.86	60.52	54.16	57.69	59.87	65.41	15.96
L15	4.39	37.40	42.78	57.20	54.86	48.50	52.03	54.21	59.75	21.62
L16	8.81	32.97	38.35	52.77	50.43	44.07	47.61	49.78	55.32	26.05
L17	7.53	49.31	54.69	69.11	66.78	60.41	63.95	66.12	71.66	9.71
L18	7.88	49.66	55.04	69.46	67.13	60.76	64.30	66.47	72.01	9.36
L19	16.74	25.05	30.43	44.85	42.51	36.15	39.69	41.86	47.40	33.97
L20	15.11	26.67	32.05	46.47	44.14	37.77	41.31	43.48	49.02	32.35
L21	11.90	29.88	35.26	49.68	47.35	40.98	44.52	46.69	52.23	29.14
L22	17.28	24.51	29.89	44.31	41.97	35.61	39.14	41.32	46.86	34.51
L23	17.29	24.49	29.88	44.29	41.96	35.60	39.13	41.31	46.85	34.52
L24	9.09	32.69	38.08	52.49	50.16	43.80	47.33	49.50	55.05	26.32
L25	2.61	44.40	49.78	64.20	61.86	55.50	59.03	61.21	66.75	14.62
L26	4.02	45.80	51.18	65.60	63.27	56.90	60.44	62.61	68.15	13.22
L27	6.77	48.56	53.94	68.36	66.02	59.66	63.19	65.37	70.91	10.46
L28	0.55	41.23	46.61	61.03	58.70	52.33	55.87	58.04	63.59	17.79
L29	3.63	38.15	43.53	57.95	55.62	49.25	52.79	54.96	60.50	20.87

III. RED values of generators with load points

Table 0.**1** .RED values between the generator and load points for fault on line 2-25

	G30	G31	G32	G33	G34	G35	G36	G37	G38	G39
L1	0.7851	0.9788	0.9764	0.9810	1.0000	0.9839	0.9912	0.9918	0.9902	0.3026
L2	0.4373	0.9445	0.9382	0.9502	1.0000	0.9579	0.9769	0.9786	0.9745	0.8222
L3	0.6801	0.8858	0.8729	0.8975	1.0000	0.9134	0.9525	0.9561	0.9475	0.8657
L4	0.8511	0.7656	0.7514	0.9137	1.0000	0.9271	0.9600	0.9727	0.9674	0.8642
L5	0.9133	0.6595	0.7366	0.9435	1.0000	0.9522	0.9738	0.9830	0.9797	0.8354
L6	0.9233	0.6335	0.7290	0.9480	1.0000	0.9560	0.9759	0.9846	0.9816	0.8467
L7	0.9245	0.6639	0.7475	0.9495	1.0000	0.9573	0.9766	0.9850	0.9821	0.7900
L8	0.9251	0.6793	0.7570	0.9503	1.0000	0.9580	0.9770	0.9852	0.9823	0.7617
L9	0.9691	0.8677	0.8998	0.9795	1.0000	0.9827	0.9905	0.9939	0.9927	0.3023
L10	0.9317	0.7832	0.5329	0.9421	1.0000	0.9511	0.9732	0.9843	0.9812	0.9010
L11	0.9285	0.7333	0.5997	0.9436	1.0000	0.9523	0.9738	0.9843	0.9812	0.8828
L12	0.9244	0.7599	0.5905	0.9359	1.0000	0.9458	0.9703	0.9826	0.9792	0.8904
L13	0.9202	0.7864	0.5813	0.9282	1.0000	0.9393	0.9667	0.9809	0.9771	0.8980
L14	0.8923	0.8004	0.6935	0.8938	1.0000	0.9102	0.9507	0.9725	0.9672	0.8928
L15	0.9025	0.8905	0.8390	0.7871	1.0000	0.8199	0.9012	0.9545	0.9456	0.9303
L16	0.9072	0.9298	0.9025	0.7413	1.0000	0.7813	0.8800	0.9468	0.9364	0.9468
L17	0.8558	0.9248	0.9039	0.8072	1.0000	0.8370	0.9105	0.9075	0.8894	0.9303
L18	0.7886	0.9099	0.8920	0.8415	1.0000	0.8660	0.9265	0.9260	0.9115	0.9056
L19	0.9609	0.9704	0.9589	0.3106	0.9999	0.9078	0.9494	0.9776	0.9732	0.9776
L20	1.0000	1.0000	1.0000	0.9999	0.0001	1.0000	1.0000	1.0000	1.0000	1.0000
L21	0.9363	0.9519	0.9331	0.8224	1.0000	0.6116	0.8386	0.9635	0.9564	0.9635
L22	0.9667	0.9748	0.9650	0.9072	1.0000	0.4370	0.7962	0.9809	0.9772	0.9809
L23	0.9652	0.9737	0.9635	0.9031	1.0000	0.6124	0.6307	0.9801	0.9762	0.9801
L24	0.9155	0.9361	0.9112	0.7644	1.0000	0.7567	0.8439	0.9516	0.9421	0.9515
L25	0.9726	0.9857	0.9817	0.9634	1.0000	0.9690	0.9830	0.2871	0.8477	0.9868
L26	0.9346	0.9659	0.9564	0.9126	1.0000	0.9261	0.9594	0.6958	0.6363	0.9684
L27	0.8981	0.9469	0.9321	0.8638	1.0000	0.8849	0.9368	0.7927	0.7522	0.9508
L28	0.9673	0.9830	0.9782	0.9563	1.0000	0.9631	0.9797	0.8480	0.3035	0.9842
L29	0.9780	0.9885	0.9853	0.9706	1.0000	0.9751	0.9863	0.8976	0.2028	0.9894

Table 0.2. RED values between the generator and load points for fault on line 26-29

	G30	G31	G32	G33	G34	G35	G36	G37	G38	G39
L1	0.8386	0.9827	0.9804	0.9815	1.0000	0.9843	0.9914	0.9172	0.9842	0.3188
L2	0.5774	0.9546	0.9487	0.9515	1.0000	0.9590	0.9775	0.7832	0.9587	0.8650
L3	0.7467	0.8901	0.8772	0.8967	1.0000	0.9126	0.9521	0.8569	0.9525	0.8858
L4	0.8793	0.7673	0.7530	0.9130	1.0000	0.9264	0.9596	0.9291	0.9727	0.8726
L5	0.9293	0.6605	0.7375	0.9430	1.0000	0.9518	0.9735	0.9580	0.9833	0.8401
L6	0.9373	0.6343	0.7297	0.9475	1.0000	0.9556	0.9756	0.9626	0.9849	0.8508
L7	0.9383	0.6647	0.7483	0.9491	1.0000	0.9570	0.9764	0.9633	0.9852	0.7941
L8	0.9388	0.6801	0.7577	0.9499	1.0000	0.9577	0.9768	0.9636	0.9854	0.7657
L9	0.9748	0.8681	0.9001	0.9793	1.0000	0.9825	0.9904	0.9850	0.9940	0.3039
L10	0.9433	0.7838	0.5334	0.9416	1.0000	0.9506	0.9729	0.9654	0.9850	0.9045
L11	0.9410	0.7340	0.6003	0.9431	1.0000	0.9519	0.9736	0.9643	0.9849	0.8865
L12	0.9372	0.7606	0.5911	0.9354	1.0000	0.9453	0.9700	0.9617	0.9834	0.8942
L13	0.9334	0.7871	0.5819	0.9276	1.0000	0.9388	0.9664	0.9592	0.9819	0.9019
L14	0.9095	0.8013	0.6942	0.8929	1.0000	0.9094	0.9503	0.9438	0.9743	0.8978
L15	0.9095	0.8904	0.8387	0.7852	1.0000	0.8184	0.9003	0.9361	0.9611	0.9322
L16	0.9096	0.9292	0.9017	0.7390	1.0000	0.7793	0.8789	0.9329	0.9554	0.9472
L17	0.8555	0.9234	0.9020	0.8031	1.0000	0.8335	0.9087	0.8893	0.9232	0.9297
L18	0.8139	0.9106	0.8925	0.8387	1.0000	0.8636	0.9251	0.8770	0.9343	0.9129
L19	0.9619	0.9702	0.9586	0.3097	0.9999	0.9070	0.9490	0.9717	0.9812	0.9778
L20	1.0000	1.0000	1.0000	0.9999	0.0001	1.0000	1.0000	1.0000	1.0000	1.0000
L21	0.9380	0.9514	0.9325	0.8209	1.0000	0.6102	0.8378	0.9539	0.9694	0.9638
L22	0.9676	0.9746	0.9647	0.9064	1.0000	0.4363	0.7958	0.9759	0.9840	0.9811
L23	0.9662	0.9735	0.9632	0.9023	1.0000	0.6117	0.6303	0.9749	0.9833	0.9802
L24	0.9177	0.9356	0.9104	0.7623	1.0000	0.7549	0.8429	0.9388	0.9594	0.9519
L25	0.7221	0.9653	0.9599	0.9538	1.0000	0.9609	0.9786	0.5839	0.9341	0.9093
L26	0.8234	0.9532	0.9420	0.8975	1.0000	0.9133	0.9524	0.7799	0.7650	0.9326
L27	0.8381	0.9394	0.9235	0.8538	1.0000	0.8764	0.9322	0.8301	0.8373	0.9312
L28	0.9300	0.9815	0.9770	0.9594	1.0000	0.9656	0.9811	0.9128	0.2922	0.9733
L29	0.9644	0.9906	0.9883	0.9793	1.0000	0.9825	0.9904	0.9557	0.1471	0.9864

Table 0.3.RED values between the generator and load points for fault on line 16-17

	G30	G31	G32	G33	G34	G35	G36	G37	G38	G39
L1	0.8306	0.9821	0.9811	0.9946	1.0000	0.9954	0.9975	0.9117	0.9683	0.3163
L2	0.5565	0.9532	0.9506	0.9858	1.0000	0.9880	0.9934	0.7689	0.9170	0.8585
L3	0.7000	0.8863	0.8801	0.9655	1.0000	0.9708	0.9840	0.8229	0.8835	0.8711
L4	0.8705	0.7669	0.7542	0.9292	1.0000	0.9401	0.9671	0.9235	0.9497	0.8700
L5	0.9263	0.6604	0.7382	0.9498	1.0000	0.9576	0.9767	0.9565	0.9714	0.8393
L6	0.9353	0.6344	0.7303	0.9527	1.0000	0.9600	0.9781	0.9618	0.9749	0.8503
L7	0.9361	0.6647	0.7489	0.9545	1.0000	0.9616	0.9789	0.9623	0.9752	0.7935
L8	0.9366	0.6801	0.7583	0.9555	1.0000	0.9624	0.9793	0.9625	0.9754	0.7651
L9	0.9738	0.8681	0.9003	0.9816	1.0000	0.9845	0.9915	0.9846	0.9898	0.3037
L10	0.9454	0.7843	0.5339	0.9415	1.0000	0.9506	0.9729	0.9678	0.9788	0.9052
L11	0.9418	0.7344	0.6008	0.9448	1.0000	0.9533	0.9744	0.9656	0.9774	0.8868
L12	0.9396	0.7611	0.5916	0.9353	1.0000	0.9453	0.9700	0.9643	0.9765	0.8951
L13	0.9374	0.7878	0.5825	0.9258	1.0000	0.9372	0.9656	0.9630	0.9757	0.9033
L14	0.9179	0.8026	0.6949	0.8866	1.0000	0.9041	0.9474	0.9515	0.9681	0.9007
L15	0.9566	0.8957	0.8388	0.7315	1.0000	0.7730	0.8754	0.9744	0.9832	0.9475
L16	0.9735	0.9363	0.9015	0.6649	1.0000	0.7167	0.8445	0.9844	0.9897	0.9679
L17	0.7341	0.9128	0.9081	0.9735	1.0000	0.9776	0.9877	0.7983	0.7694	0.8913
L18	0.7209	0.9026	0.8973	0.9704	1.0000	0.9750	0.9863	0.8077	0.8128	0.8835
L19	0.9888	0.9731	0.9585	0.2785	0.9999	0.8806	0.9345	0.9934	0.9957	0.9865
L20	1.0000	1.0000	1.0000	0.9999	0.0001	1.0000	1.0000	1.0000	1.0000	1.0000
L21	0.9818	0.9563	0.9324	0.7700	1.0000	0.5672	0.8142	0.9893	0.9929	0.9780
L22	0.9905	0.9771	0.9647	0.8798	1.0000	0.4138	0.7835	0.9944	0.9963	0.9885
L23	0.9901	0.9761	0.9631	0.8745	1.0000	0.5882	0.6175	0.9941	0.9961	0.9880
L24	0.9759	0.9419	0.9103	0.6948	1.0000	0.6978	0.8116	0.9858	0.9906	0.9708
L25	0.7037	0.9646	0.9626	0.9892	1.0000	0.9909	0.9950	0.5729	0.8811	0.9038
L26	0.7875	0.9534	0.9509	0.9859	1.0000	0.9880	0.9934	0.7624	0.6029	0.9225
L27	0.7628	0.9346	0.9311	0.9801	1.0000	0.9832	0.9908	0.7786	0.6787	0.9081
L28	0.8938	0.9767	0.9755	0.9929	1.0000	0.9940	0.9967	0.8813	0.2867	0.9613
L29	0.9285	0.9843	0.9835	0.9952	1.0000	0.9960	0.9978	0.9200	0.1915	0.9739

Bibliography

[1] V. Madami, M. Adamiak, and M. Thakur, “Design and implementation of wide area special protection schemes,” in *Proceedings of 57th Annu. Conf. Prot. Relay Eng. 2004*, pp. 35–44, 2004.

[2] A. G. Phadke, “Synchronized phasor measurements in power systems,” *IEEE Comput. Appl. Power*, vol. 6, no. 2, pp. 10–15, 1993.

[3] D. E. Echeverría, J. L. Rueda, J. C. Cepeda, D. G. Colomé, and I. Erlich, “Comprehensive approach for prediction and assessment of power system transient stability in real-time,”in *Proceedings of IEEE PES Innovative Smart Grid Technologies*,pp. 1–5, 2013.

[4] F. R. Gomez, A. D. Rajapakse, U. D. Annakkage, and I. T. Fernando, “Support vector machine-based algorithm for post-fault transient stability status prediction using synchronized measurements,” *IEEE Trans. Power Syst.*, vol. 26, no. 3, pp. 1474–1483, 2011.

[5] Power System Engineering Research Center, Final Project Report on the December 2010,“System Protection Schemes : Limitations , Risks , and Management,” 2010.

[6] CIGRE Working Group C4.34, “Application of phasor measurement units for monitoring power,” September, 2017.

[7] P. Kundur J Paserba, V Ajjarappu,G Andersson, A Bose,C Canizares, N Hatziargyriou, D Hill, A Stankovic, C Taylor, T Cutsem,and V Vittal, “Definition and Classification of Power System Stability,” *IEEE Trans. Power Syst.*, vol. 19, no.

2, pp. 1387–1401, 2004.

[8] C. W. Taylor, D. C. Erickson, K. E. Martin, R. E. Wilson, and V. Venkatasubramanian, “WACS - Wide-area stability and voltage control system: R&D and online demonstration,”in *Proceedings of IEEE,* vol. 93, no. 5, pp. 892–906, 2005.

[9] P. F. Le Roux and R. C. Bansal, “Transient stability control by means of under-frequency load shedding and a hybrid control scheme,” *J. Energy South. Africa,* vol. 28, no. 4, pp. 41–53, 2017.

[10] Y. R. Omar, I. Z. Abidin, S. Yusof, H. Hashim, and H. A. Abdul Rashid, “Under Frequency Load Shedding (UFLS): Principles and implementation,”in *Proceedings of IEEE Int. Conf. Power Energy,* no. 1, pp. 414–419, 2010.

[11] A. Ketabi and M. H. Fini, “Adaptive underfrequency load shedding using particle swarm optimization algorithm,” *Journal for Applied Research and Technology,* vol. 15, pp. 54–60, 2017.

[12] S. Manson, G. Zweigle, and V. Yedidi, “Case study: An adaptive underfrequency load-shedding system,” *IEEE Trans. Ind. Appl.*, vol. 50, no. 3, pp. 1659–1667, 2014.

[13] U. Rudez and R. Mihalic, “Analysis of underfrequency load shedding using a frequency gradient,” *IEEE Trans. Power Deliv.*, vol. 26, no. 2, pp. 565–575, 2011.

[14] A. Derviškadić, Y. Zuo, G. Frigo, and M. Paolone, “Under Frequency Load Shedding based on PMU Estimates of Frequency and ROCOF,”in *Proceedings of IEEE PES Innovative Smart Grid Technologies Conf Europe* pp. 1–6, 2018.

[15] G. G. Karady, and J. Gu, “A Hybrid Method for Generator Tripping,” vol. 17, no. 4, pp. 1102–1107, 2002.

[16] F. D. Galiana, “Analysis of Contingencies Leading to Islanding and Cascading Outages,”in *Proceedings of IEEE Power Tech Conf.*, Laussane, pp. 63–67, 2007.

[17] Z. Xing, J. Han, Y. U. Zhihong, and Z. Xiaoxin, “A Generator Tripping Control Method based on Trajectory Sensitivity Analysis and Pattern Search,”in *Proceedings of 34th Chinese Control Conf. (CCC)*,pp. 9043–9047, 2015.

[18] M. A. Rahman, I. Ashraf, and H. D. Alsharari, “HVDC system for National and Cross Border Grid Interconnections in Saudi Arabia,” *IOSR J. Eng.*, vol. 2, no. 4, pp. 529–537, 2012.

[19] W. Shao and V. Vittal, “LP-based OPF for corrective FACTS control to relieve overloads and voltage violations,” *IEEE Trans. Power Syst.*, vol. 21, no. 4, pp. 1832–1839, 2006.

[20] X.-P. Zhang, L. Yao, B. Chong, C. Sasse, and K. R. Godfrey, “FACTS and HVDC technologies for the development of future power systems,”in *Proceedings of Int. Conf. Futur. Power Syst.*, vol. 2005, pp. 241–247, 2005.

[21] Naihu Li, Yan Xu, and Heng Chen, “FACTS-based power flow control in interconnected power system,” *IEEE Trans. Power Syst.*, vol. 15, no. 1, pp. 257–262, 2000.

[22] G. Beck, W. Breuer, D. Povh, and D. Retzmann, “Use of FACTS and HVDC for Power System Interconnection and Grid Enhancement,” *Power GEN Middle East 2006*, pp. 1–33, 2006.

[23] V. Vittal, “System islanding using minimal cutsets with minimum net flow,”in *Proceedings of IEEE PES Power Syst. Conf. Expo. 2004.*, pp. 967–972, 2004.

[24] G. Xu and V. Vittal, “Slow coherency based cutset determination algorithm for large

power systems," *IEEE Trans. Power Syst.*, vol. 25, no. 2, pp. 877–884, 2010.

[25] S. Shahnawaz Ahmed, N. C. Sarker, A. B. Khairuddin, M. R. B. A. Ghani, and H. Ahmad, "A Scheme for Controlled Islanding to Prevent Subsequent Blackout," *IEEE Power Eng. Rev.*, vol. 22, no. 11, p. 55, 2002.

[26] Z. Lin, F. Wen, J. Zhao, and Y. Xue, "Controlled islanding schemes for interconnected power systems based on coherent generator group identification and wide-area measurements," *J. Mod. Power Syst. Clean Energy*, vol. 4, no. 3, pp. 440–453, 2016.

[27] S. Fu and Z. Xu, "An intelligent approach for system separation to prevent a blackout," in *Proceedings of 2010 Int. Conf. Power Syst. Technol. Technol. Innov. Mak. Power Grid Smarter, POWERCON2010*, 2010.

[28] H. Mehrjerdi, S. Lefebvre, D. Asber, and M. Saad, "Graph partitioning of power network for emergency voltage control," in *Proceedings of 2013 9th Asian Control Conf. ASCC 2013*, pp. 1–6, 2013.

[29] L. Ding, F. M. Gonzalez-longatt, P. Wall, V. Terzija, and S. Member, "Two-Step Spectral Clustering Controlled Islanding Algorithm," *IEEE Trans. Power Syst.*,vol. 28, no. 1, pp. 75–84, 2013.

[30] Y. Ohura, M Suzuki, K Yanagihashi, K Omata,and T Nagamura, "A predictive out-of-step protection system based on observation of the phase difference between substations," *IEEE Trans. Power Deliv.*, vol. 5, no. 4, pp. 1695–1704, 1990.

[31] V. Vittal, W. Kliemann, D. G. Chapman, A. D. Silk, Y. Xni, and D. J. Sobajic, "Determination of generator groupings for an islanding scheme in the manitoba hydro system using the method of normal forms," *IEEE Trans. Power Syst.*, vol. 13,

no. 4, pp. 1345–1351, 1998.

[32] I. Kamwa, R. Grondin, and Y. Hebert, “Wide-area measurement based stabilizing control of large power systems-a decentralized/hierarchical approach,” *IEEE Trans. Power Syst.*, vol. 16, no. 1, pp. 136–153, 2001.

[33] A. De La Quintana and R. Palma-Behnke, “Challenges for special protection systems in the Chilean electricity market,” in *Proceedings of IEEE Power Energy Soc. Gen. Meet.*, pp. 1–5, 2013.

[34] C. R. Chen, W. T. Tsai, and H. Y. Chen, “System simulation and implementation of sips in Taiwan,” *Math. Probl. Eng.*, vol. 2014, 2014.

[35] M. Bahrman, “HVDC Transmission,” *IEEE PSCE*, vol. 5, no. 2, pp. 22–31, 2007.

[36] Manitoba Hydro, “Needs For and Alternatives To Chapter 5 – The Manitoba Hydro System, Interconnections and Export Markets,” no. August, 2013.

[37] H . Seyedi , M . Sanaye, “Design of New Load Shedding Special Protection Schemes for a Double Area Power System,” *Am. J. Appl. Sci.*, vol. 6, no. 2, pp. 317–327, 2009.

[38] M P Bahrman, L Balu, and N Bergstrom, “Dynamic Performance Characteristics of North American HVDC Systems for Transient and Dynamic Stability Evaluations,” *IEEE Trans. Power Appar. Syst.*, vol. PAS-100, no. 7, pp. 3356–3364, 1981.

[39] J. De La Ree, V. Centeno, J. S. Thorp, and A. G. Phadke, “Synchronized phasor measurement applications in power systems,” *IEEE Trans. Smart Grid*, vol. 1, no. 1, pp. 20–27, 2010.

[40] S. B. Matta and K. Seethalekshmi, “Islanding Detection and Controlled Islanding In Emerging Power Systems Key issues and challenges,” *Int. Res. J. Eng. Technol.*,

vol. 4, no. 6, pp. 1045–1059, 2017.

[41] D. R. Gurusinghe, “Application of Wide Area Synchrophasor Measurements for Improved Real-Time Monitoring and Control of Power Systems,” PhD Dissertation,University of Manitoba,Canada, November, 2016.

[42] F. Hashiesh, H. E. Mostafa, A. R. Khatib, I. Helal, and M. M. Mansour, “An intelligent wide area synchrophasor based system for predicting and mitigating transient instabilities,” *IEEE Trans. Smart Grid*, vol. 3, no. 2, pp. 645–652, 2012.

[43] PowerTech Labs Inc, “TSAT Transient Security Assessment Tool,” 2007.

[44] D. R. Gurusinghe and A. D. Rajapakse, “Post-disturbance transient stability status prediction using synchrophasor measurements,” *IEEE Trans. Power Syst.*, vol. 31, no. 5, pp. 3656–3664, 2016.

[45] A. G. Phadke and J. S. Thorp, *Synchronized Phasor Measurements and Their Applications*. 2008.

[46] N. Fan, and F. Pan, “Locating Phasor Measurements and Detecting Cutset Angles in Power Systems,”in *Proceedings of IEEE PES Innovative Smart Grid Technologies Conference,Asia*, pp. 1–7, 2011.

[47] J. Ballance, B. Bhargava, and G. D. Rodriguez, “Use of synchronized phasor measurement system for enhancing AC-DC power system transmission reliability and capability,”*CIGRE Session C1-210*, pp. 1–12, 2004.

[48] K. Visakha, D. Thukaram, and L. Jenkins, “Transmission charges of power contracts based on relative electrical distances in open access,” *Electr. Power Syst. Res.*, vol. 70, no. 2, pp. 153–161, 2004.

[49] G. Yesuratnam and D. Thukaram, “Congestion management in open access based

on relative electrical distances using voltage stability criteria," *Electr. Power Syst. Res.*, vol. 77, no. 12, pp. 1608–1618, 2007.

[50] M. Belkacemi and N. Harid, "Fast Reduction and Modification of Power System Sparse Matrices," *Electr. Power Components Syst.*, vol. 32, no. 4, pp. 367–373, 2004.

[51] O. Alsaç, B. Stott, and W. F. Tinney, "Sparsity-oriented compensation methods for modified network solutions," *IEEE Trans. Power Appar. Syst.*, vol. PAS-102, no. 5, pp. 1050–1060, 1983.

[52] P. A. Trodden, W. A. Bukhsh, A. Grothey, and K. I. M. McKinnon, "MILP islanding of power networks by bus splitting,"in *Proceedings of IEEE Power Energy Soc. Gen. Meet.*, 2012.

[53] K. Sun, D. Z. Zheng, and Q. Lu, "Splitting strategies for islanding operation of large-scale power systems using OBDD-based methods," *IEEE Trans. Power Syst.*, vol. 18, no. 2, pp. 912–923, 2003.

[54] H. You, V. Vittal, and X. Wang, "Slow Coherency-Based Islanding," *IEEE Trans.Powr Syst*, vol. 19, no. 1, pp. 483–491, 2004.

[55] S. Xu and S. Miao, "Three-stage method for intentional controlled islanding of power systems," *J. Mod. Power Syst. Clean Energy*, vol. 6, no. 4, pp. 691–700, 2018.

[56] H. Song, J. Wu, and K. Wu, "A wide-area measurement systems-based adaptive strategy for controlled islanding in bulk power systems," *Energies*, vol. 7, no. 4, pp. 2631–2657, 2014.

[57] N. Saharuddin, I. Zainal Abidin, H. Mohklis, A. Abdullah, and K. Naidu, "A Power System Network Splitting Strategy Based on Contingency Analysis," *Energies*, vol.

11, no. 2, p. 434, 2018.

[58] C. G. Wang, B. H. Zhang, Z. G. Hao, J. Shu, P. Li, and Z. Q. Bo, “A novel real-time searching method for power system splitting boundary,” *IEEE Trans. Power Syst.*, vol. 25, no. 4, pp. 1902–1909, 2010.